New Computational Framework for Biomechanical

Multibody System Applications

BY

FLORENTINA MARINA GANTOI

B.Sc. in Mechanical Engineering, Pitesti University, Romania, 2006

THESIS

Submitted as partial fulfillment of the requirements
for the degree of Doctor of Philosophy in Mechanical Engineering
in the Graduate College of the
University of Illinois at Chicago, 2013

Chicago, Illinois

Defense Committee:

Professor Ahmed Shabana, Chair and Advisor, Mechanical Engineering
Mike Brown, Mechanical Engineering
Craig Foster, Civil and Materials Engineering
Carmen Lilley, Mechanical Engineering
Thomas Royston, Mechanical Engineering

This thesis is dedicated to my sister Lidia and her husband Silviu who always supported me to pursue my professional goals with unconditional love.

ACKNOWLEDGEMENTS

I would like to thank my graduate advisor Dr. Ahmed Shabana for his extensive guidance, valuable suggestions, and persistent encouragement during my studies at the University of Illinois at Chicago. Your advice on both research as well as on my career have been invaluable. I would also like to thank my committee members: Dr. Michael Brown, Dr. Craig Foster, Dr. Carmen Lilley, and Dr. Thomas Royston for their constructive advice. I am particularly grateful for my co-advisor Dr. Michael Brown for his tremendous help that allowed me to complete my thesis.

I owe thanks to all my colleagues at the Dynamic Simulation Laboratory I worked over the years. I learn something new from each one of them and for that I am very grateful.

Lastly, I would like to thank my family for all their love and encouragement. For my parents, who raised me with a love of science and supported me in all my pursuits. And most of all for my loving, supportive, encouraging, and patient husband Julian for his help and support during the program.

TABLE OF CONTENTS

TABLE OF CONTENTS (continued)

TABLE OF CONTENTS (continued)

LIST OF TABLES

LIST OF FIGURES

LIST OF FIGURES (continued)

LIST OF FIGURES (continued)

SUMMARY

Most of the computational finite element (FE)-based bio-mechanics models employ static or quasi-static assumptions. These models fail to capture the response of the human body and its joints to high speed cyclic loading. They also fail to accurately capture the change in the system motion that is governed by highly nonlinear differential and algebraic equations. This thesis aims at addressing this important issue by developing a new computational framework for modeling human body and its joints, with particular interest in the knee joint mechanics. The new computational framework is based on successful integration of multibody system (MBS) and large displacement FE algorithms. In this new computational framework, the *absolute nodal coordinate formulation* (ANCF) is used as the basis for the description of the rigid geometry as well as the deformation of the very flexible ligaments. ANCF finite elements have many desirable features that can be exploited in modeling complex bio-mechanics systems. These elements can be used to capture the deformations of the ligament cross sections, allow for the use of general material laws that are suited for developing accurate ligament models, have a constant inertia matrix that lead to an optimum sparse matrix structure, and their kinematic description is consistent with the description used in computational geometry methods, thereby allowing for converting CAD models to FE meshes without geometry distortion. The new computational framework used in this thesis also allow for modeling more general boundary conditions at the ligament bone insertion sites. The approach described in this thesis can be used to develop more realistic models of the human body joints and is applicable to future research studies on ligaments, muscles and soft tissues (LMST).

Specifically, the main contributions of this thesis can be summarized as follows:

1. This investigation clearly demonstrates that different models for the bone/ligament insertion sites can be developed. To this end, two different sets of clamped end conditions at the ligament/bone insertion site are examined using nonlinear large displacement ANCF finite elements. The first set of end conditions, called the *partially clamped joint*, eliminates only the translations and rotations at a point, allowing for the cross section stretch and shear at the ligament/bone connection. The second joint, called the *fully clamped joint*, eliminates all the translation, rotation, and deformation degrees of freedom of the cross section at the ligament/bone insertion sites. In the case of the fully clamped joint, the gradient vectors do not change their length and orientation, allowing for the use of the constant strain assumptions. The partially clamped joint, on the other hand, allows for the change in length and relative orientation of the gradient vectors at the bone/ligament insertion site, leading to the cross section deformation induced by knee movements.
2. The thesis reports a new numerical comparative study to demonstrate the effect of the boundary conditions at the insertion site on the ligament deformations. Two different ANCF finite element models are used in the first chapter; the first model employs the fully parameterized three-dimensional beam element, while the second model employs the three-dimensional cable element. The three-dimensional fully parameterized beam element allows for a straight forward implementation of a Neo-Hookean constitutive model that can be used to accurately predict the large displacement as experienced in knee flexation and rotation.

At the ligament/bone insertion site, the ANCF fully parameterized beam element is used to define a fully or partially constrained joint; while the ANCF cable element can only be used to define one joint type. The fully and partially clamped joint constraints are satisfied at the position, velocity, and acceleration levels using a dynamic formulation that is based on an optimum sparse matrix structure.

3. A new method is proposed for developing ANCF surfaces that can be used in the description of the rigid geometry of the bones. Besides modeling the ligaments deformation, it is demonstrated that ANCF can also be used in modeling the contact geometry in biomechanics applications. Two ANCF approaches can be used to model the rigid contact surface geometry. In the first approach, fully parameterized ANCF volume elements are converted to surface geometry using parametric relationship that reduces the number of independent coordinate lines. This parametric relationship can be defined analytically or using a spline function representation. In the second approach, an ANCF surface that defines a gradient deficient thin plate element is used. This second approach does not require the use of parametric relations or spline function representations. These two geometric approaches shed light on the generality of and the flexibility offered by the ANCF geometry as compared to computational geometry (CG) methods such as B-splines and NURBS (**N**on-**U**niform **R**ational **B**-**S**plines). Furthermore, because B-spline and NURBS representations employ a rigid recurrence structure, they are not suited as general analysis tools that capture different types of joint discontinuities.

ANCF finite elements, on the other hand, lend themselves easily to geometric description and can additionally be used effectively in the analysis of ligaments, muscles, and soft tissues (LMST). In this thesis, ANCF finite elements are used to define the femur/tibia rigid body contact surface geometry. Two different contact formulations are used in this investigation to predict the femur/tibia contact forces; the *elastic contact formulation* where penetrations and separations at the contact points are allowed, and the *constraint contact formulation* where the non-conformal contact conditions are imposed as constraint equations, and as a consequence, no separations or penetrations at the contact points are allowed. For both formulations, the contact surfaces are described in a parametric form using surface parameters that enter into the ANCF finite element geometric description. A set of nonlinear algebraic equations that depend on the surface parameters is developed and used to determine the location of the contact points. These two contact formulations are implemented in a general MBS algorithm that allows for modeling rigid and flexible body dynamics.

4. The formulation of the insertion site partially clamped joint is not unique, different partially clamped joint models can be developed, and these models are associated with different joint coordinate systems. The relationship between the ligament/bone insertion site boundary conditions and the choice of the joint coordinate system is explained in this thesis. The thesis examines the use of two different frames in the formulation of the ligament/bone constraints. These two frames are the tangent and the cross section frames.

The tangent frame is a coordinate system selected such that one of its axes is tangent to the space curve defined by the beam centerline, while in the cross section frame the coordinate system is selected such that two of its axes lie in the plane that defines the beam cross section. In order to formulate the connectivity conditions using *the tangent* and *cross section frame*, a large displacement three-dimensional ANCF beam element is used.

5. Most existing beam formulations assume that the cross section of the beam remains rigid regardless of the amplitude of the displacement. ANCF finite elements, however, allow for the deformation of the cross section and lead to a more general beam models that capture the coupling between different modes of displacements. One of the main contributions of this thesis is to examine the effect of the order of interpolation on the modes of deformation of the beam cross section using ANCF finite elements; this is particularly important in the bio-mechanics applications. To this end, a new two-dimensional shear deformable ANCF beam element is developed. The new finite element employs a higher order of interpolation, and allows for new cross section deformation modes that cannot be captured using previously developed shear deformable ANCF beam elements. The element developed in this thesis relaxes the assumption of the planar cross section; thereby allowing for including the effect of *warping* as well as for different stretch values at different points on the element cross section. The displacement field of the new element is assumed to be cubic in the axial direction and quadratic in the transverse direction.

Using this displacement field, more expressions for the element extension, shear and the cross section stretch can be systematically defined. Measures of the shear angle, extension, and cross section stretch can also be systematically defined using coordinate systems defined at the element material points. Using these local coordinate systems, expressions for a nominal shear angle are obtained. The differences between the cross section deformation modes obtained using the new higher order element and those obtained using the previously developed lower order elements are highlighted. Numerical examples are presented in order to compare the results obtained using the new finite element and the results obtained using previously developed ANCF finite elements.

CHAPTER 1

INTRODUCTION

1.1. Motivation and Objectives

Most investigations on human body motion are focused on the simulation of human tasks based on the assumption that the joints that constrain the relative motion of the system components are ideal or perfect joints. Furthermore, most of the finite element based investigations are based on static or quasi-static assumptions. In order to better understand the performance of the human body mechanics, it is necessary to develop realistic and detailed models that more accurately describe the characteristics of the human joints. An important example of which is the knee joint. This joint is the largest synovial joint in the body and the most complex with six degrees of freedom in load bearing physiological motion. The stiffness and stability of the joint are provided by complex interactions between muscles, ligaments, articulating cartilage and menisci. The individual role of each element in overall response of the joint can substantially alter with structural changes in the other components, boundary conditions, flexion angle, load magnitudes and load combinations. Integrating FE methods and multibody system (MBS) algorithms is necessary for developing accurate and detailed biomechanics models. This is particularly important given the fact that most biomechanics finite element models are not suited for capturing accurately the dynamic modes of ligament and muscle deformations because, as previously mentioned, these models are based on static or quasi static assumptions.

The aim of this thesis is to introduce a new computational environment for modeling ligament dynamics and the contact geometry in bio-mechanics applications based on the

integration of the finite element *absolute nodal coordinate formulation* (ANCF) and multibody system (MBS) algorithms. In this unified computational environment, one method will be used for the development of the geometry as well as the analysis. One of the objectives of this thesis is to investigate ligament dynamics under a prescribed motion and ligament/bone insertion site constraints. In order to examine ligament/bone connectivity, two large displacement three-dimensional ANCF finite elements are used to obtain two different knee joint models that have different modes of deformation. Both three-dimensional finite elements are based on a nonlinear elasticity theory that accounts for geometric nonlinearities due to large displacements and rotations. Furthermore, two different sets of clamped end conditions are examined: the fully clamped joint and the partially clamped joint. The *partially clamped joint*, eliminates only the translations and rotations at a point, allowing the cross section to stretch and shear at bone/ligament insertion site. The second joint; called the *fully clamped joint*, eliminates all the translation, rotation and deformation degrees of freedom of the cross section at the bone/ligament intersection. For the partially clamped joint, two sets of end conditions expressed in terms of the orthonormal vectors that define *the tangent* and *the cross section* frame are considered. The *tangent frame* is a coordinate system selected such that one of the frame axes is tangent to the space curve defined by the beam centerline, while in the *cross section frame* the coordinate system is selected such that two of its axes lie in the plane that defines the beam cross section.

Another objective of this thesis is the development of two general contact formulations based on ANCF finite elements for bio-mechanics applications; the *elastic contact formulation* where penetrations and separations at the contact points are allowed, and the *constraint contact formulation* where the non-conformal contact conditions are imposed as constraint equations,

and as a consequence, no separations or penetrations at the contact points are allowed. ANCF finite elements are also used to describe the contact surface geometry.

Most beam finite elements are based on a kinematic description that assumes that the element cross section remains rigid regardless of the amount of deformation and loading. Therefore, these elements are not suited for capturing the change of the dimensions of the ligament and muscle cross sections. This shows how the assumption of the cross section rigidity can be relaxed using new ANCF finite elements. The thesis proposes a new shear deformable element that allows systematically for capturing the cross section deformation as well as warping.

1.2. Background

The dynamics of mechanical systems consisting of interconnected rigid and deformable components that undergo large translations and rotations has been the subject of a large number of investigations. Such mechanical systems are known in the literature as Multibody Systems (MBS). Multibody dynamic theory can be divided into two main categories: rigid body mechanics and structural mechanics in which the deformation effect is taken into consideration.

Computational biomechanics is an important branch of the field of MBS dynamics. The use of the MBS methodologies allowed for making significant progress in the study and simulation of biomechanical applications (Guess et al., 2010).There are several methods in the literature for studying the kinematics and dynamics of rigid and deformable bodies that experience large rotations and translations. One of the most widely used for modeling small deformation and large rotation problems is the floating frame of reference (FFR) formulation.

This formulation describes the rigid and flexible body motion correctly in the case of small deformation. When the body experiences large deformation, however, it is not recommended to use the FFR formulation that employs linear mode. ANCF finite elements are more suited for the solution of the large rotation and large deformation problems as in case of the knee joint. ANCF finite elements are also consistent with the computational geometry methods.

Before defining the scope and organization of this thesis, a literature survey on some of the important topics discussed in this investigation is provided.

1.2.1. Absolute Nodal Coordinate Formulation (ANCF)

The finite element methods are numerical procedures that can be applied to a large class of engineering problems (Saed Moavani, 2008). In fact the finite element method is the most widely used numerical approach in the study of the deformation of the elastic components in MBS applications. These systems represent a large number of industrial and technological applications such as robotics, machines, vehicles and biomechanical systems. Very complicated problems can be solved by dividing a structure into small elements, obtain the algebraic or differential equations for each element, and then solving the system of equations for the entire structure. ANCF finite elements are used to solve large deformation and large rotation MBS problems. In this formulation, displacements and slopes at the nodal points are used as nodal coordinates. Some of the desirable features of ANCF include the constant mass matrix of the finite elements, zero centrifugal and Coriolis forces, and the simplicity of imposing some of the joint constraints. Moreover, ANCF allows for a straight forward implementation of general constitutive equations.

Classical Euler-Bernoulli beam theory neglects the shear effect and assumes that the cross section of the beam remains rigid and perpendicular to the beam neutral axis when the

beam deforms. In Timoshenko beam theory, on the other hand, the cross section is permitted to rotate with respect to a Frenet frame defined at material points on the beam centerline. While Timoshenko beam theory accounts for the shear effect, it also assumes that the cross sections remain planar, but are not restrained to be perpendicular to the bending axis. Most existing finite element beam formulations also use this assumption of rigid and planar cross section. In some of these finite element formulations, the displacement of the cross section in the planar analysis is defined by two translation coordinates and one rotation coordinate. In the spatial analysis, six coordinates are used; three translations and three rotations. In some finite element formulations, the translations and rotations of the cross section are defined as field variables using independent interpolations (Crisfield and Moita, 1991). By using the translation and rotation fields, one can develop expressions for the strains that enter into the formulation of the constitutive equations and elastic forces of the beam. Because of the nature of the coordinates used, most existing finite element formulations, however, lead to highly nonlinear inertia matrix in the spatial large displacement analysis of beam problems.

Fully parameterized ANCF finite elements, on the other hand, relax the assumption of the rigidity of the element cross section; allowing for the cross section to deform (Abbas et al., 2010; Dufva et al., 2005; Garcia-Vallejo et al., 2004 and 2007; Gerstmayr et al., 2008; Gerstmayr and Irshik, 2008; Gerstmayr and Matikainen, 2005; Nachbagauer et al., 2010; Kerkkanen et al., 2005; Koyama eta al., 2006; Sopanen and Mikkola, 2003; Sugiyama et al., 2006; Sugiyama and Soda, 2009; Tian et al., 2010). ANCF finite elements can also be used to capture the coupling between the cross section deformation, and the extension and bending of the finite element (Hussein et al., 2007). Nonetheless, the cross section deformation modes depend on the order of interpolation

used. Linear interpolation in the transverse direction allows for a stretch of the cross section, nonetheless, the cross section remains planar and the stretch does not depend on the location of the material points on the cross section. Furthermore, linear interpolation in the transverse direction does not allow for capturing the effect of warping. In order to capture the warping effect and allow for the variation of the stretch at material points on the cross section, higher order interpolation in the transverse direction needs to be used as explained in this thesis.

1.2.2. Review of the Existing Knee Models

From the mathematical point of view, knee models can be divided in to phenomenological and anatomical models. While the fist category describes the response of the knee without considering anatomical parts of the knee joint, the anatomical models describe accurate mechanical properties for each part. Furthermore, from the kinetic point of view anatomical models can be evaluated in static, quasi-static or dynamic conditions. Most of the knee models are static and quasi-static, but in the last decade the number of the dynamic models has also increased (Bertozzi et al., 2008). Most of the dynamic models are focused in studying only some aspects of the knee joint behavior, for this reason more realistic and detailed knee models are necessary to be developed.

The knee joint is one of the largest and most complex joint of the human body. The knee sustains high forces and moments and is situated between the bodyôs two longest lever arms (the femur and the tibia), making it particularly susceptible to injury. The stiffness and stability of the joint are provided by complex interactions between muscles, ligaments, articulating cartilage and menisci. The individual role of each element in overall response of the joint can substantially alter with structural changes in the other components, boundary conditions, flexion angle, load

magnitudes and load combinations. The knee joint must support motion in the frontal plane (abduction and adduction), the sagittal plane (extension and flexion), and the transverse plane (external and internal rotation) allowing the femur and tibia to rotate, twist, and slide relative to one another (Bartel et al., 2006; Silva et al., 2007; Yamaguchi, 2001).

The study of the human body motion as a multibody system (MBS) is a challenging research field that has witnessed significant developments over the last years. In general, most of the investigations focused on the simulation of human tasks based on the assumption that the joints that constrain the relative motion of the system components are ideal or perfect joints (Machado et al., 2010). The motion of the natural knee joint is determined by the geometry of the joint surfaces; constrained by the ligaments, the joint capsule, soft tissues and the active muscle forces acting across the joint (Bartel et al., 2006). In this thesis, the joint capsule, soft tissues, and muscle forces are not taken in consideration.

There are several finite elements models that discuss tibia-femoral contact, but most are limited to simple boundary conditions and are based on quasi-static assumptions (Blankvoort et al., 1996; Bendjaballah et al., 1995; Mclean et al., 2003; Donahue et al., 2002). In a 2004 survey that addressed three-dimensional knee contact models (Bey et al., 2004), it was found that current MBS knee models (Blankvoort et al., 1991; Abdel-Rahmen et al., 1997; Piazza and Delp, 2001; Elias et al., 2004) are either quasi-static with deformable contact or dynamic with rigid contact.

Machado discussed the most relevant contact models used in biomechanics applications: Elastic contact force based on the Hertzian contact theory, Kelvin and Voigt linear model, Hunt and Crossley or Lankarani and Nikravesh contact models which are based on a modified

Hertzian theory are some of the common contact force models used to model contact mechanics of the knee joint (Machado, 2012).

Advanced knee models can be analyzed using either finite element or multi-body algorithms but more recently, studies in biomechanics show the importance of MBS models in combination with finite element methods in the field of biomechanical modeling (Guess et al., 2010; Engel et al., 2011). This combination can provide important information about knee joint mechanics.

1.3. Scope and Organization of the Thesis

This thesis is organized in six chapters including this introductory chapter. In this section, the organization and scope of the thesis as well as a summary of the contents and contributions of its chapters are presented.

In **Chapter 2**, four models are developed to discuss both the ligament dynamics under a prescribed motion and ligament/bone insertion site constraints. Two models allow for the deformation of the ligament cross section at the ligament/bone connection, while the other models do not allow for such modes of cross section deformation. In order to examine ligament/bone connectivity, two large displacement three-dimensional beam and cable finite elements are used to develop two different knee joint models that have different modes of deformation. Both three-dimensional finite elements are based on a nonlinear elasticity theory that accounts for geometric nonlinearities due to large displacements and rotations. The results obtained using the two finite element formulations are compared and the convergence of the models is examined. To illustrate the application of the two finite element formulations, the

study utilizes the methods of constrained dynamics to simulate the motion of a simplified knee model of the lateral and medial collateral ligaments with anatomically correct size and insertion geometry relative to the femur, tibia and fibula. The ligaments structural flexibility is modeled using the large displacement finite element absolute nodal coordinate formulation (ANCF). The ANCF fully parameterized three-dimensional beam element used in Chapter 2 allows for a straight forward implementation of a Neo-Hookean constitutive model that accurately represents the ligament deformations as experienced in knee flexion and rotation. These fully parameterized ANCF elements also capture the cross section deformations, thereby allowing for developing different models for the ligament/bone insertion site constraints.

In the case of conventional structural beam finite elements, a maximum of six boundary conditions can be imposed at a nodal point; with the maximum number defining the conventional clamped end conditions. However, in the case of fully parameterized spatial ANCF finite elements, one can use three translation coordinates and nine position vector gradients at the node. In this case, six boundary conditions on the translations and rotations at a material point do not eliminate the deformation modes at this point. One can then define several types of joints; two of them are investigated in this thesis. The first, called the *partially clamped joint*, while the second, called the *fully clamped joint*. Other partially clamped joints that have a number of constraint equations larger than six and less than the number of constraint equations employed in the fully clamped joint can also be developed in a straight forward manner. A clear definition of which joint is actually used in the dynamic modeling is particularly important in developing accurate FE/MBS models of the knee.

In order to accurately determine the locations of the contact points the use of accurate description of the shapes of the two contact surfaces is necessary. This is accomplished in **Chapter 3** of the thesis using ANCF finite elements. The methods adopted allow for the use of complex geometry for the contact surfaces based on full parameterization. These methods also allow for the use of spline representations to define the contact surface geometry when analytical description cannot be found. In one method, ANCF volume geometry is converted to surface geometry using a parametric relationship that reduces the number of independent coordinate lines. In the second method, ANCF surfaces can be directly used without the need for using the parametric relationship. Both ANCF beam and plate elements can be used to model complex structures by changing the magnitude of the gradient vectors in the reference strain-free configurations. Two formulations; the elastic and constraint, are used in this chapter to predict the contact forces. A set of nonlinear algebraic equations that depend on the surface parameters is developed and used to determine the location of the contact points. In both methods, the assumptions of non-conformal contact are used. In the constraint method, the normal contact forces are obtained as reaction forces using the technique of Lagrange multipliers. In the elastic contact formulation, penetration between the bodies is allowed; this penetration and its derivative enter into the calculation of the contact forces.

Chapter 4 is concerned with the investigation of two models that have two different formulations for the bone/ligament insertion site constraints. It is shown that the formulation of the clamped joint constraints when fully parameterized ANCF finite elements are used is not unique. The partially clamped joint, which allows for the deformation of the cross section at the bone/ligament insertion sites, can be defined using different orthogonal vectors that define

different joint frames. The case of the *partially clamped joint* is discussed in Chapter 4 using two sets of orthogonal vectors that are associated with two different joint frames. The first is called the *tangent frame*, while the second is called the *cross section frame*. The relation between the two frames is shown using the knee joint model developed in Chapter 2. In order to formulate the constraint equations of joints between two bodies modeled using two different formulations, one needs to properly define a set of joint coordinate systems that are used to describe the connectivity conditions. The cross section and tangent frame allow for the deformation of the cross section at the ANCF/rigid body connection. In order to examine this connectivity using *the tangent* and *cross section frame*, one large displacement three-dimensional finite beam elements is used to develop the computer knee joint models.

In **Chapter 5**, a new **t**wo-**d**imensional **b**eam **e**lement with **16**-degree of freedom (TDBE16) is developed and used to study the deformation of the element cross section. The new shear deformable TDBE16 has eight nodal coordinates per node. These nodal coordinates are two position coordinates that define the location of the node in the global coordinate system, four displacement gradient coordinates, and two curvature coordinates. The use of these coordinates allow for increasing the order of interpolation in the transverse direction, thereby capturing the warping effect and allowing for the variation of the stretch along cross section lines. The fundamental differences between the shear representations in Timoshenko beam and TDBE12 (**t**wo-**d**imensional **b**eam **e**lement with **12** nodal coordinates) and TDBE16 models are highlighted. It is shown that the shear angle in Timoshenko beam theory requires the definition of a local frame; while the TDBE12 and TDBE16 shear strain definitions that enter into the formulation of the elastic forces do not require introducing such a local frame. TDBE16 is a fully

parameterized ANCF finite element that leads to a constant mass matrix, allows for the use of general constitutive equations and general continuum mechanic approach in the formulation of the elastic forces, and captures modes that couple the deformation of the cross section, and extension and bending of the beam. The results, obtained using the TDBE16 model, are compared with the results obtained using the TDBE12 model in order to examine the effect of the order of interpolation on the deformation of the cross section.

The thesis ends with **Chapter 6** which gives summary of and conclusions drawn from this investigation.

CHAPTER 2

LIGAMENTS DEFORMATION

The focus of this chapter is to study the mechanics of the knee joint shown in Figure 1 using new ligament/bone insertion site constraint models that require the integration of multibody system and large displacement finite element algorithms. Two different sets of clamped end conditions at the ligament/bone insertion site are examined using nonlinear large displacement *absolute nodal coordinate formulation* (ANCF) finite elements. The first set of end conditions, called the *partially clamped joint*, eliminates only the translations and rotations at a point, allowing for the cross section stretch and shear at the ligament/bone connection. The second joint, called the *fully clamped joint*, eliminates all the translation, rotation and deformation degrees of freedom of the cross section at the ligament/bone insertion site. In the case of the fully clamped joint, the gradient vectors do not change their length and orientation, allowing for the use of the constant strain assumptions. The partially clamped joint, on the other hand, allows for the change in length and relative orientation of the gradient vectors at the bone/ligament insertion site, leading to the cross section deformation induced by knee movements. Nansonôs formula is applied as a measure of the deformation of the cross section in the case of the partially clamped joint. In this study, the major bones in the knee joint consisting of the femur, tibia, fibula are modeled as rigid bodies; while the ligaments structures are modeled using the large displacement ANCF finite elements. Two different ANCF finite element models are developed in this chapter; the first model employs the fully parameterized three-dimensional beam element shown in Figure 2, while the second model employs the three-dimensional cable element shown in Figure 3.

The three-dimensional fully parameterized beam element allows for a straight forward implementation of a Neo-Hookean constitutive model that can be used to accurately predict the large displacement as experienced in knee flexation and rotation. At the ligament bone insertion site, the ANCF fully parameterized beam element is used to define a fully or partially constrained joint; while the ANCF cable element can only be used to define one joint type. The fully and partially clamped joint constraints are satisfied at the position, velocity, and acceleration levels using a dynamic formulation that is based on an optimum sparse matrix structure. The approach described in this investigation can be used to develop more realistic models of the knee and is applicable to future research studies on ligaments, muscles and soft tissues (LMST). In particular, the partially clamped joint representation of the ligament/bone insertion site constraints can be used to develop improved structural mechanics models of the knee.

2.1 Knee Joint

The knee joint is the junction of the femur (thigh bone or upper leg bone) and the tibia (shin bone or larger bone of the lower leg) known as the tibio-femoral joint with a third sesamoid bone called the patella (knee cap) and attached patella tendon. The patella provides protection for the knee and leverage for the quadriceps femoris muscle which cross anterior to the tibio-femoral joint to insert on the tibia. This chapter will consider only the tibio-femoral joint without the contribution of the patella and patella tendon (sometimes referred to as the patello-femoral joint).

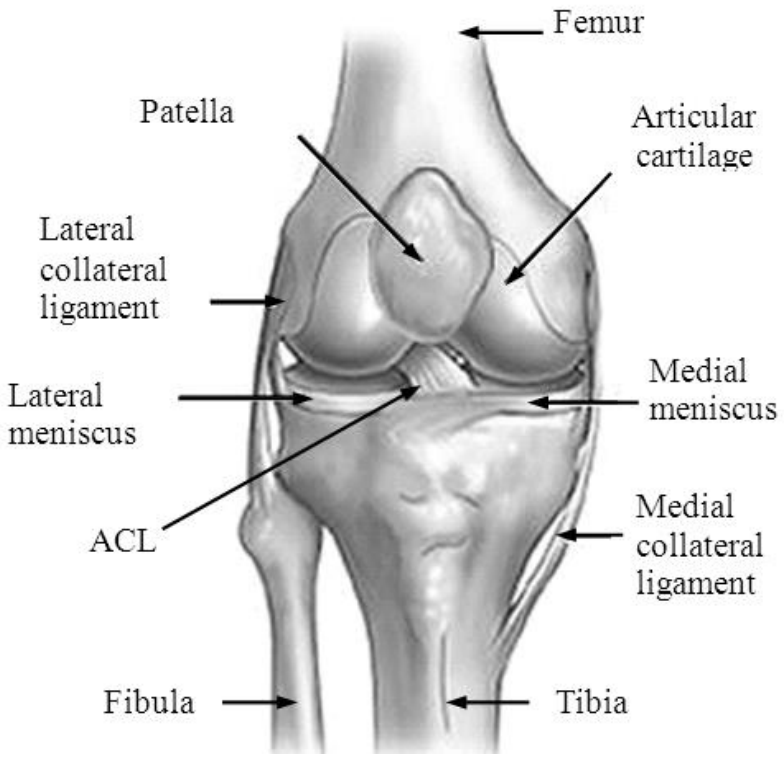

Figure 1 Anatomy of the knee (http://www.aclsolutions.com/anatomy.php)

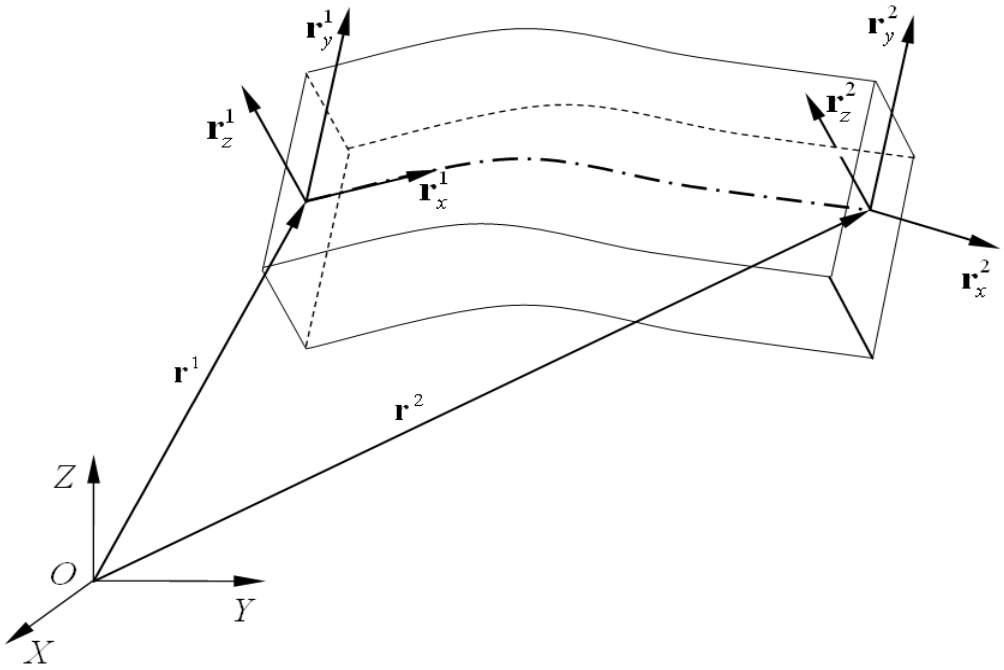

Figure 2 ANCF beam element

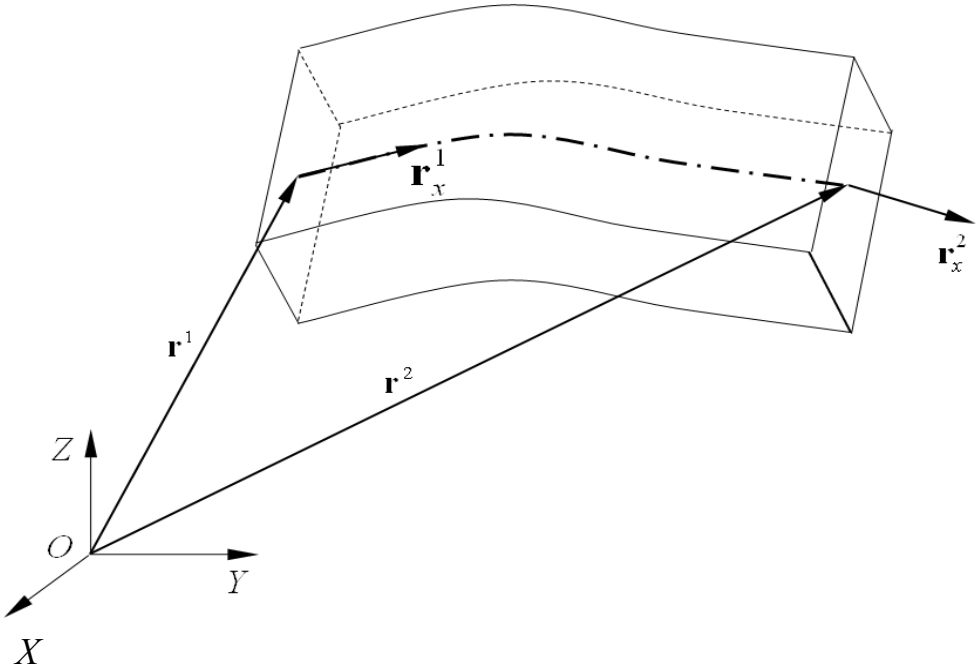

Figure 3 ANCF cable element

The intercondylar regions of the distal end of the femur and the proximal end of the tibia are partially covered with articular cartilage and connected menisci; cartilage is a tough, elastic material that helps absorb shock and assists the knee joint to move smoothly.

The menisci are c-shaped pads of connective tissue that are divided into two crescent-shaped discs positioned between the tibia and femur on the lateral and medial side of each knee. The two menisci in each knee act as shock absorbers, cushioning the lower part of the leg from the weight of the rest of the body, as well as enhancing stability and providing a smooth surface for joint articulation. In addition the knee joint is surrounded by fluid-filled sacs called bursae that serve as gliding surfaces to reduce friction between the bones and tendons (Bartell et al., 2006).

2.1.1. Ligaments and Knee Model

A ligament is composed of tough fibrous material and functions to control excessive motion by limiting joint mobility. The four major stabilizing ligaments of the knee are the medial and lateral collateral ligaments (MCL and LCL, respectively), and the anterior and posterior cruciate ligaments (ACL and PCL, respectively). The superficial fibers of the MCL are anchored superiorly to the medial femoral epicondyle descending anteriorly to attach to the posterior tibia and resist widening of the inside of the joint, or prevent ñopening-upò of the knee.

The posterior fibers of the MCL (deep MCL) attach to the medial meniscus structure; and during knee flexion, these fibers and those attached to the femur twist and help stabilize the medial meniscus. The LCL is attached superiorly to the lateral femoral epicondyle and inferiorly to the lateral surface of the fibular head. The LCL and MCL help stabilize the motion in the sagittal plane such that the LCL is the primary restraint to varus (abduction) rotation and the

superficial portion of the MCL is the primary restraint to valgus (adduction) rotation (Nordin and Frankel, 2001). The two cruciate ligaments (ACL, PCL) are located in the intercondylar region of the knee and interconnect the femur and tibia in a cross linkage arrangement. The ACL helps prevent anterior displacement of the tibia relative to the femur and the PCL resists posterior translation of the tibia relative to the femur (Nordin and Frankel, 2001). The remainder of the applied load not absorbed by the ligaments is absorbed by the remainder of the knee structure.

The knee functions to allow movement of the leg and is critical to normal walking. The knee flexes (bends) normally to a maximum of 135 degrees and extends (straightens) to 0 degrees. The bursae, or fluid-filled sacs, serve as gliding surfaces for the tendons to reduce the force of friction as these tendons move. The knee is a weight-bearing joint such that the menisci serve to evenly load the surface during weight- bearing and also adds in disbursing joint fluid for joint lubrication. There are additional ligaments and tendons as well as a number of bursa and sections of fat pad and dense tissue that are part of the knee capsule, that contribute to knee stability.

2.1.2. Muscles

There are two major groups of muscles at the knee. The quadriceps femoris muscle comprises four muscles on the anterior thigh that work to straighten the leg from a bent position. The hamstring muscle consists of three muscles located in the posterior compartment of the thigh which flex the leg at the knee joint and extend the thigh at the hip joint.

2.1.3. Tendons

Tendons are tough cords of tissue that connect muscle to bone. In the knee, the quadriceps femoris tendon connects the quadriceps muscle to the patella extending to insert on the posterior

tibia providing power to extend the leg. The collective hamstring tendons insert into the lateral surface of the head of the fibula and medially to the tibia (Drake et al., 2005).

This part of the thesis is focused on developing a new non-incremental forward dynamic finite element/multibody system framework for the ligament-to-bone insertion site constraints subjected to cyclic motion. It is not the intent of this chapter investigation to develop a full knee model capturing the mechanics as the femur and tibia rotate, twist, and slide relative to one another; but to demonstrate the fundamental issue related to modeling the ligament-to-bone insertion site. Two joint conditions are developed with constraints that either allow for the cross section deformation at the ligament/bone connections or preclude such deformation. Before discussing the ligament/bone boundary conditions, the finite elements used in the ligament modeling are first presented.

2.2. Ligament Finite Element Models

It is clear from the description of the knee joint presented in the preceding section that the ligament/bone connection is not rigid. While different dynamic models that employ different material properties can be developed for the knee joint, this investigation is only focused on developing new finite element/multibody system models for the ligament/bone insertion site constraints. Some of these models capture the cross section deformation at the insertion site using structural finite elements such as beams. This can be achieved by using the fully parameterized ANCF beam elements that allow for the deformation of the element cross section. The use of such fully parameterized ANCF elements allows developing different joint types including fully and partially clamped joints. On the other hand, the ANCF gradient deficient

cable element, which is simpler, does not allow for the deformation of the cross section, and therefore, it can be used with only one joint type.

2.2.1. Fully Parameterized ANCF Beam Element

Most existing finite element beam formulations assume that the element cross section remains rigid as the beam deforms. Such element formulations, therefore, cannot capture the deformation of the ligament cross section. Furthermore, most of these beam element formulations are based on linear or nonlinear classical beam theory and do not allow for a straight forward implementation of general constitutive equations. To address these modeling deficiencies, fully parameterized ANCF beam elements that capture the cross section deformations and allow for a straight forward implementation of general constitutive equations are used in this chapter to model the ligament mechanics. Using the fully parameterized ANCF beam element shown in Figure 1, the position vector $\mathbf{r}$ of an arbitrary point on element e can be defined in a global coordinate system XYZ as $\mathbf{r} = \mathbf{S}(x, y, z)\mathbf{e}$, where $\mathbf{S}(x, y, z)$ is the element shape function matrix, $\mathbf{e}$ is the vector of nodal coordinates, and x, y and z are the element local coordinates. The vector of element nodal coordinates $\mathbf{e}$ can be defined for the three-dimensional beam element as $\mathbf{e} = \left[\left(\mathbf{e}^1\right)^T \quad \left(\mathbf{e}^2\right)^T \right]^T$, where superscripts 1 and 2 refer, respectively, to the first and second nodes on the element. The nodal coordinates at node k can be written as follows (Shabana, 2008):

$$\mathbf{e}^k = \left[\left(\mathbf{r}^k\right)^T \quad \left(\partial \mathbf{r}^k / \partial x\right)^T \quad \left(\partial \mathbf{r}^k / \partial y\right)^T \quad \left(\partial \mathbf{r}^k / \partial z\right)^T \right]^T \tag{2.1}$$

where $\mathbf{r}^k$ is the global position vector of node *k*, and $\mathbf{r}_x^k = \partial \mathbf{r}^k / \partial x$, $\mathbf{r}_y^k = \partial \mathbf{r}^k / \partial y$ and $\mathbf{r}_z^k = \partial \mathbf{r}^k / \partial z$ define the position vector gradients at the node *k*. This representation ensures inter-element continuity of the global position vector gradients at the nodal points without making any assumptions on the magnitude of the rotation or deformation within the element (Sugiyama et al., 2003). In this thesis a transversely isotropic, hyper-elastic, quasi-incompressible constitutive material model is used for the knee ligaments.

The vector of generalized elastic forces can be obtained as $\mathbf{Q}_k = \left(\partial U / \partial \mathbf{e} \right)^T$, where U is the strain energy function. In the case of ligaments, the expression for the strain energy function can be written as (Peña et al., 2006)

$$U = \int_V \left((1/2D)(\ln J)^2 + C_1 \left(\mathrm{tr}(\bar{\mathbf{C}}) - 3 \right) + F_2 \right) dV \tag{2.2}$$

Where V is the element volume, D is the inverse of the bulk modulus; C_1 is the Neo-Hookean constant; $J = \det(\mathbf{J}) = |\mathbf{J}|$ is the determinant of the matrix of position vector gradients $\mathbf{J}$; $\mathrm{tr}(\bar{\mathbf{C}})$ is the trace of the matrix $\bar{\mathbf{C}} = J^{-2/3}\mathbf{C}$, where $\mathbf{C} = \mathbf{J}^T\mathbf{J}$ is the right Cauchy-Green deformation tensor; and F_2 is a function of the stretch λ that is defined as, $\lambda = \mathbf{a}_0^T \mathbf{C} \mathbf{a}_0$ (Peña et al., 2006) . In this equation, $\mathbf{a}_0$ is a unit vector in the initial direction of the ligament fibers. The strain energy density function that accounts for the collagen fibers F_2 is defined as (Weiss et al., 1996).

$$\left.\begin{array}{ll} \lambda \cdot \partial F_2 / \partial \lambda = 0 & \lambda < 1 \\ \lambda \cdot \partial F_2 / \partial \lambda = C_3 \left(e^{C_4(\lambda - 1)} - 1 \right) & 1 \le \lambda < \lambda^* \\ \lambda \cdot \partial F_2 / \partial \lambda = C_5 \lambda + C_6 & \lambda \ge \lambda^* \end{array}\right\} \tag{2.3}$$

where $C_3, C_4, C_5,$ and C_6 are material constants, and λ^* is the stretch at which collagen fibers start to be straightened (Peña et al., 2006). The vector of generalized elastic forces can then be obtained as

$$\left(\mathbf{Q}_k\right)^T = \int_V \left(\left(\frac{1}{D}\frac{\ln J}{J} - \frac{2C_1}{3} J^{-5/3} \mathrm{tr}\left(\mathbf{C}\right) \right) \frac{\partial J}{\partial \mathbf{e}} + C_1 J^{-2/3} \frac{\partial \left(\mathrm{tr}\left(\mathbf{C}\right)\right)}{\partial \mathbf{e}} + \frac{\partial F_2}{\partial \lambda}\frac{\partial \lambda}{\partial \mathbf{e}} \right) dV \tag{2.4}$$

In order to eliminate all possible degrees of displacement and deformation at a node in the case of a three-dimensional fully parameterized ANCF element, twelve constraint equations must be imposed (three for the translations, three for the rotations, and six for the strain components). Furthermore, since fully parameterized ANCF elements have a complete set of gradient vectors, the Green-Lagrange strain tensor can be defined for the element as $\boldsymbol{\varepsilon} = \left(\mathbf{J}^T\mathbf{J} - \mathbf{I}\right)/2$. For example, the normal strains are $\varepsilon_{11} = \left(\mathbf{r}_x^T\mathbf{r}_x - 1\right)/2$, $\varepsilon_{22} = \left(\mathbf{r}_y^T\mathbf{r}_y - 1\right)/2$ and $\varepsilon_{33} = \left(\mathbf{r}_z^T\mathbf{r}_z - 1\right)/2$. One can show that at $\xi = 0$, $x = 0$ and $\varepsilon_{22} = \left(\mathbf{r}_y^{1^T}\mathbf{r}_y^1 - 1\right)/2$, $\varepsilon_{33} = \left(\mathbf{r}_z^{1^T}\mathbf{r}_z^1 - 1\right)/2$; while at $\xi = 0.5, x = 0.5l$, and the normal strains are $\varepsilon_{22} = \left(0.25\left(\mathbf{r}_y^1 + \mathbf{r}_y^2\right)^T\left(\mathbf{r}_y^1 + \mathbf{r}_y^2\right) - 1\right)/2$, $\varepsilon_{33} = \left(0.25\left(\mathbf{r}_z^1 + \mathbf{r}_z^2\right)^T\left(\mathbf{r}_z^1 + \mathbf{r}_z^2\right) - 1\right)/2$. At $\xi = 1, x = l$, and the normal strains are $\varepsilon_{22} = \left(\mathbf{r}_y^{2^T}\mathbf{r}_y^2 - 1\right)/2$, $\varepsilon_{33} = \left(\mathbf{r}_z^{2^T}\mathbf{r}_z^2 - 1\right)/2$. The axial strain can be calculated in the same manner. These closed form strain expressions which measure the stretch of the element cross section can be used to verify the numerical results of the finite element/multibody system knee joint model obtained in this chapter.

2.2.2. Gradient Deficient ANCF Cable Element

The gradient deficient ANCF cable element, which does not allow for shear deformation, has two nodes Figure 3. Each node has six coordinates; three translational coordinates $\mathbf{r}$ and three gradient coordinates defined by the vector $\mathbf{r}_x$. Therefore, the vector of nodal coordinates has eight elements and is defined as (Gerstmayr and Shabana, 2006)

$$\mathbf{e} = \left[\mathbf{r}^T \left(x = 0 \right) \quad \mathbf{r}_x^T \left(x = 0 \right) \quad \mathbf{r}^T \left(x = l \right) \quad \mathbf{r}_x^T \left(x = l \right) \right]^T \tag{2.5}$$

The global position vector $\mathbf{r}$ of the material point P on the cable element can be defined using the element shape functions and the nodal coordinate vector as $\mathbf{r} = \mathbf{S}(x)\mathbf{e}$ where $\mathbf{S}$ is the element shape function matrix expressed in terms of the element spatial coordinate x. This shape function is defined in Appendix A of the thesis. Since the cable element has one gradient vector only, the general continuum mechanics approach cannot be used to formulate the element elastic forces. The strain energy of the cable element can be written as

$$U = \frac{1}{2}\int_0^l EA\left(\varepsilon_{11}\right)^2 dx_1 + \frac{1}{2}\int_0^l EIk^2 dx_1 \tag{2.6}$$

where E is the modulus of elasticity, A is the element cross section area, I is the second moment of area, and k is the curvature.

2.3. Partially Clamped Joint

In this section, the formulation of the partially clamped joint, also called *rigid* or *bracket joint* is discussed. This joint, which can be used to connect rigid, flexible, and very flexible bodies eliminates six degrees of freedom, and therefore, requires six constraint equations. The degrees

of freedom eliminated are three relative translation coordinates and three relative rotations between two coordinate systems on the two bodies connected by the joint. Therefore, in the case of very flexible bodies modeled using the fully parameterized ANCF finite elements, the partially clamped joint does not eliminate all the degrees of freedom at the joint node, allowing the finite element to deform at this node. Different joint frames can be used to impose the partially and fully clamped joint constraints Figure 4 (Sugiyama et al., 2003; and Hussein et al., 2009). In this chapter, the *cross-section frame* is used.

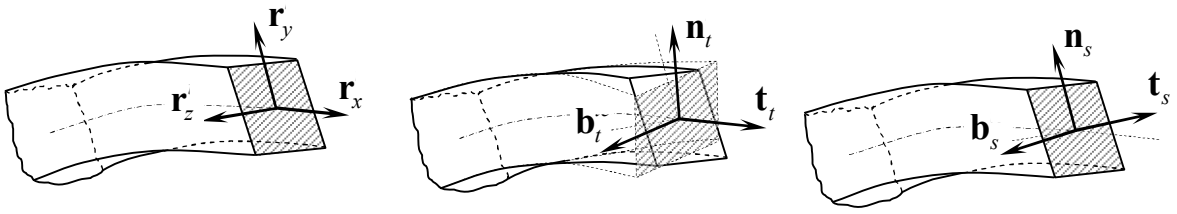

(a) Gradients (b) Tangent frame (c) Cross section frame

Figure 4 ANCF joint coordinate systems

2.3.1. Cross - Section Frame

The cross section frame, used in this thesis, is a coordinate system selected such that two of its axes lie in the plane that defines the beam cross section as shown in Figure 4c. Let $\mathbf{t}_s$, $\mathbf{n}_s$ and $\mathbf{b}_s$ be three orthogonal vectors defined at an arbitrary point on the beam centerline of an element *e*. A vector on the cross section of the beam can be defined as $\mathbf{n}_s = \mathbf{r}_y \big/ \left|\mathbf{r}_y\right|$, where $\mathbf{r}_y = \partial\mathbf{r}/\partial y$ and $\left|\mathbf{r}_y\right|$ is the Euclidian norm of $\mathbf{r}_y$ defined by $\sqrt{\mathbf{r}_y^T\mathbf{r}_y}$. A unit vector $\mathbf{t}_s$ normal to both $\mathbf{n}_s$ and $\partial\mathbf{r}/\partial z$ can be defined as

$$\mathbf{t}_s = \frac{\mathbf{n}_s \times \mathbf{r}_z}{\left| \mathbf{n}_s \times \mathbf{r}_z \right|} \tag{2.7}$$

where $\mathbf{r}_z = \partial \mathbf{r} / \partial z$. A unit vector $\mathbf{b}_s$ can then be defined as $\mathbf{b}_s = \mathbf{t}_s \times \mathbf{n}_s$. One can show that the unit vector $\mathbf{b}_s$ lies in the cross section plane that contains the gradient vectors $\mathbf{r}_y$ and $\mathbf{r}_z$. The orthogonal triad $\mathbf{t}_s$, $\mathbf{n}_s$ and $\mathbf{b}_s$ can be used to define the orthogonal transformation matrix $\mathbf{A}_s$ as $\mathbf{A}_s = \left[\mathbf{t}_s \quad \mathbf{n}_s \quad \mathbf{b}_s \right]$ (Weed et al., 2008).

2.3.2. Constraint Equations

The three nodal translations and the unit vectors that define the orientation of the flexible body frame at the joint definition point can be used in the absolute nodal coordinate formulation to impose six constraint equations for the partially clamped joint. For example, using this approach, a very flexible body modeled using the absolute nodal coordinate formulation can be attached to a rigid body or a flexible body modeled using the *floating frame of reference* (FFR) formulation.

In the knee joint example, the ligaments are very flexible and can be effectively modeled using the absolute nodal coordinate formulation, while the tibia and femur can be modeled as rigid bodies Figure 5 (Weed et al., 2008). The partially clamped joint eliminates all the relative translational and rotational degrees of freedom at the ligament/bone connection. Note that partially clamped joints used to connect finite elements of bodies modeled using the absolute nodal coordinate formulation can be formulated using simple linear connectivity conditions.

However, when two bodies are modeled using two different formulations that employ two different sets of generalized coordinates, the algebraic constraint equations of the partially clamped joint are nonlinear functions of these generalized coordinates. Consider, for example, a

very flexible ANCF body that is connected to a rigid body or to a flexible FFR body using a partially clamped joint; the resulting algebraic constraint equations are highly nonlinear functions of the system coordinates.

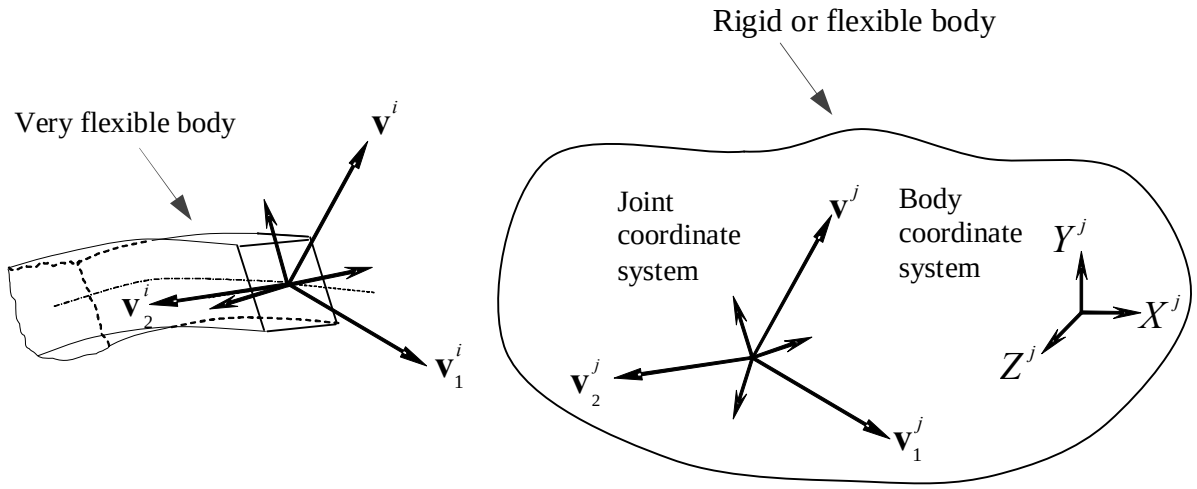

Figure 5 Coordinate systems used in the joint formulation

The six constraint equations of the partially clamped joint can be written as follows (Hussein et al., 2009):

$$\mathbf{C}\left(\mathbf{q}^i, \mathbf{q}^j\right) = \begin{bmatrix} \mathbf{r}_P^i - \mathbf{r}_P^j \\ \mathbf{v}^{i\mathrm{T}} \mathbf{v}_1^j \\ \mathbf{v}^{i\mathrm{T}} \mathbf{v}_2^j \\ \mathbf{v}_2^{i\mathrm{T}} \mathbf{v}_1^j \end{bmatrix} = \mathbf{0} \tag{2.8}$$

where $\mathbf{q}^i$ and $\mathbf{q}^j$ are the position coordinates of the bodies connected by the joint, $\mathbf{r}_P^i$ and $\mathbf{r}_P^j$ are the global position vectors of the joint definition point P on bodies i and j, respectively, $\mathbf{v}^i$

and $\mathbf{v}_1^i$ are two vectors defined on body i; and $\mathbf{v}_1^j$ and $\mathbf{v}_2^j$ are two vectors defined on body j (Hussein et al., 2009). In the case of the FFR formulation, the vector $\mathbf{r}_P^k, k = i, j$, can be written as

$$\mathbf{r}_P^k = \mathbf{R}^k + \mathbf{A}^k \bar{\mathbf{u}}_P^k, \qquad k = i, j \tag{2.9}$$

In this equation, $\mathbf{R}^k$ is the global position vector of the origin of body k coordinate system, $\mathbf{A}^k$ is the transformation matrix that defines the orientation of this coordinate system with respect to the global system, and $\bar{\mathbf{u}}_P^k$ is the local position vector of the joint definition point with respect to body k coordinate system. The first vector equation in Equation 2.8 prevents the relative translations between the two bodies, while the remaining three scalar equations prevent the relative rotations between the two bodies. Equation 2.8 does not impose constraints on the strains in the case of a fully parameterized ANCF finite element, allowing for the deformation of the cross section.

The constraint Jacobian matrix of the partially clamped joint as defined by the Equation 2.8 is

$$\mathbf{C}_{\mathbf{q}} = [\mathbf{C}_{\mathbf{q}^i} \;\; \mathbf{C}_{\mathbf{q}^j}] = \begin{bmatrix} \mathbf{H}_P^i & -\mathbf{H}_P^j \\ \mathbf{v}^{i\mathrm{T}} \mathbf{H}_1^j & \mathbf{v}_1^{j\mathrm{T}} \mathbf{H}^i \\ \mathbf{v}^{i\mathrm{T}} \mathbf{H}_2^j & \mathbf{v}_2^{j\mathrm{T}} \mathbf{H}^i \\ \mathbf{v}_2^{i\mathrm{T}} \mathbf{H}_1^j & \mathbf{v}_1^{j\mathrm{T}} \mathbf{H}_2^i \end{bmatrix} = \mathbf{0} \tag{2.10}$$

where the Jacobian matrices $\mathbf{H}_P^i$, $\mathbf{H}_P^j$, $\mathbf{H}^i$, $\mathbf{H}_2^i$, $\mathbf{H}_1^j$ and $\mathbf{H}_2^j$ are defined as follows:

$$\left.\begin{aligned} \mathbf{H}_P^i &= \frac{\partial \mathbf{r}_p^i}{\partial \mathbf{q}^i}, \quad \mathbf{H}_P^j = \frac{\partial \mathbf{r}_p^j}{\partial \mathbf{q}^j}, \quad \mathbf{H}^i = \frac{\partial \mathbf{v}^i}{\partial \mathbf{q}^i}, \\ \mathbf{H}_2^i &= \frac{\partial \mathbf{v}_2^i}{\partial \mathbf{q}^i}, \quad \mathbf{H}_1^j = \frac{\partial \mathbf{v}_1^j}{\partial \mathbf{q}^j}, \quad \mathbf{H}_2^j = \frac{\partial \mathbf{v}_2^j}{\partial \mathbf{q}^j} \end{aligned}\right\} \tag{2.11}$$

As discussed in previous publications, in order to have simpler formulation for the constraint equations; one can choose, without any loss of generality, the vectors defined on the ANCF body to be $\mathbf{v}^i = \mathbf{n}_s$, $\mathbf{v}_1^i = \mathbf{b}_s$ (Hussein et al., 2009).

2.3.3. Cross Section Deformation

As previously mentioned, the partially clamped joint allows for the deformation of the cross section; while in the case of the fully clamped joint, the gradient vectors are constrained such that the cross section remains the same at the joint definition point as the ligament deforms. In this chapter, the deformation of the ligament cross section is measured using *Nanson's formula* which defines the ratio of the area in the deformed (current) configuration to the area in the undeformed (reference) configuration (Ogden, 1984; Shabana, 2008). This formula is given by

$$\frac{ds}{dS} = \frac{J}{\left(\mathbf{n}^T \mathbf{J}\mathbf{J}^T \mathbf{n}\right)^{1/2}} \tag{2.12}$$

In this equation, dS and ds are the areas of an infinitesimal surface in the reference and current configurations, respectively; $\mathbf{n}$ is a unit vector normal to the area in the current configuration; and $J = |\mathbf{J}|$ is the determinant of the matrix of position vector gradients. In the case of the fully parameterized ANCF beam element considered in this chapter, one can show that the preceding equation reduces to the simple form $(ds/dS) = |\mathbf{r}_y \times \mathbf{r}_z|$ (Hussein et al., 2009).

2.4. Fully Clamped Joint

The fully clamped joint formulation eliminates all the translation, rotation, and deformation degrees of freedom at the joint node. Therefore, the cross section of the finite element at the joint node does not deform. Let $\mathbf{r}_x^i, \mathbf{r}_y^i$, and $\mathbf{r}_z^i$ be the gradient vectors at an arbitrary node on the ANCF body i. One can always define three orthogonal unit vectors $\mathbf{v}_1^j$, $\mathbf{v}_2^j$, and $\mathbf{v}_3^j$ at the joint node on the FFR body j. The twelve constraint equations of the fully clamped joint can then be written as follows:

$$\mathbf{C}(\mathbf{q}^i, \mathbf{q}^j) = \begin{bmatrix} \mathbf{r}_P^i - \mathbf{r}_P^j \\ \mathbf{r}_x^i - \mathbf{v}_1^j \\ \mathbf{r}_y^i - \mathbf{v}_2^j \\ \mathbf{r}_z^i - \mathbf{v}_3^j \end{bmatrix} = \mathbf{0} \tag{2.13}$$

In this equation, $\mathbf{r}_P^i$ and $\mathbf{r}_P^j$ are the same as defined in the preceding section. One may choose not to constrain all the strains by eliminating some constraint equations in Equation 2.13. Other possibilities of constraints at clamped joints when ANCF finite elements are used to model one of the bodies of the joint were proposed in the literature (Garcia-Vallejo et al., 2007; Garcia-Vallejo et al., 2008). Furthermore, Equation 2.13 can be slightly modified to account for the effect of initial stretch of the ligaments. This can be accomplished by relaxing some of the conditions of the orthonormality of the vectors $\mathbf{v}_1^j$, $\mathbf{v}_2^j$, and $\mathbf{v}_3^j$.

The constraint Jacobian matrix of the fully clamped joint is defined as

$$\mathbf{C}_{\mathbf{q}} = [\mathbf{C}_{\mathbf{q}^i} \;\; \mathbf{C}_{\mathbf{q}^j}] = \begin{bmatrix} \mathbf{H}^{\,i}_{P} & -\mathbf{H}^{\,j}_{P} \\ \mathbf{H}^{\,i}_{x} & -\mathbf{H}^{\,j}_{1} \\ \mathbf{H}^{\,i}_{y} & -\mathbf{H}^{\,j}_{2} \\ \mathbf{H}^{\,i}_{z} & -\mathbf{H}^{\,j}_{3} \end{bmatrix} = \mathbf{0} \tag{2.14}$$

The matrices that appear in this equation are defined as

$$\left.\begin{aligned} \mathbf{H}^{\,i}_{P} &= \frac{\partial \mathbf{r}^{\,i}_{P}}{\partial \mathbf{q}^{\,i}}, \quad \mathbf{H}^{\,i}_{x} = \frac{\partial \mathbf{r}^{\,i}_{x}}{\partial \mathbf{q}^{\,i}}, \quad \mathbf{H}^{\,i}_{y} = \frac{\partial \mathbf{r}^{\,i}_{y}}{\partial \mathbf{q}^{\,i}}, \quad \mathbf{H}^{\,i}_{z} = \frac{\partial \mathbf{r}^{\,i}_{z}}{\partial \mathbf{q}^{\,i}}, \\ \mathbf{H}^{\,j}_{P} &= \frac{\partial \mathbf{r}^{\,j}_{P}}{\partial \mathbf{q}^{\,j}}, \quad \mathbf{H}^{\,j}_{1} = \frac{\partial \mathbf{v}^{\,j}_{1}}{\partial \mathbf{q}^{\,j}}, \quad \mathbf{H}^{\,j}_{2} = \frac{\partial \mathbf{v}^{\,j}_{2}}{\partial \mathbf{q}^{\,j}}, \quad \mathbf{H}^{\,j}_{3} = \frac{\partial \mathbf{v}^{\,j}_{3}}{\partial \mathbf{q}^{\,j}} \end{aligned}\right\} \tag{2.15}$$

The dimensions of the matrices in this equation, as in the case of the partially clamped joint, depend on the formulation used in the dynamic modeling of the bodies connected by the joint.

Of particular importance in the study of knee mechanics is how the application of the two different joint definitions (the partially and fully clamped joints) affect the stress concentrations and deformation at the ligament/bone insertions sites. These insertion sites are noted as direct and indirect. The direct insertion site is a well-defined transition from the ligament fibrils to zones of fibrocartilage and calcified fibrocartilage, terminating at approximately right angles in the bone outer structure. An example of a direct insertion site is the femoral attachment of the MCL (Benjamin et al., 2006, Weiss et al., 2001). Finite element analysis predicts that the ligament deformation at the insertion site can vary significantly which can be captured with the partially clamped joint (Moffat et al., 2008).

The indirect insertion has a more gradual transition with the fibers attaching to the bone obliquely without the fibrocartilage zones as seen in the direct insertion site. An example of an indirect insertion site is the tibia attachment of the MCL (Weiss et al., 2001). It is reported in the

literature that the largest stress concentration can occur at the distal end of the MCL (the tibia attachment) which also can be modeled with the partially clamped joint (Moffat et al., 2008).

2.5. Numerical Results

In the numerical study presented in this section, the use of the ANCF beam and cable elements in the nonlinear dynamic analysis of the knee joint model is investigated. Numerical results using the Neo-Hookean material model are obtained for the partially and fully clamped joint models based on the fully parameterized ANCF finite elements. A method based on the integration of multibody system and large deformation finite element algorithms is introduced for modeling the dynamics of the knee joint model shown in Figure 1 (Weed et al., 2008). In this model the tibia, femur and fibula are modeled as rigid bodies; while the two ligaments are modeled using the three-dimensional ANCF beam and cable elements. The goal of this chapter is to develop a new computational framework for the computer aided analysis of a non-incremental forward dynamic knee model integrating multibody system and large displacement finite element algorithms. In order to maintain the focus on the development of the complex computational algorithms demonstrated in this thesis, the approach applies the newly developed framework to a simplified knee model such that the femur and tibia are modeled using a revolute joint which eliminates the translations and rotation in the frontal and transverse planes allowing only rotation of the femur relative to the tibia in the sagittal plane. The prescribed displacement is simulated in the analysis by properly selecting the revolute joint axis of rotation of the femur with respect to the tibia. In this thesis the fibula is connected to the tibia using rigid joint, constraining all the translations

and rotations of the fibula with respect to the tibia, which is assumed to be rigidly attached to the ground.

The LCL is assumed clamped to the fibula and femur. This ligament is positioned vertically lengthwise and rotated 19 degrees from the vertical of the femur. It has a length of 66.6 mm and elliptical cross-section radii of 3.4 mm and 2.3 mm. The LCL femoral insertion site is 19.5 mm above the inferior tip of the femur with the fibular insertion site located 43.5 mm below the tibial plateau (LaPrade et al., 2007). The anterior fibers of the MCL are clamped to the femur and tibia. The ligament has a length of 94.8 mm with cross-section radii of 7 mm and 2.3 mm; and it is attached vertically and lengthwise to the femur 32.8 mm above the inferior tip of the femur. Its tibial attachment is 62 mm below the tibial plateau (Meister et al., 2000). Table I shows other dimensions and inertia properties of the model; while Table II shows the values of the ligament material coefficients used in this thesis. The MCL and LCL are exposed to residual stresses as all biological soft tissues. The residual longitudinal strain in the MCL and LCL is assumed to be 0.04 (Weed et al., 2008). The knee joint model used in this thesis is shown in Figure 6. A preliminary model of the knee joint showed the two ligaments (LCL, MCL) contained a high oscillation to in-plane and out-plane bending that is not present in normal physiological motion. These oscillations may be a result of the selection of a constitutive model that does not account for ligament viscoelasticity as observed in cyclic motion, does not account for the ligament compression due to the surrounding knee capsule, and does not take into account the additional restraint of the deep MCL fibers connected to the medial meniscus. To correct this situation the two-ligament model was modified by adding internal damping to absorb the

oscillations. This damping simulates the knee capsule consisting of various soft tissues, muscles and fat composites that surround and contain the two exterior ligaments.

Therefore, in the current model damper elements are added to damp out the high frequencies in the LCL and MCL. The mid-point of the MCL is connected to the tibia by a linear damping element with a damping coefficient 5 N.s/m and along its length by a series of four damping elements with an assumed damping coefficient of 1 N.s/m each along the length of the ligament. These elements represent the surrounding tissue encompassing the knee capsule as well as the MCL deep fiber connection to the medial meniscus structure. The knee model used is solved by giving the femur a prescribed flexation. The angle of flexation is governed by the following equation:

$$\theta = \frac{1}{2}\theta_{\max}\left(1-\cos\left(2\pi t/\tau\right)\right) \tag{2.16}$$

where t is the simulation time, $\theta_{\max} = 45^{o}$ and $\tau = 0.2$ s. From the previous equation, the angle of flexation θ oscillates between zero and $\theta_{\max}$. The angle θ reaches $\theta_{\max}$ when $t = \tau/2$, and it becomes zero again when the first cycle is completed at $t = \tau$. The results obtained show convergence can be achieved by using 8 finite elements along the MCL and LCL structures (Hussein et al., 2009). The loading scenario considered is a combined compression load of 1150 N with a valgus torque of 10 Nm applied to the femur.

The change in the length of the MCL and LCL for the case of the fully clamped joint during the flexion- extension is shown in Figure 7, and for the partially clamped joint case in Figure 8. The axial strains of the midpoint in both cases of fully and partially clamped joint are presented in Figures 9 and 10. The results of the ligament length and axial strains presented in

Figures 7-10 show a good agreement between the cable and beam element models. While the results of the cable element model are shown in all these figures, it is important to remember that the cable element model allows only for the use of one joint type that does not permit for the cross section deformation. Figures 11 - 14 show the normal strain for the MCL and LCL for the partially and fully clamped joint. In the case of the fully clamped joint the normal strain is constant because of the ligaments pretension (The pretension was assumed to be homogenous in the entire beam). Figure 15 shows the change in the cross sections at the midpoints of the MCL and LCL using Nansonôs formula. This change in the cross section dimension can be effectively captured using the fully parameterized ANCF beam element employed in this chapter. The results presented in Figure 15 for the fully clamped joint case show that the area in any current configuration is reduced. It is important to note that the insertion site mechanics must allow stress concentrations in the ligament which can only be captured using the partially clamped joint.

Table I DIMENSIONS AND INERTIA OF THE FEMUR AND TIBIA (ISCAN, 2005)

Body Name	Length (cm)	m(kg)	I_{xx}(kg m^2)	I_{yy}(kg m^2)	I_{zz} (kg m^2)
Femur	40	7.516	0.354614	0.354614	0.004604
Tibia	40	3.537	0.166880	0.166880	0.002166

Table II LIGAMENT MATERIAL COEFFICIENTS (MPA) (WEED ET AL, 2008)

Ligament	C_1	C_2	C_3	C_4	C_5	λ^*	D
MCL	1.44	0.0	0.57	48.0	467.1	1.063	0.00126
LCL	1.44	0.0	0.57	48.0	467.1	1.063	0.00126

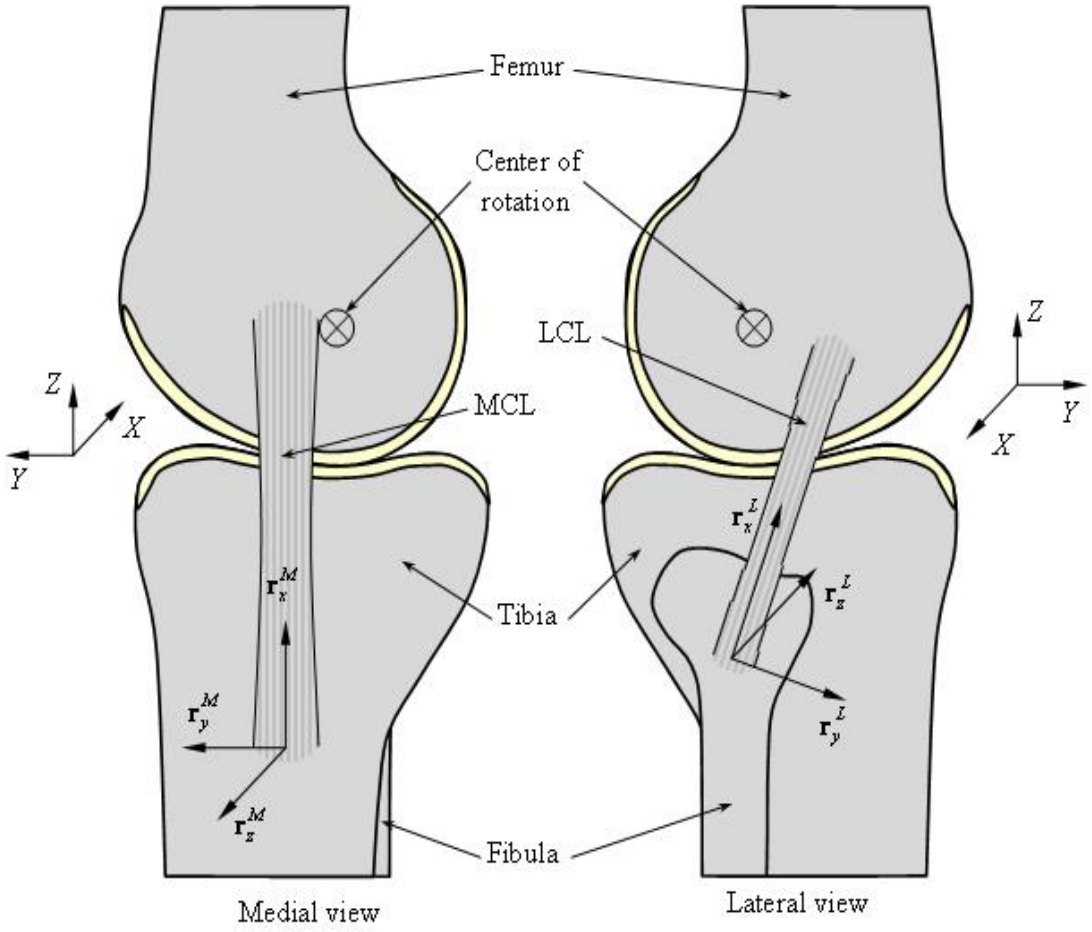

Figure 6 Knee joint model

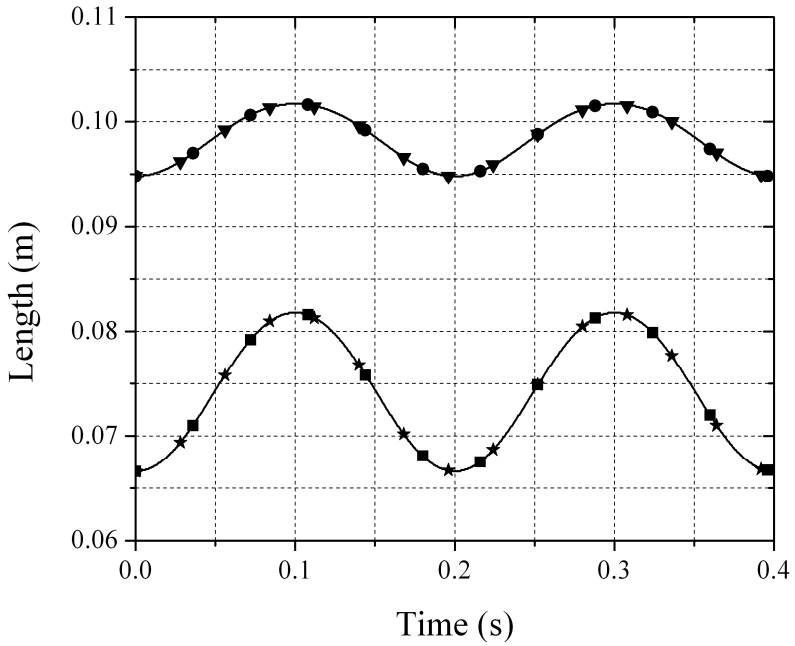

Figure 7 Length in the case of the fully clamped joint
(—■— LCL beam elements, —●— MCL beam elements,
—★— LCL cable elements, —▼— MCL cable elements)

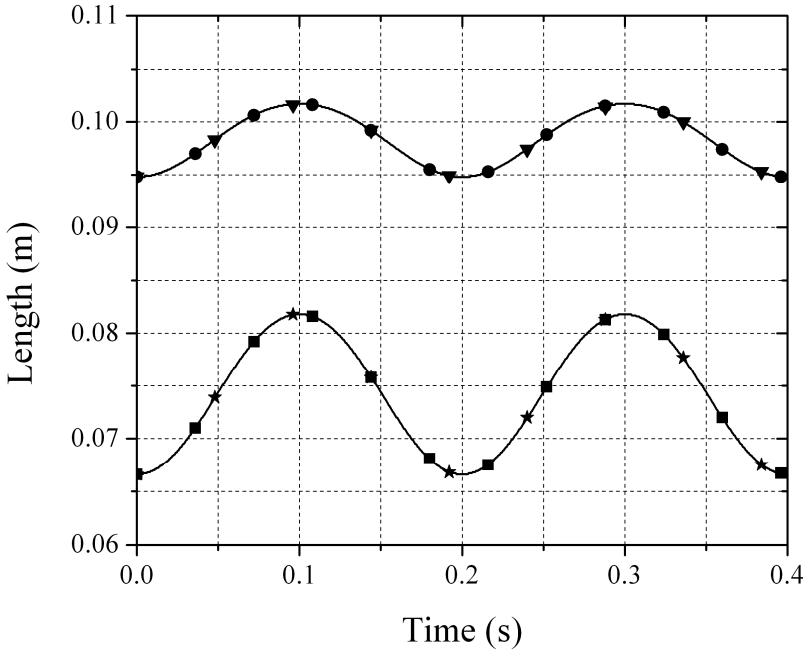

Figure 8 Length in the case of the partially clamped joint
(—■— LCL beam elements, —●— MCL beam elements,
—★— LCL cable elements, —▼— MCL cable elements)

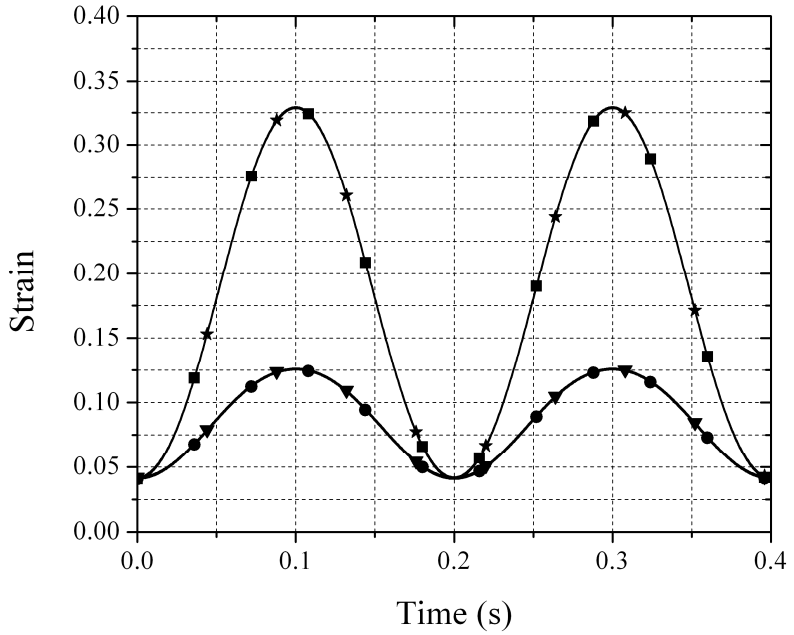

Figure 9 Axial strain of the midpoint in the case of the fully clamped joint
(—■— LCL beam elements, —●— MCL beam elements,
—★— LCL cable elements, —▼— MCL cable elements)

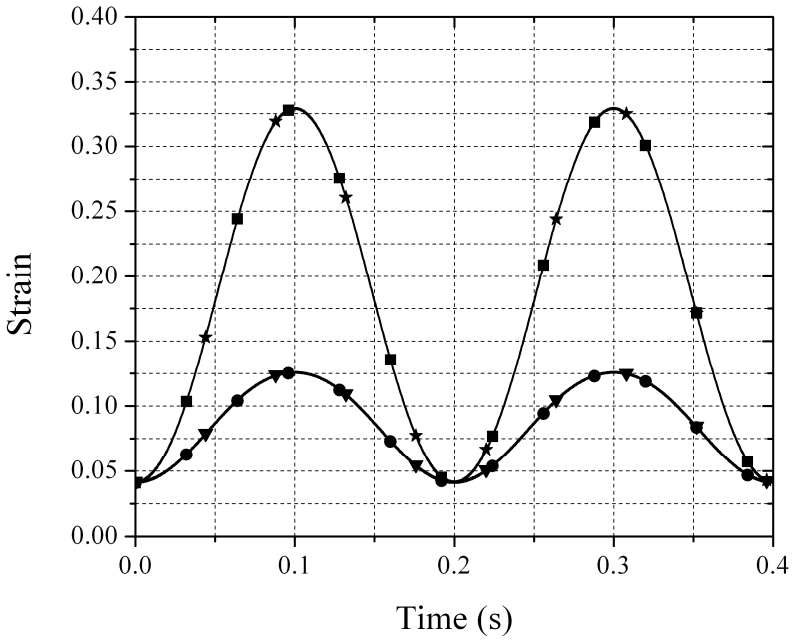

Figure 10 Axial strain of the midpoint in the case of the partially clamped joint
(—■— LCL beam elements, —●— MCL beam elements,
—★— LCL cable elements, —▼— MCL cable elements)

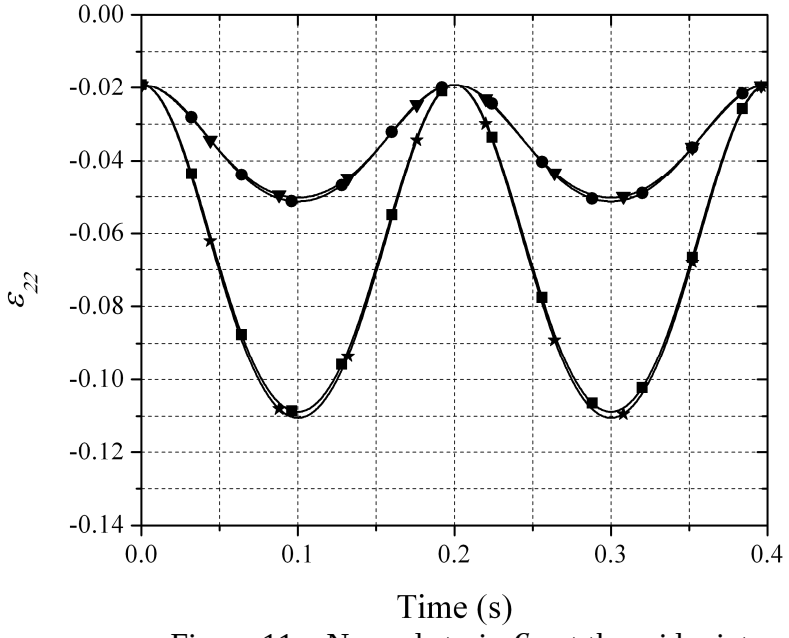

Figure 11 Normal strain $\mathcal{E}_{22}$ at the midpoint
(—■—LCL partially clamped, —●— MCL partially clamped,
—★—LCL fully clamped, —▼— MCL fully clamped)

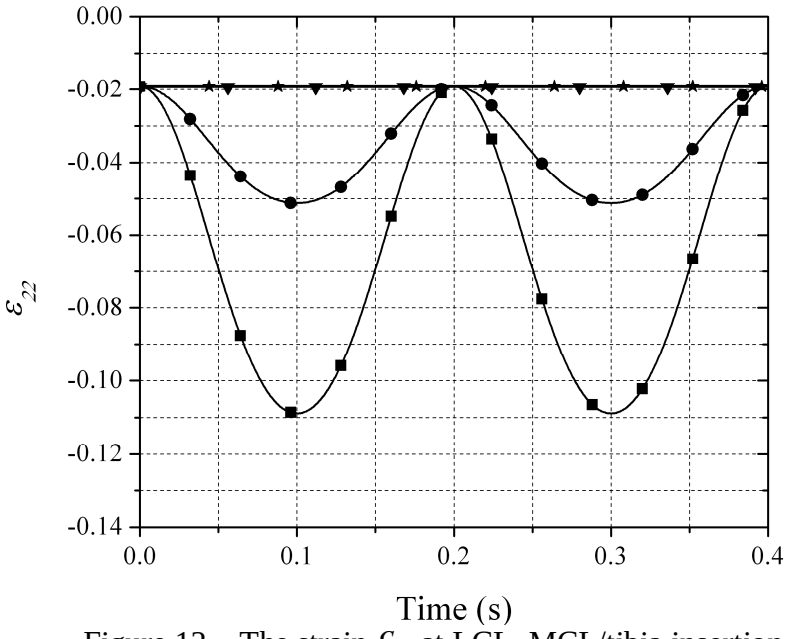

Figure 12 The strain $\mathcal{E}_{22}$ at LCL, MCL/tibia insertion site
(—■—LCL partially clamped, —●— MCL partially clamped,
—★—LCL fully clamped, —▼— MCL fully clamped)

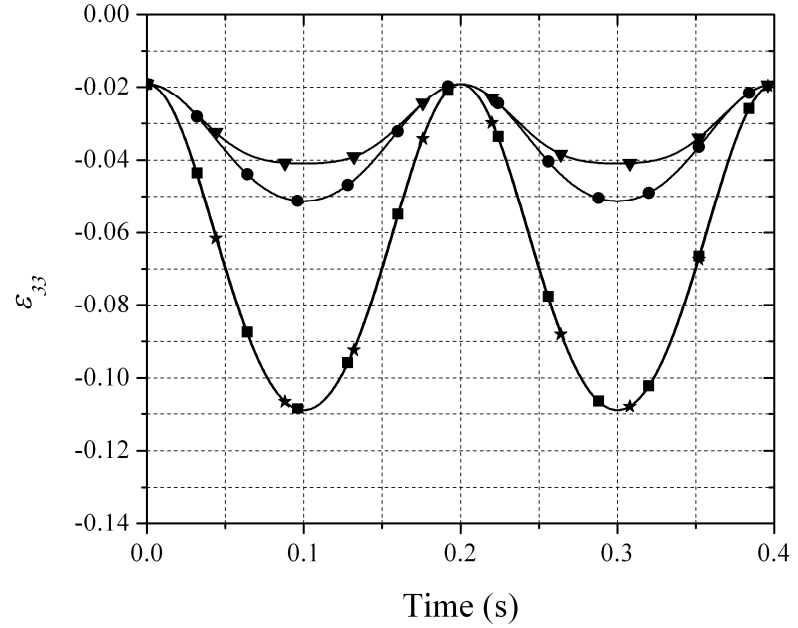

Figure 13 Normal strain $\mathcal{E}_{33}$ at the midpoint
(LCL partially clamped, MCL partially clamped,
LCL fully clamped, MCL fully clamped)

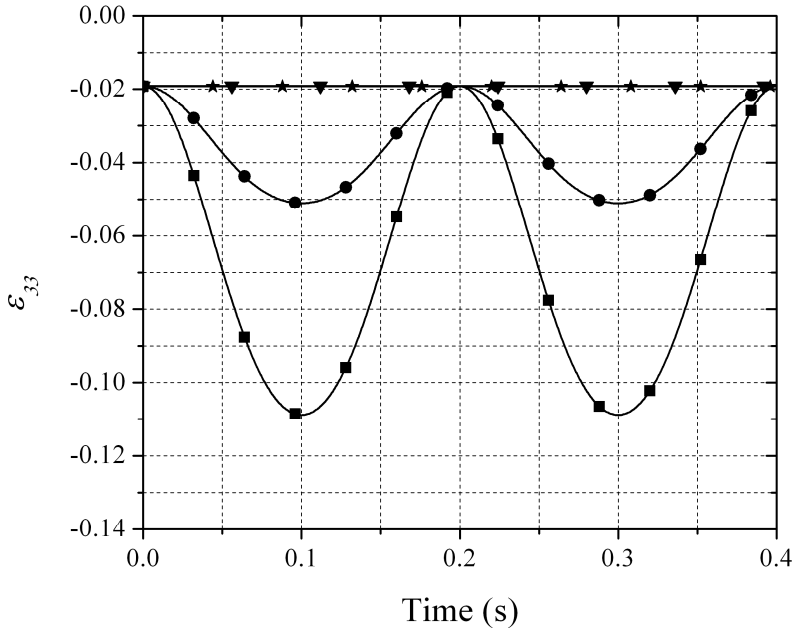

Figure 14 The strain $\mathcal{E}_{33}$ at LCL, MCL/tibia insertion site
(LCL partially clamped, MCL partially clamped,
LCL fully clamped, MCL fully clamped)

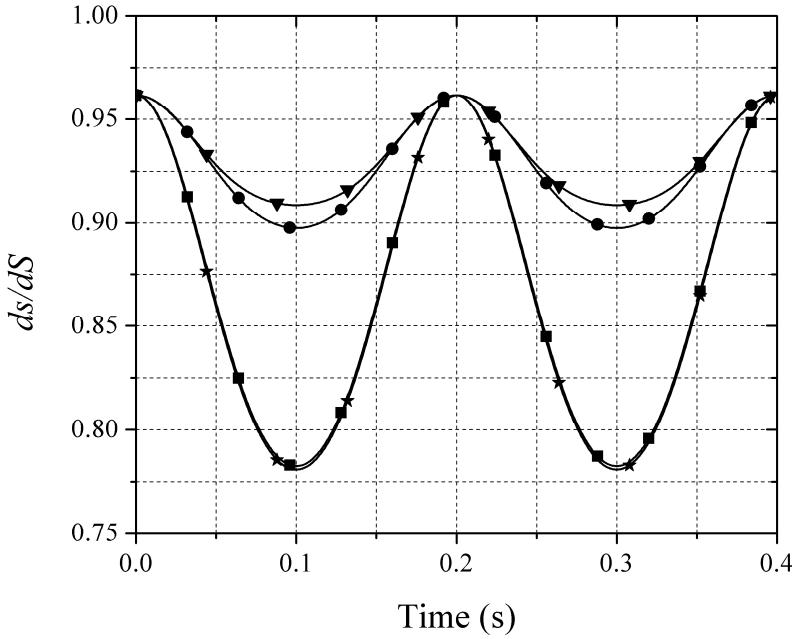

Figure 15 Deformation of the cross section area at the midpoint (—■—LCL partially clamped, —●— MCL partially clamped, —★—LCL fully clamped, —▼— MCL fully clamped)

2.6. Concluding Remarks

In this chapter, new finite element/multibody system models are developed for the ligament/bone insertion site constraints. Two ANCF finite elements are employed in this chapter; the first is the fully parameterized beam element, while the second is the gradient deficient cable element. The fully parameterized ANCF beam element allows for using different ligament/bone insertion site constraint models. The partially and fully clamped ligament/bone joints are considered. The partially clamped joint allows for the cross section deformation at the ligament/bone insertion site. This cross section deformation can be measured using Nansonôs formula.

The analysis reported in this chapter has shown that the fully parameterized ANCF beam element allows for more modes of deformation at the knee ligament/bone insertion site as compared to the gradient deficient cable element which cannot capture the expected change in the ligament cross section. The numerical results demonstrate that the new computational finite element/multibody framework using the simplified two ligament model with either the beam or cable element can yield useful data in regard to the change in length and strains of either the LCL or MCL regardless of the insertion site constraints (fully clamped or partially clamped). In addition, the analysis demonstrates that the ligament-to-bone direct connection which is a progression of elastic type fibrocartilage, collagen and bone that can deform (as a result of stress concentrations) under a prescribed cyclic motion precludes the application of the fully clamped beam which does not allow such deformation (Benjamin M, et al. 2006).

The data shows higher strains for both ligaments than the quasi-static finite element models reported in the literature (Weiss et al., 2001; Peña et al., 2006). The higher strains are the result of the integration of the fully parameterized ANCF beam finite element model into a

dynamic multibody computational framework that captures the large displacement and change in the ligament cross section resulting from the prescribed cyclic motion. High strains are also justified in the simple model considered in this chapter, because two ligaments only were considered and the femur is subjected to a relatively high speed of rotation. The two ligaments considered carry the entire load which in reality is shared by other ligaments and tissues of the knee joint.

CHAPTER 3

CONTACT GEOMETRY

In previous chapter, the sliding between the femur and tibia was modeled by using a kinematic revolute joint placed at a specific location in the model with only the two outside ligaments (MCL, LCL) providing stability. This joint allows only rotation of the femur relative to the tibia in the sagittal plane. One goal of the current chapter is to improve the kinematic and force knee joint model by allowing more degrees of freedom of the femur with respect to the tibia and include the two interior cruciate ligaments (ACL and PCL). Having additional degrees of freedom requires the use of a femur/tibia contact force model that was not required when the kinematic revolute joint was used by the authors in previous chapter.

Two ANCF approaches can be used to model the rigid contact surface geometry. In the first approach, fully parameterized ANCF volume elements are converted to surface geometry using parametric relationship that reduces the number of independent coordinate lines. This parametric relationship can be defined analytically or using a spline function representation. In the second approach, an ANCF surface that defines a gradient deficient thin plate element is used. This second approach does not require the use of parametric relations or spline function representations. These two geometric approaches shed light on the generality of and the flexibility offered by the ANCF geometry as compared to computational geometry (CG) methods such as B-splines and NURBS (**N**on-**U**niform **R**ational **B**-**S**plines). Furthermore, because B-spline and NURBS representations employ a rigid recurrence structure, they are not suited as general analysis tools that capture different types of joint discontinuities. ANCF finite elements,

on the other hand, lend themselves easily to geometric description and can additionally be used effectively in the analysis of ligaments, muscles, and soft tissues (LMST), as demonstrated in this thesis using the knee joint as an example. In this chapter, ANCF finite elements are used to define the femur/tibia rigid body contact surface geometry. The same ANCF finite elements are also used to model the MCL and LCL ligament deformations as shown in the previous chapter. Two different contact formulations are used in this thesis to predict the femur/tibia contact forces; the *elastic contact formulation* where penetrations and separations at the contact points are allowed, and the *constraint contact formulation* where the non-conformal contact conditions are imposed as constraint equations, and as a consequence, no separations or penetrations at the contact points are allowed. For both formulations, the contact surfaces are described in a parametric form using surface parameters that enter into the ANCF finite element geometric description. A set of nonlinear algebraic equations that depend on the surface parameters is developed and used to determine the location of the contact points. These two contact formulations are implemented in a general MBS algorithm that allows for modeling rigid and flexible body dynamics.

3.1. ANCF Geometry and Kinematics

The geometry of the knee joint models reported in the literature varies (Guess et al., 2010, Ashraf et al., 2003); some models have symmetric femoral and tibial components while others are unsymmetrical. While the general geometry description used in this thesis allows for modeling arbitrary shapes, symmetric surfaces are used in the knee joint model considered in this thesis. Two steps are employed in the computational algorithm used to obtain the numerical

solution of the femur/tibia contact problem. In the first step, the locations of the points of contact between the femur and tibia are determined. This first step is purely geometric and requires the use of accurate description of the shapes of the femur and tibia surfaces. This is accomplished in this investigation using ANCF finite elements. In the second step, the geometry results are used to determine the femur/tibia contact forces. To this end, two different contact formulations, the elastic and constraint contact formulations, are used. The results obtained using these two different contact formulations that lead to models with different number of degrees of freedom will be compared. The accuracy of the forces predicted using these two different formulations depends strongly on the accuracy of the geometry results obtained in the first step. The methods adopted in this thesis allow for the use of complex geometry for the contact surfaces based on full parameterization. Figure 16 shows the profiles used in this chapter for tibia surface and for the lateral and medial condyle of the femur. These methods also allow for the use of spline representations to define the contact surface geometry when analytical description cannot be found.

3.2. ANCF Beam Element

As previously mentioned, ANCF finite elements can be used in the geometry description as well as in the dynamic force analysis. All B-spline and NURBS representations can be converted without geometry distortion to ANCF/FE meshes using a linear transformation. The converse, however, is not true, that is, not all ANCF representations can be converted to B-spline or NURBS representation (Shabana, 2012). Because ANCF finite elements can accurately describe the geometry of the femur and tibia rigid surfaces, different geometry models that employ

different ANCF finite elements can be used. In this chapter, we consider two ANCF elements as examples; these elements are the fully parameterized ANCF three-dimensional beam element shown in Figure 17, and the gradient deficient ANCF thin plate element shown in Figure 18. Other ANCF elements such as the fully parameterized plate element can also be used. The numerical results, however, will be obtained using the fully parameterized three-dimensional beam element that requires the use of the spline function representation to define a surface. This element is chosen because it can also be used to model the ligament mechanics.A surface can be described in terms of two parameters (coordinate lines). When ANCF beam elements are used, the global position vector $\mathbf{r}^{ij}$ of an arbitrary point on the fully parameterized beam element j of body i can be defined using the element shape function matrix $\mathbf{S}^{ij}$ and the vector of nodal coordinates $\mathbf{e}^{ij}$ as $\mathbf{r}^{ij} = \mathbf{S}^{ij}(x, y, z)\mathbf{e}^{ij}(t)$, where t is time, and x, y, and z are the local element coordinates. The vector of nodal coordinates $\mathbf{e}^{ij}$ consists of absolute position and gradient coordinates. The element has two nodes, and each node has twelve coordinates that define the global position vector of the node and the three gradient vectors $\mathbf{r}_x^{ij} = \partial \mathbf{r}^{ij} / \partial x, \mathbf{r}_y^{ij} = \partial \mathbf{r}^{ij} / \partial y$, and $\mathbf{r}_z^{ij} = \partial \mathbf{r}^{ij} / \partial z$ (Shabana, 2012). The representation $\mathbf{r}^{ij} = \mathbf{S}^{ij}(x, y, z)\mathbf{e}^{ij}(t)$ describes a volume since three parameters (coordinate lines) x, y, and z are used for this fully parameterized element. The ANCF representation allows for systematically converting this volume geometry to surface geometry. This can be accomplished by eliminating one of the independent parameters by expressing this parameter in terms of the other two. For example, the use of the functional relationship $z = f(y)$ converts the ANCF volume geometry to surface geometry in the case of the beam element. In this case, the ANCF representation can be written as

$\mathbf{r}^{ij} = \mathbf{S}^{ij}\left(x, y, f\left(y\right)\right)\mathbf{e}^{ij}\left(t\right)$, where $f\left(y\right)$ is a known a function that can be used to define the surface shape. A more general function relationship such as $z = f\left(x, y\right)$ can also be used.

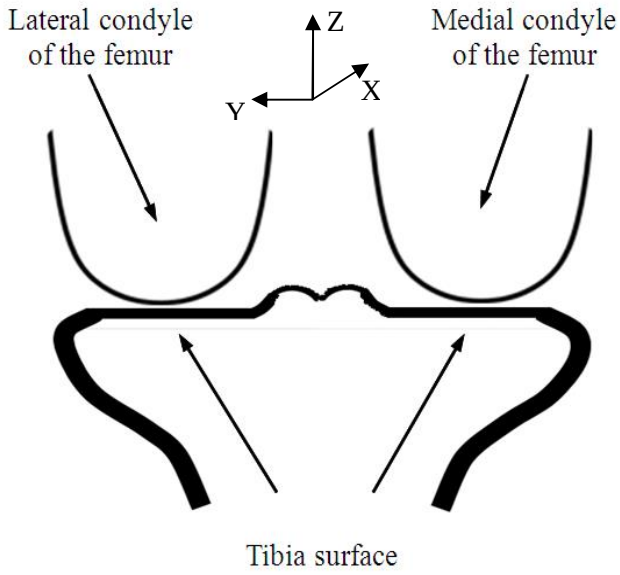

Figure 16 Femur and tibia profile

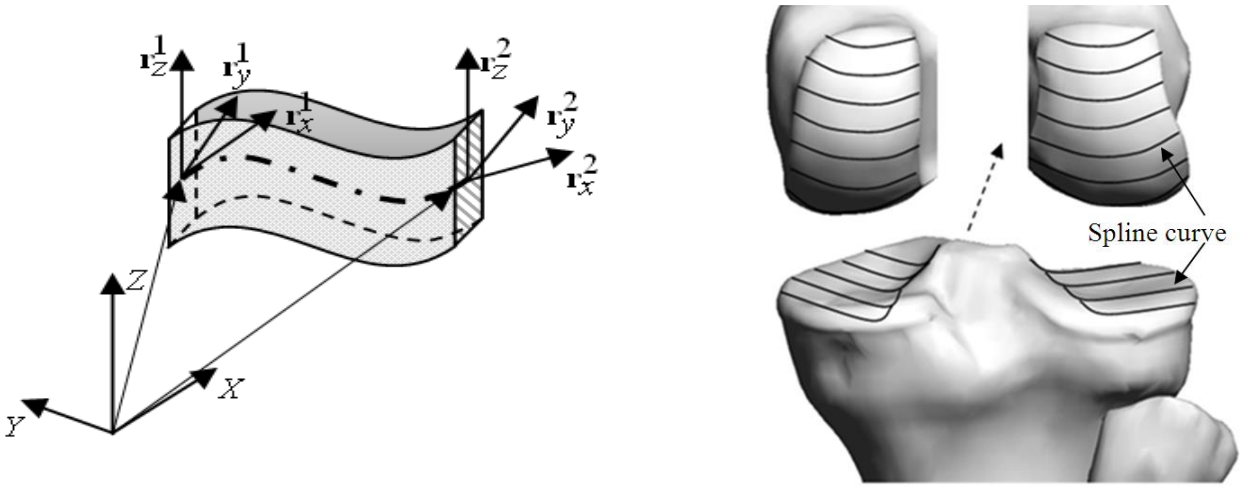

Figure 17 ANCF 3D beam element

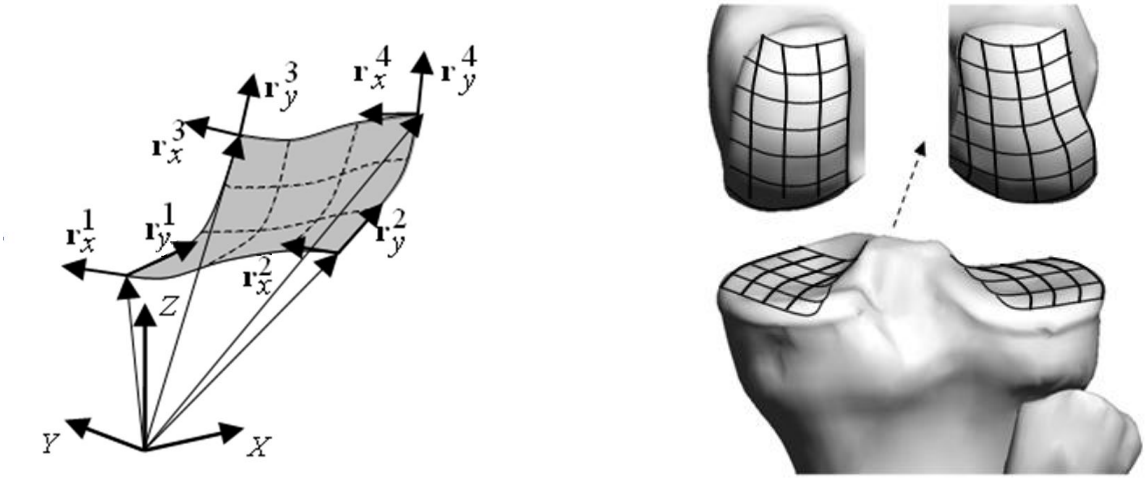

Figure 18 ANCF thin plate element

3.2.1. ANCF Thin Plate Element

Another ANCF finite element that can be used to describe the surface geometry is the gradient deficient thin plate element shown in Figure 18. This element has four nodes, each of which has nine nodal coordinates. Only the two parameters x and y are used to define the thin plate element geometry. In this case, one can write the global position vector on the element mid-surface as $\mathbf{r}^{ij} = \mathbf{S}^{ij}\left(x, y\right)\mathbf{e}^{ij}\left(t\right)$. The vector of element nodal coordinates in this case consists of the node position vector and the two gradient vectors $\mathbf{r}_x^{ij} = \partial \mathbf{r}^{ij} / \partial x$ and $\mathbf{r}_y^{ij} = \partial \mathbf{r}^{ij} / \partial y$. This leads to an element with thirty six degrees of freedom. Both ANCF beam and plate elements can be used to model tapered structures by changing the magnitude of the gradient vectors in the reference strain-free configurations. Using the gradient vectors, ANCF tapered elements can be easily obtained.

3.2.2. Computational Geometry Methods

It is shown in the literature that all Bezier and B-spline curve representations used in CAD systems can be converted to ANCF finite elements, without any geometry distortion, using a linear transformation (Sanborn et al., 2009). This unique ANCF feature allows for establishing a simple and efficient interface between CAD systems and FE/MBS analysis software. Nonetheless, B-spline curves and surfaces are based on rigid recurrence formulas that do not provide the flexibility offered by FE formulations. For this reason, not all ANCF finite elements can be converted to B-spline representations. An example of these ANCF finite elements that cannot be converted to B-spline representation is the thin plate element previously discussed in this section. B-spline surfaces are governed by the recurrence

relationship $\mathbf{r}(u,v)=\sum_{i=0}^{n}\sum_{j=0}^{m}N_{i,p}(u)N_{j,q}(v)\mathbf{P}_{i,j}$, where u and v are the parameters; $N_{i,p}(u)$ and $N_{j,q}(v)$ are B-spline basis functions of degree p and q, respectively; and $\mathbf{P}_{i,j}$ are a bidirectional set of control points. A cubic B-spline surface can be converted to a higher dimensional ANCF plate element that has four nodes, each of which has the nodal coordinate vectors $\mathbf{r},\partial\mathbf{r}/\partial x,\partial\mathbf{r}/\partial y$, and $\partial^2\mathbf{r}/\partial x\partial y$ (Mikkola and Shabana, 2012). Note that the resulting element, which has curvatures in addition to the gradients as nodal coordinates, has forty eight nodal coordinates as compared to the lower dimensional thirty-six degree of freedom ANCF thin plate element previously discussed in this chapter. While, for the geometry description, the increase in the dimensionality of the element may not be a concern, such an increase in the element dimension can be an issue in the analysis. B-spline and NURBS surface representations do not offer the flexibility of using lower dimensional models for a given order of interpolation because of the rigid recurrence formulas used.

3.2.3. Surface Parameterization

In general, four surface parameters can be used to describe the geometry of the two surfaces in contact. The surface parameters can be written in a vector form as

$$\mathbf{s}=\begin{bmatrix}s_1^i & s_2^i & s_1^j & s_2^j\end{bmatrix}^T \tag{3.1}$$

where superscripts i and j refer to bodies i (femur) and j (tibia), respectively. Using these parameters, the location of the contact point P can be defined, respectively, in the coordinate systems of bodies i and j as

$$\bar{\mathbf{u}}_P^i\left(s_1^i, s_2^i\right) = \begin{bmatrix} x^i\left(s_1^i, s_2^i\right) \\ y^i\left(s_1^i, s_2^i\right) \\ z^i\left(s_1^i, s_2^i\right) \end{bmatrix}^T, \qquad \bar{\mathbf{u}}_P^j\left(s_1^j, s_2^j\right) = \begin{bmatrix} x^j\left(s_1^j, s_2^j\right) \\ y^j\left(s_1^j, s_2^j\right) \\ z^j\left(s_1^j, s_2^j\right) \end{bmatrix} \tag{3.2}$$

The tangents to the surface at the contact point are defined in body i coordinate system as

$$\bar{\mathbf{t}}_1^k = \frac{\partial \bar{\mathbf{u}}_P^i}{\partial s_1^k}, \quad \bar{\mathbf{t}}_2^k = \frac{\partial \bar{\mathbf{u}}_P^k}{\partial s_2^k}, \quad k = i, j \tag{3.3}$$

Using these tangent vectors, the normal vector can be defined as $\bar{\mathbf{n}}^k = \bar{\mathbf{t}}_1^k \times \bar{\mathbf{t}}_2^k$. The parameterization used in Equation 3.2 for the surfaces, as well as the tangent and the normal vectors, can be used to describe the geometry of the femur and tibia surfaces Figure 19. This parameterization allows for the description of general surfaces and also allows for the use of numerical or tabulated data to define the contact surface geometry. When the ANCF beam elements are used to describe the contact surface geometry, one can assume $x = s_1^k$ and $y = s_2^k, k = i, j$. In this case, $d\mathbf{r} = \left(\partial \mathbf{r}/\partial x\right) dx + \left(\partial \mathbf{r}/\partial y\right) dy + \left(\partial \mathbf{r}/\partial z\right) dz$. Using the functional relationship, $z = f\left(y\right)$, one can write $d\mathbf{r} = \left(\partial \mathbf{r}/\partial x\right) dx + \left(\left(\partial \mathbf{r}/\partial y\right) + \left(\partial \mathbf{r}/\partial z\right)\left(\left(\partial f\left(y\right)/\partial y\right)\right)\right) dy$. In the case of more general surfaces, the function relationship $z = f\left(x, y\right)$ can be used. In this case, one has $d\mathbf{r} = \left(\left(\partial \mathbf{r}/\partial x\right) + \left(\partial \mathbf{r}/\partial z\right)\left(\left(\partial f\left(x, y\right)/\partial x\right)\right)\right) dx + \left(\left(\partial \mathbf{r}/\partial y\right) + \left(\partial \mathbf{r}/\partial z\right)\left(\left(\partial f\left(x, y\right)/\partial y\right)\right)\right) dy$. These differential relationships can be used to define the tangent and normal vectors as well as their derivatives that enter into the formulations of the kinematics and force equations when complex femur and tibia surfaces are used. As shown by Equations 3.2 and 3.3, two of the surface parameters (s_1^i, s_2^i) are used to define the location of the contact point in the coordinate system $X^i Y^i Z^i$ of body i, while the other two parameters $(s_1{}^j, s_2{}^j)$ define the location of the

contact point in body j coordinate system $X^jY^jZ^j$. The location of the origin and the orientation of the two body coordinate systems are defined, respectively, by the vector $\mathbf{R}^k$ and the transformation matrix $\mathbf{A}^k$, $k = i, j$. Using this description, the global position vector of an arbitrary point on the surface of the two bodies can be written as

$$\mathbf{r}^k = \mathbf{R}^k + \mathbf{A}^k \bar{\mathbf{u}}^k, \quad k = i, j \tag{3.4}$$

where $\bar{\mathbf{u}}^k$ is the local position vector that defines the location of an arbitrary point on the surface of body i or body j with respect to the respective body coordinate system. Differentiation of the preceding equation with respect to time defines the absolute velocity and acceleration vectors of the arbitrary point on the surfaces of the two bodies.

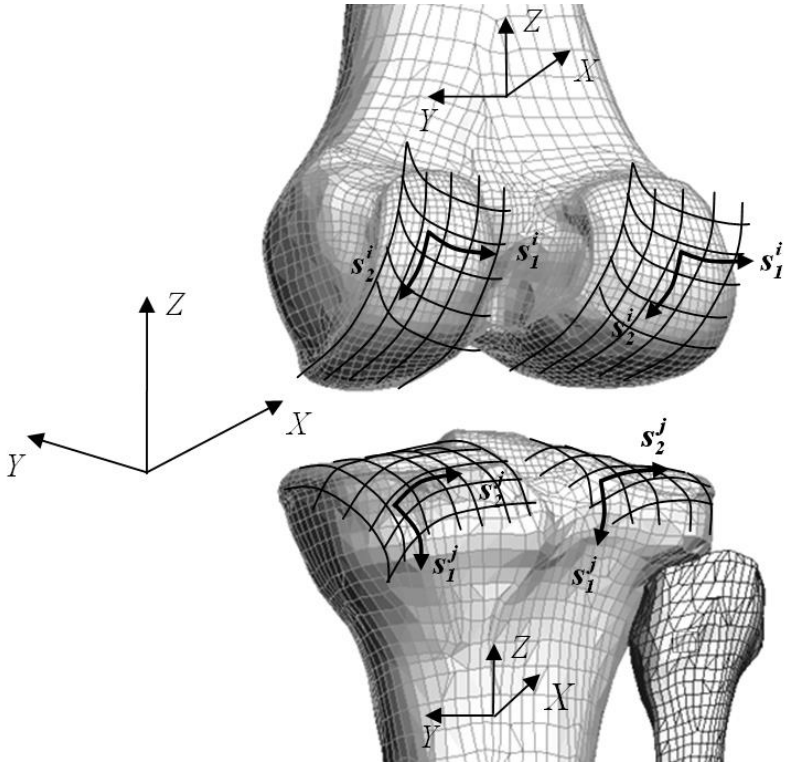

Figure 19 Surface parameterization

3.3. Femur/Tibia Elastic Contact Formulation

The geometry description methods discussed in the preceding section are general and can be used to describe the surfaces of two arbitrary bodies i and j. In this section and the following section, two different contact formulations that can be used to predict the forces of contact between the femur, denoted as body f, and the tibia, denoted as body t, are discussed. These are the elastic and constraint contact formulations.

In the elastic approach, the contact conditions are not considered as kinematic constraints that must be satisfied at the position, velocity, and acceleration levels. Therefore, no degrees of freedom are eliminated, and the femur has six degrees of freedom with respect to the tibia. The contact conditions, which allow for small penetrations at the contact points, are used to obtain the surface parameters that define the location of the contact points. In the elastic contact formulation, four algebraic equations are solved, for each contact, to determine the four parameters that describe the geometry of the femur and tibia surfaces. These four equations can be written as

$$\left.\begin{aligned} &\mathbf{t}_1^t \cdot \left(\mathbf{r}^f - \mathbf{r}^t\right) = 0, \quad \mathbf{t}_2^t \cdot \left(\mathbf{r}^f - \mathbf{r}^t\right) = 0 \\ &\mathbf{t}_1^f \cdot \mathbf{n}^t = 0, \quad \mathbf{t}_2^f \cdot \mathbf{n}^t = 0 \end{aligned}\right\} \tag{3.5}$$

where $\mathbf{t}_1^k$ and $\mathbf{t}_2^k, k = f, t$, are the tangents to the tibia and femur surfaces at the potential contact point, $\mathbf{r}^{ft} = \mathbf{r}^f - \mathbf{r}^t$ is the vector that defines the relative position of the point on the femur with respect to the point on the tibia; and $\mathbf{n}^t$ is the normal to the tibia surface at the potential contact point. Because the tangent and the normal vectors are functions of the surface parameters, and assuming that the generalized coordinates of the femur and tibia are known, one can write the set

of algebraic equations of Equation 3.5 in a vector form as **E(s) = 0**, where **E** is the vector of nonlinear algebraic equations that can be solved using an iterative Newton-Raphson algorithm for the surface parameters that define the potential non-conformal contact points. This requires evaluating the Jacobian matrix of the algebraic equations and iteratively solving the following system for each contact to determine the Newton differences associated with the surface parameters:

$$\begin{bmatrix} \mathbf{t}_1^t \cdot \mathbf{t}_1^f & \mathbf{t}_1^t \cdot \mathbf{t}_2^f & \dfrac{\partial \mathbf{t}_1^t}{\partial s_1^t} \cdot \mathbf{r}^{ft} - \mathbf{t}_1^t \cdot \mathbf{t}_1^t & \dfrac{\partial \mathbf{t}_1^t}{\partial s_2^t} \cdot \mathbf{r}^{ft} - \mathbf{t}_1^t \cdot \mathbf{t}_2^t \\ \mathbf{t}_2^t \cdot \mathbf{t}_1^f & \mathbf{t}_2^t \cdot \mathbf{t}_2^f & \dfrac{\partial \mathbf{t}_2^t}{\partial s_1^t} \cdot \mathbf{r}^{ft} - \mathbf{t}_2^t \cdot \mathbf{t}_1^f & \dfrac{\partial \mathbf{t}_2^t}{\partial s_2^t} \cdot \mathbf{r}^{ft} - \mathbf{t}_2^t \cdot \mathbf{t}_1^t \\ \dfrac{\partial \mathbf{t}_1^f}{\partial s_1^f} \cdot \mathbf{n}^t & \dfrac{\partial \mathbf{t}_1^f}{\partial s_2^f} \cdot \mathbf{n}^t & \dfrac{\partial \mathbf{n}^t}{\partial s_1^t} \cdot \mathbf{t}_1^f & \dfrac{\partial \mathbf{n}^t}{\partial s_2^t} \cdot \mathbf{t}_1^f \\ \dfrac{\partial \mathbf{t}_2^f}{\partial s_1^f} \cdot \mathbf{n}^t & \dfrac{\partial \mathbf{t}_2^f}{\partial s_2^f} \cdot \mathbf{n}^t & \dfrac{\partial \mathbf{n}^t}{\partial s_1^t} \cdot \mathbf{t}_2^f & \dfrac{\partial \mathbf{n}^t}{\partial s_2^t} \cdot \mathbf{t}_2^f \end{bmatrix} \begin{bmatrix} \Delta s_1^f \\ \Delta s_2^f \\ \Delta s_1^t \\ \Delta s_2^t \end{bmatrix} = - \begin{bmatrix} \mathbf{t}_1^t \cdot \mathbf{r}^{ft} \\ \mathbf{t}_2^t \cdot \mathbf{r}^{ft} \\ \mathbf{t}_1^f \cdot \mathbf{n}^t \\ \mathbf{t}_2^f \cdot \mathbf{n}^t \end{bmatrix} \tag{3.6}$$

In this equation, $\Delta s_1^f, \Delta s_2^f, \Delta s_1^t$, and Δs_2^t are the Newton differences. Convergence is achieved when the norm of the violation of the algebraic equations or the norm of Newton differences is less than a specified tolerance. Having determined the vector of the surface parameters, the penetration δ can be calculated as $\delta = \mathbf{r}^{ft} \cdot \mathbf{n}^t$. Knowing the penetration and its time derivative, the normal contact force can be evaluated using the following equation:

$$F = -K_h \delta^{3/2} - C\dot{\delta}|\delta| \tag{3.7}$$

where K_h is a constant that depends on the surface curvatures and the elastic properties, and C is an assumed damping coefficient. The time rate of penetration, $\dot{\delta}$, can be evaluated as the dot product of the relative velocity vector between the contact points on the femur and the tibia and

the normal vector to the surface at the contact point. The absolute value of the penetration, $|\delta|$, is introduced in the preceding equation in order to guarantee that the contact force is zero when the penetration is zero.

3.4. Femur/Tibia Constraint Contact Formulation

In this section, the constraint contact formulation is briefly discussed in order to highlight the basic differences between the two force approaches that will be used in this investigation. The surface geometric description of the femur and tibia is assumed to be the same in both formulations. In the case of the constraint contact formulation, the femur has five degrees of freedom with respect to the tibia since the motion along the normal to the surfaces at the contact point is not allowed.

The contact points on the surfaces must coincide during the dynamic simulation avoiding penetration and separation between the two bodies. Another condition is that the normals to the surfaces at the contact point must remain parallel. These conditions define the following five nonlinear algebraic constraint equations that are required to describe the non-conformal contact between the femur and tibia:

$$\left.\begin{array}{l} \mathbf{t}_1^t \cdot \left(\mathbf{r}^f - \mathbf{r}^t\right) = 0, \quad \mathbf{t}_2^t \cdot \left(\mathbf{r}^f - \mathbf{r}^t\right) = 0 \\ \mathbf{t}_1^f \cdot \mathbf{n}^t = 0, \quad \mathbf{t}_2^f \cdot \mathbf{n}^t = 0, \quad \mathbf{n}^t \cdot \left(\mathbf{r}^f - \mathbf{r}^t\right) = 0 \end{array}\right\} \tag{3.8}$$

The vectors that appear in this equation are the same as defined in the preceding section. In order to eliminate the four surface parameters associated with each contact, four contact constraint equations are selected such that their Jacobian matrix is a non-singular square matrix. The four

equations are chosen from Equation 3.8 by excluding the last equation that defines the relative motion along the normal to the surface at the contact point. This equation can be added to the system differential equations of motion in order to determine the normal contact force using the technique of Lagrange multipliers. The MBS algorithm used in this investigation ensures that the contact constraints of Equation 3.8 are satisfied at the position, velocity, and acceleration levels. In general the kinematic constraint equations imposed on the motion of the multibody system can be expressed in a vector form as $\mathbf{C}(\mathbf{q},\mathbf{s},t)=\mathbf{0}$, where $\mathbf{C}$ is the vector of constraint functions, $\mathbf{q}$ is the vector of the system generalized coordinates, $\mathbf{s}$ is the vector of surface parameters, and t is time (Shabana et al., 2008). In this constraint contact formulation, the geometric surface parameters are treated as dependent variables and are systematically eliminated from the equation of motion. Only one Lagrange multiplier associated with the contact constraints is used and this Lagrange multiplier defines the normal contact force. Using this constraint approach, no separation or penetration between the tibia and femur at the contact point is allowed.

3.5. Ligament Modeling

The use of ANCF beam elements to describe the femur and tibia rigid surface geometry was discussed in Section 3.3. The same ANCF beam elements can be used in the deformation analysis of the ligaments, muscles, and soft tissues (LMST) as described in Chapter 2. The dynamics of the MCL and LCL will be examined using ANCF meshes that capture the ligament large displacements and the cross section deformations, and allow for the use of general material models. This sheds light on the potential use of ANCF finite elements in the successful **i**ntegration of **c**omputer **a**ided **d**esign and **a**nalysis (I-CAD-A).

The necessary knee joint stability for optimal daily function is provided by the interaction of various articulations, menisci, ligaments as well as muscle forces (Nordin et al., 2001). Ligaments are connective tissue that connects bones to other bones, and are an important part of knee anatomy. The predominant kinematic characteristics of the knee are determined by the curvatures of the femoral and tibial articulating surfaces as well as by the orientation of the knee (Kapandji, 1970).

The ligaments control the passive motion of the knee joint while the dynamic stability of the joint is provided by muscular movements. The tibio-femoral joint is supported by the collateral ligaments (LCL, MCL), and the two cruciate ligament (ACL, PCL). For a better description of their behavior it is important to know their components. Ligaments structure consists of network of collagenous fibers that can have different lengths and complex orientations. Constitutive models describe their performance by predicting large deflections and deformations. Because of their structure, most fibrous soft tissues are assumed to be continuous fiber. This type of material has a single preferred direction (a material that is reinforced by only one family of fibers) and it is usually modeled as transversely isotropic hyper-elastic material (Leondes, 2007).

As was mentioned earlier, this work is a continuation of the previous chapter where only two of the ligaments MCL and LCL were modeled using ANCF finite elements. The implementation of such general material models with ANCF structural beam elements was demonstrated in previous studies (Mohamed et al., 2010, Weed et al., 2008).This chapter will extend the MCL and LCL model to include the tibio femoral contact and the two cruciate ligaments.

3.5.1. Anterior Cruciate Ligament (ACL)

The ACL is one of the four major ligaments of the knee. It provides primary restraint to anterior displacement of the tibia as well as rotational stability. The kinematics of the ACL has received much attention due to its important role in normal knee function as well as in ligament reconstruction (Mow et al., 1997). The ligament is the primary restraint against anterior tibial displacement and internal rotation of the tibia at the knee. Non-contact ACL injuries occur when a high force at the joint in the direction of either internal rotation or anterior tibial translation exceeds the tensile strength of the ligament (Milner, 2008). The ACL is modeled in this study using a linear spring damper element with a length of 0.0342 m, and stiffness of 200000 N/m (Kennedy et al., 1974, Bartel et al., 2006).

3.5.2. Posterior Cruciate Ligament (PCL)

This ligament, which connects the tibia to the femur, is located at the center of the knee, behind ACL. The PCL is reported to be stronger than the ACL, and is not injured as often as the ACL (Amis et al., 2003). The configuration of the PCL allows the ligament to resist forces pushing the tibia posterior relative to the femur. The function of the PCL is to prevent the femur from sliding off the anterior edge of the tibia and to prevent the tibia from displacing posterior to the femur. The PCL is modeled in this study using a linear spring damper element with a length of 0.0375 cm, and stiffness of 200000 N/m (Wang, 2002, Bartel et al., 2006).

3.5.3. Menisci

A meniscus is a disk of fibrocartilage that serves as a pad between the ends of bones in the knee joint, provides stability and distributes the whole body weight across knee joint. Menisci are two

ñcò shape pads that help distribute the loads from the femoral condyles to the tibial plateaus (Bartel et al., 2006). The main function of the menisci is to transmit joint loads from the femur to the tibia (Machado et al., 2010).

There are few studies in the literature based on knee joint models that include menisci. Penã et al. presented in their research a three-dimensional finite element model of the knee that includes femur, tibia, all four major ligaments, articular cartilage and menisci. In this study the meniscal tissues were assumed to be single phase linear elastic, isotropic and homogenous materials. Their model describes the importance of the combined role of the menisci and ligaments in the stability of the joint (Penã et al., 2006). Another study provides a method that develops a new representation of the knee with menisci within a dynamic three-dimensional MBS framework (Guess et al., 2010). The meniscus model includes elements (linearly elastic isotropic materials) connected through 6×6 stiffness matrices. One of the limitations of the method is that the menisci provide only a secondary kinematic constraint during walking.

In this thesis a different approach for modeling the menisci is presented employing formulas for tangential forces and spin moment (Vollebregt, 2008). These formulas are given by

$$F_x = D\left(\mathbf{v}^f - \mathbf{v}^t\right)^T \mathbf{t}_1, \quad F_y = D\left(\mathbf{v}^f - \mathbf{v}^t\right)^T \mathbf{t}_2, \quad M_1 = D_1\left(\boldsymbol{\omega}^f - \boldsymbol{\omega}^t\right)^T \mathbf{n} \tag{3.9}$$

where $\mathbf{v}^f$ and $\mathbf{v}^t$ are the absolute velocities of the bodies at the contact point (femur/tibia), $\boldsymbol{\omega}^f$ and $\boldsymbol{\omega}^t$ are the absolute angular velocities of the bodies in contact, $\mathbf{t}_1$ and $\mathbf{t}_2$ are unit tangent vectors on the tibia at the point of contact, $\mathbf{n}$ is the unit normal vector at the point of contact, and D and D_1 are assumed in this investigation to have constant values of 50 N.s/m and 100 N.s, respectively. In addition to these forces, a spring-damper system is applied in parallel at the

main points of contact between the femur and tibia to resist stresses or shocks applied to the joint (Fung, 1993). The spring stiffness and damping coefficients are sized to allow a smooth motion during knee joint flexion.

3.6. Multibody System Equations

ANCF finite elements allow for successful integration of CAD geometry and FE/MBS algorithms that are designed to solve the differential and the algebraic equations of complex physics and engineering systems. In this section, the dynamic equations used in the present chapter and the knee joint model previously presented in Chapter 2 are briefly discussed.

3.6.1. Multi-Formulation MBS Approach

In order to be able to efficiently solve the resulting nonlinear dynamic equations of complex biomechanics systems, a multi-formulation approach that allows for modeling bodies with different degrees of flexibility must be used. One can use either the floating frame of reference (FFR) formulation or rigid body formulation to model the tibia, fibula, and femur. In the current work the bones are modeled as rigid bodies that can be modeled using the rigid body Newton-Euler equations which employ reference coordinates that define the location and orientation of the rigid body coordinate system. The FFR formulation employs coupled reference and elastic coordinates and can be used to model bodies that experience small deformations. ANCF finite elements can be used for the geometry description and for the analysis of large deformations. Joint constraints that describe insertion site kinematics and specified motion trajectories are formulated using a set of nonlinear algebraic constraint equations that are adjoined to the system differential equations of motion using the technique of Lagrange multipliers. The following

augmented form of the equations of motion is used to obtain the vector of reference, elastic, and ANCF accelerations (Shabana, 2005):

$$\begin{bmatrix} \mathbf{m}_{rr} & \mathbf{m}_{rf} & \mathbf{0} & \mathbf{C}_{\mathbf{q}r} \\ \mathbf{m}_{fr} & \mathbf{m}_{ff} & \mathbf{0} & \mathbf{C}_{\mathbf{q}f} \\ \mathbf{0} & \mathbf{0} & \mathbf{m}_{aa} & \mathbf{C}_{\mathbf{q}a} \\ \mathbf{C}_{\mathbf{q}_r} & \mathbf{C}_{\mathbf{q}_f} & \mathbf{C}_{\mathbf{q}_a} & \mathbf{0} \end{bmatrix} \begin{bmatrix} \ddot{\mathbf{q}}_r \\ \ddot{\mathbf{q}}_f \\ \ddot{\mathbf{q}}_a \\ \boldsymbol{\lambda} \end{bmatrix} = \begin{bmatrix} \mathbf{Q}_r \\ \mathbf{Q}_f \\ \mathbf{Q}_a \\ \mathbf{Q}_c \end{bmatrix} \tag{3.10}$$

In this equation, subscripts r, f, and a refer, respectively, to reference, elastic and absolute nodal coordinates; $\mathbf{m}_{rr}$, $\mathbf{m}_{rf}$, $\mathbf{m}_{fr}$, $\mathbf{m}_{ff}$ are the inertia sub-matrices that appear in the FFR formulation; $\mathbf{m}_{aa}$ is the constant symmetric mass matrix associated with the ANCF finite elements; this matrix is an identity matrix when Cholesky coordinates are used (Shabana, 2005); $\mathbf{C}_{\mathbf{q}_r}$, $\mathbf{C}_{\mathbf{q}_f}$, and $\mathbf{C}_{\mathbf{q}_a}$ are the Jacobians of the constraint equations associated, respectively, with the reference, elastic, and ANCF coordinates, $\boldsymbol{\lambda}$ is the vector of Lagrange multipliers, and $\mathbf{Q}_c$ is the quadratic velocity vector that results from the differentiation of the constraint equations twice with respect to time. The generalized coordinates, $\mathbf{q}_r$ and $\mathbf{q}_f$ are the coordinates used in the FFR formulation to describe the motion of rigid and flexible bodies that experience small deformations. The vector $\mathbf{q}_a$ is the vector of ANCF coordinates used to describe the motion of flexible bodies that may undergo large displacement, deformations, and change in the cross section.

3.6.2. Solution Algorithm

By solving the preceding equation, the independent accelerations can be identified and integrated forward in time in order to determine the independent coordinates and velocities. Knowing the

independent coordinates, the nonlinear kinematic constraint equations can be solved for the dependent coordinates using an iterative Newton-Raphson algorithm. Knowing all the coordinates and the independent velocities, the dependent velocities can be determined using the algebraic constraint equations at the velocity level. The use of this procedure ensures that the constraint equations are satisfied at the position, velocity, and acceleration levels.

3.7. Numerical Results

In the numerical study presented in this section, the use of the contact formulations discussed in this chapter in the nonlinear dynamic analysis of the knee joint model is investigated. A method based on the integration of geometry, MBS, large deformation FE algorithms, and contact formulations is introduced for modeling the dynamics of the knee joint model. Three-dimensional ANCF beam elements are used to model both the femur and tibia contact surface geometry and the MCL and LCL deformations. The femur/tibia interaction forces are predicted using two different contact formulations; the elastic and constraint contact formulations. In the knee joint model considered in this study, the femur, tibia, fibula are considered as rigid bodies, the LCL and MCL are modeled using ANCF finite elements, and the ACL and PCL are modeled using spring-damper elements. All the ligaments are assumed to have pretension. The lengths, masses, and mass moments of inertia of the femur and tibia are given in Table I while the physical properties and insertion sites of the ligaments are given in Table III. Damping coefficients used for the ligaments were calculated using the simple formula $c_{ligament} = 2\xi\sqrt{km}$, where c is the damping parameter, ξ is the damping factor, k is the stiffness coefficient, and m represents the mass.

3.7.1. Simulation Scenarios

In order to demonstrate the use of the proposed approach for modeling the knee joint mechanics, two very dynamic scenarios are considered. In the first scenario, lower speed motion is considered, while in the second scenario an extremely high speed motion is considered. This latter case demonstrates the applicability of the approach for modeling other biological systems.

The knee model used is assumed to be subjected to a prescribed femur flexation; with the angle of flexation is governed by the equation $\theta = 0.5\theta_{\max}\left(1-\cos(2\pi t/\tau\right)$, where t is time, $\theta_{\max} = 45$ deg, and $\tau = 0.2$ s for the lower speed scenario and $\tau = 1$s for the extreme motion scenario. The center of this prescribed rotation lies at the point at which the two cruciate ligaments cross each other, approximately 0.017 m from the contact point in vertical direction. This is the point about which the bones rotate relative to each other in the sagittal plane during flexion and extension. The residual longitudinal strain is approximately 3-5% in the ligaments of the synovial joints. (Song et al, 2004). In this study the initial strain of the ligaments was assumed to be 4% for the ANCF MCL and LCL models, and 5% for the cruciate ligaments. The insertion sites and lengths of the LCL and MCL ligaments are the same as the ones used in Chapter 2. The fibula is connected to the tibia using rigid joint, constraining all the translations and rotations of the fibula with respect to the tibia. In the elastic approach, the contact conditions are not considered as kinematic constraints that must be satisfied at the position, velocity, and acceleration levels. Therefore, no degrees of freedom are eliminated, and the femur has six degrees of freedom with respect to the tibia. However, since the rotation of the femur is specified the femur has five degrees of freedom with respect to the tibia. These degrees of freedom are

controlled by the ligament stiffness forces. The anatomical knee joint model is presented in Figure 1, while the femur and tibia profiles are shown in Figure 16.

3.7.2. Simulation Results for the Slower Motion Scenario

In the slow motion scenario, the knee angle changes from 0 to 45 degrees within 0.5 seconds, this equivalent to one cycle per second. In this case the results of the X-displacements of the femur center of mass presented in Figures 20 - 21 show a good agreement between the elastic contact formulation (ECF) and embedded constraint contact formulation (ECCF) models. The first contact C1 is on the lateral side of the knee joint, while the second contact C2 is on the medial side. The magnitudes of the contact forces obtained using the elastic and constraint formulations are compared in Figures 22 and 23 for the two contacts C1 and C2. These magnitudes depend also on the length and insertion points of the cruciate ligaments. In equilibrium the femur is not in alignment with the tibia and the weight of the femur and any reaction force results in an angulation of the joint surface. Since the joint reaction force must be perpendicular to the contact surface, a stretching of the collateral (MCL and LCL) and cruciate (ACL and PCL) ligaments result, accompanied by a high tensile force in each ligament. The joint compressive forces consist of the vertical component of the reaction forces and the tension in the patella tendon, and the quadriceps and hamstring muscles are accounted for in the computational model developed in this chapter by increased ligament tensile forces. The sum of the contact forces between the lateral and medial sides of the knee joint is shown in Figure 24. The contact forces are relatively high due too high initial tension in the cruciate ligaments and relatively high speed rotation of the femur. The four ligaments considered in the model carry the entire load

which in reality is shared by other tendons, muscles, and tissues of the knee joint; for this reason relatively high initial tension was added to the ACL and PCL.

As previously mentioned, the geometry of the femur and tibia surfaces are described in this investigation using four surface parameters. The deformations of the cruciate ligaments, which are modeled using spring damper elements, are shown in Figures 25 and 26. Figure 27 shows the change in the cross section at the midpoint of the MCL using Nansonôs formula, while Figure 28 shows the axial strain at the midpoint for the medial collateral ligament. The results presented in these figures are based on the assumption that the two condyles have the same shape. In reality, the two condyles have different geometries, and therefore, there is a lack of symmetry. As previously mentioned in the chapter, symmetry was used in order to be able to develop a simpler contact model with results that can be easily interpreted.

3.7.3. Simulation Results for the Extreme Motion Scenario

The extreme motion scenario demonstrates that the proposed FE/MBS approach can be used for very fast dynamic cases unlike most of the FE knee joint models which are based on quasi-static assumptions. This scenario can be applied to other biological systems (not human), and the results of this scenario can also be compared with the results previously presented in the second chapter of this thesis using the very high speed. Figure 29 shows comparison between the mid-point axial strain results predicted using the model proposed in this chapter and the model previously developed (Chapter 2) in which the effects of the cruciate ligaments, meniscus and contact formulation were not taken into consideration. As expected, the strains in the lateral and medial ligaments, predicted using the approach presented in this chapter, are much lower than the ones found in the first chapter of this thesis. Figures 30 and 31 show the normal contact

forces at the lateral and medial sides of the knee in the extreme case scenario. Forces are relatively high due to high initial tension in the cruciate ligaments and the very high speed rotation of the femur. The maximum value of the medial contact force is larger than the maximum value of the lateral contact force. This conclusion is in agreement with what reported in the literature that the medial condyle carries more load than the lateral condyle (Cheng, 1988).

3.7.4. Limitations, Repeatability, and Validation of the Model

It is important to point out that the current model does not have representations of the patella, patellar tendon, joint capsule, skin and muscles. Attachment of the medial meniscus periphery to the tibial cartilage is not modeled. Geometry of the knee structures was obtained using a physical knee model. This may induce inaccuracy in insertion sites of the cruciate ligaments. Furthermore, the femur and tibia surfaces are assumed to be symmetric in order to simplify and check the results of the contact geometry and forces. The material properties of the ligaments are based on the model proposed by Pena et al. (2006); these material properties are not specimen-specific. It is difficult to validate the present model because of the limited amount of experimental data that describe the dynamics behavior of the human knee joint. Most of the data that describe the joint response are obtained using static or quasi-static models.

Because the model presented in this chapter allows for the simulation of very dynamic scenarios, at this point, the validation can only be based on qualitative evaluation of joint response by comparison with data published in the literature, and with data presented in the previous chapter.

In order to allow others to reproduce the model presented in the thesis, more information needs to be provided. For simplicity, the contour of the tibial plateau was described as a straight

line, while the femur surface was approximated by a sixth order polynomial with constant coefficients $A_0 = 0.018$, $A_1 = -3 \cdot 10^{-4}$, $A_2 = -93$, $A_3 = 15$, $A_4 = 1.6 \cdot 10^{6}$, $A_5 = -6.7 \cdot 10^{4}$, $A_6 = -2.4 \cdot 10^{10}$. Dimensions and inertia properties of the femur and tibia are presented in Table I. Physical properties and insertion sites of the lateral and medial ligaments are presented in the numerical results section and for the cruciate ligaments are presented in Table III.

In order to validate the model presented in this chapter, two loadings are considered. This allows comparing the results of the new knee joint model with the results presented in Chapter 2, and Sasaki and Neptun (2010). The first loading scenario considered is a combined compression load of 1150N with a valgus torque of 10 Nm applied to the femur. As compared with the results presented in Chapter 2, the results presented in Figure 29, as expected, show a decrease in the lateral and medial ligament strains due to the addition of the cruciate ligaments and the use of the new contact formulation presented in this chapter. In order to compare the contact force results of the new knee joint model with the results of the contact forces presented by Sasaki and Neptun (2010), in addition to the prescribed motion of the femur, a compressive force of 737 N which represents the body weight was applied to the femur. Knowing that the model presented Sasaki and Neptun includes the patella and muscles forces which are not included in the model developed in this chapter, the differences in the results obtained using the two models are acceptable.

Table III PHYSICAL PROPERTIES AND INSERTION SITES OF THE LIGAMENTS (MOMMERSTEEG ET AL, 1994, MACHADO, 2009)

Ligament	Xf [m]	Yf[m]	Zf [m]	Xt [m]	Yt [m]	Zt [m]	L_0 (m)	K (N/mm)	C (Ns/m)
ACL	-0.012	-0.005	-0.18	0.012	0.003	0.197	0.0342	200	1226.1
PCL	0.007	0.01	-0.18	-0.013	-0.005	0.192	0.0375	200	1226.1

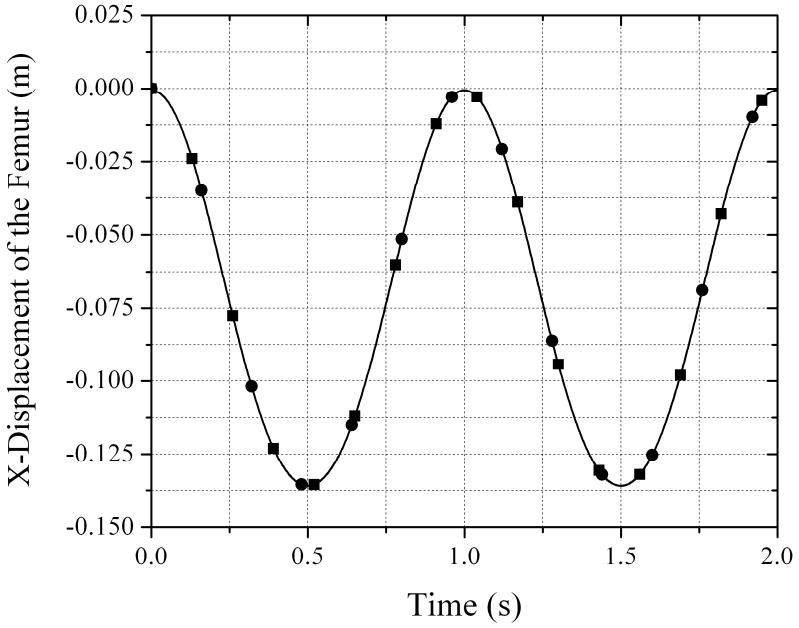

Figure 20 X- Displacement of the femur's center of mass
(—●— ECF, —■— ECCF)

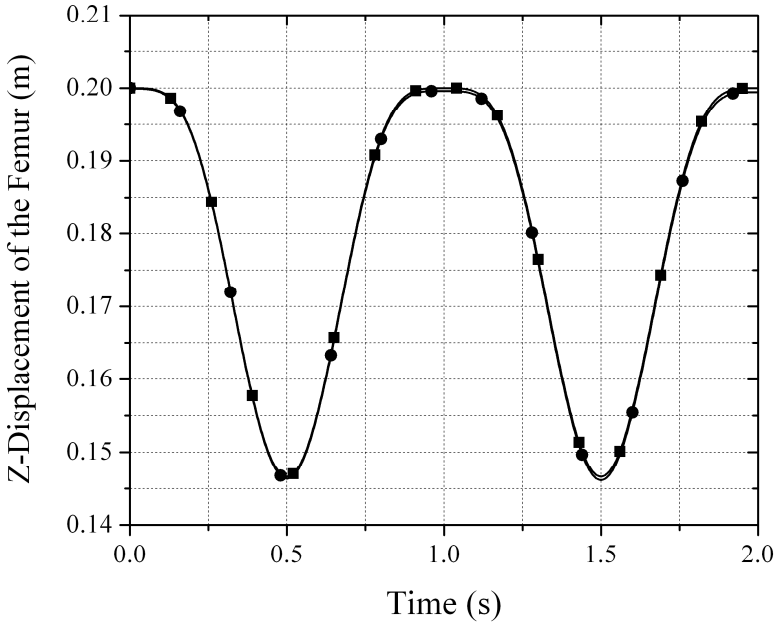

Figure 21 Z- Displacement of the femur's center of mass
(—●—ECF, —■— ECCF)

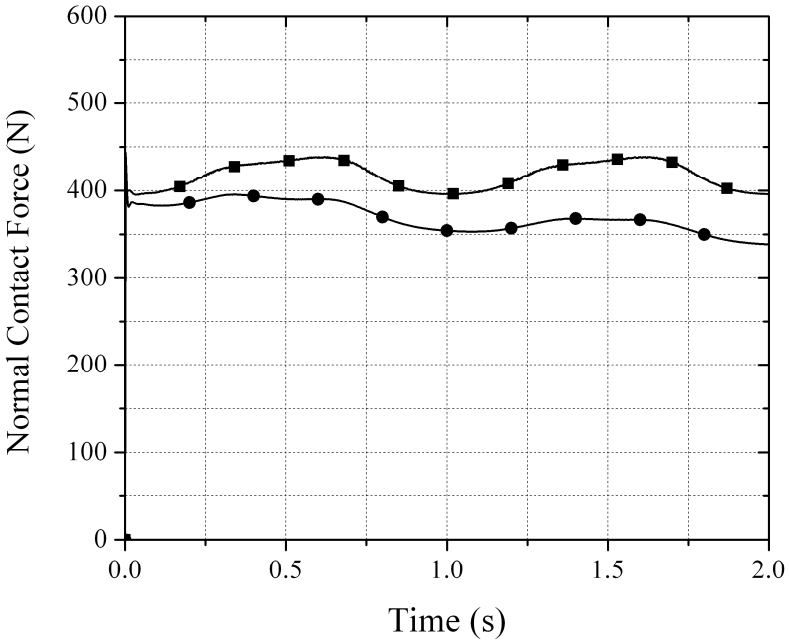

Figure 22 Normal contact force for the knee lateral side
(—●— ECF, —■— ECCF)

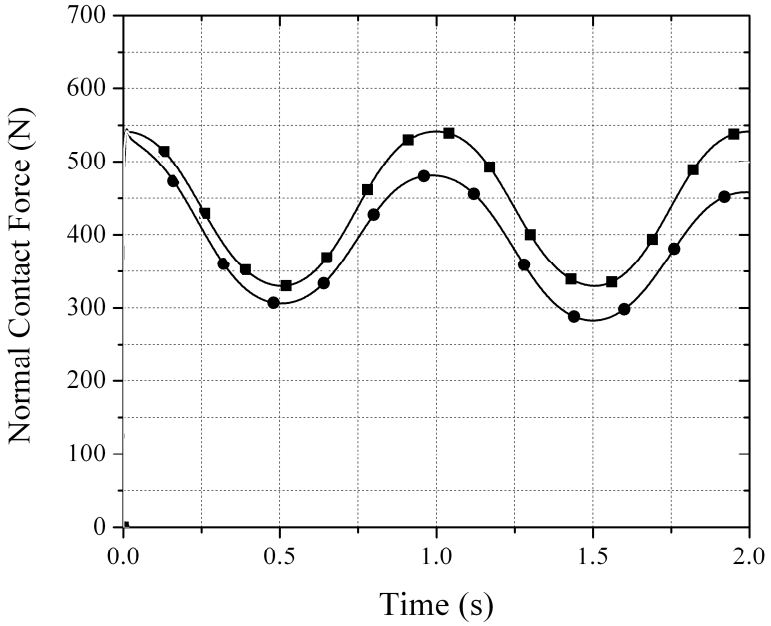

Figure 23 Normal contact force for the knee medial side
(—●— ECF, —■— ECCF)

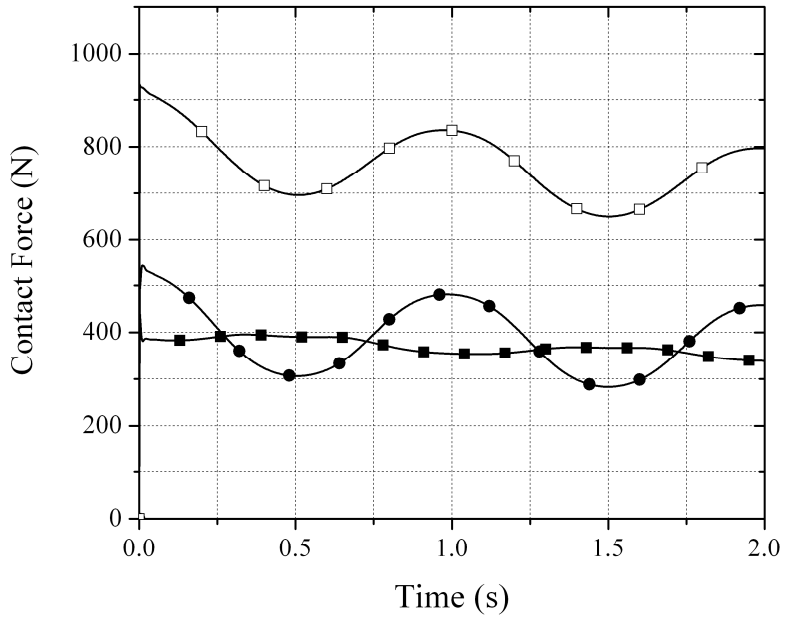

Figure 24 Sum of normal contact forces (ECF)
(Ƶ lateral side,—■— medial side, —□—sum)

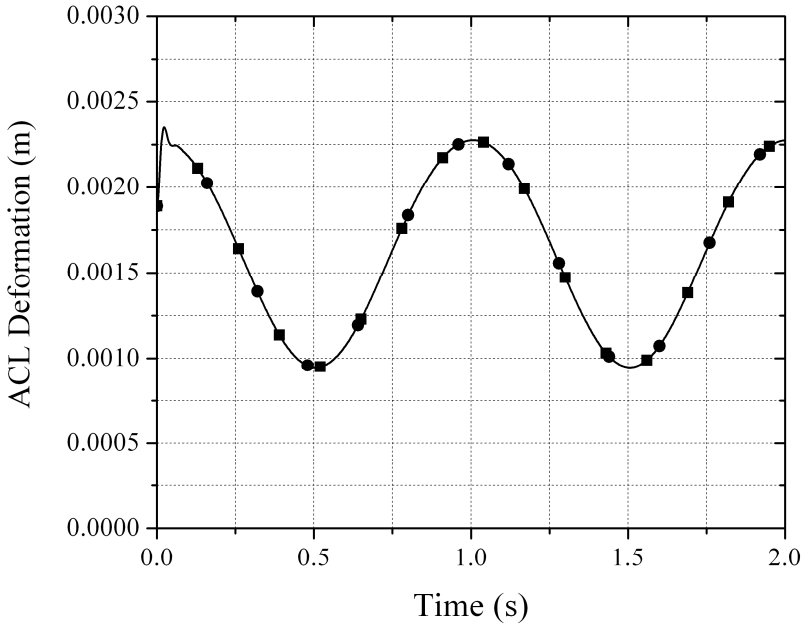

Figure 25 Deformation of the ACL ligament
(—●—ECF, —■— ECCF)

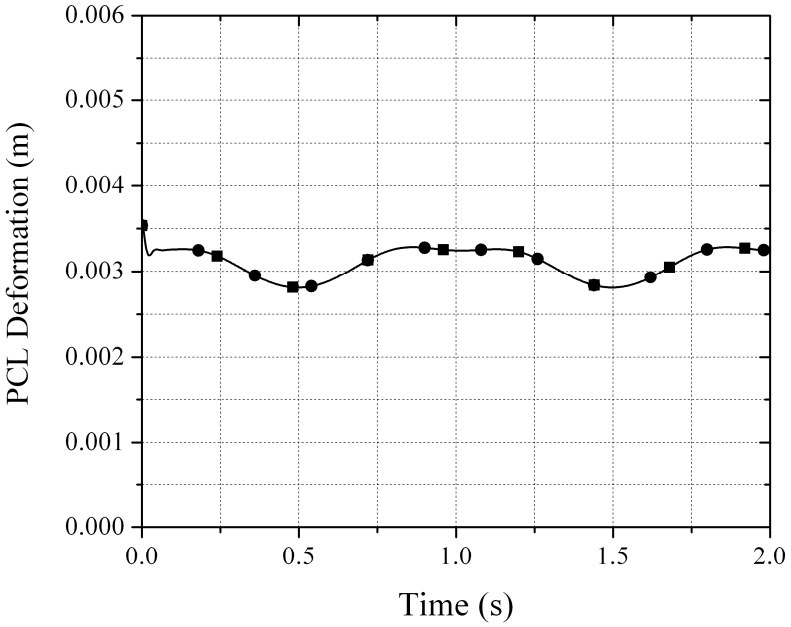

Figure 26 Deformation of the PCL ligament
(—●— ECF, —■— ECCF)

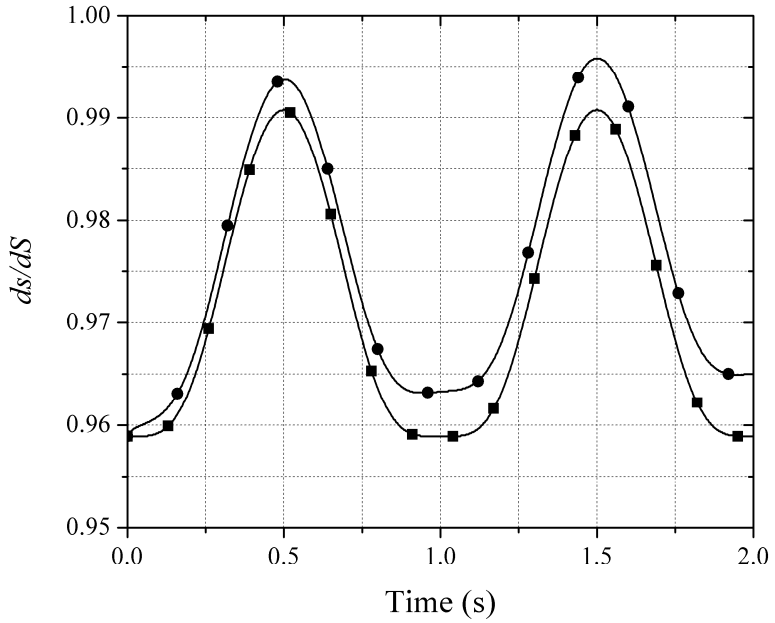

Figure 27 MCL cross section deformation at the midpoint
(—●— ECF, —■— ECCF)

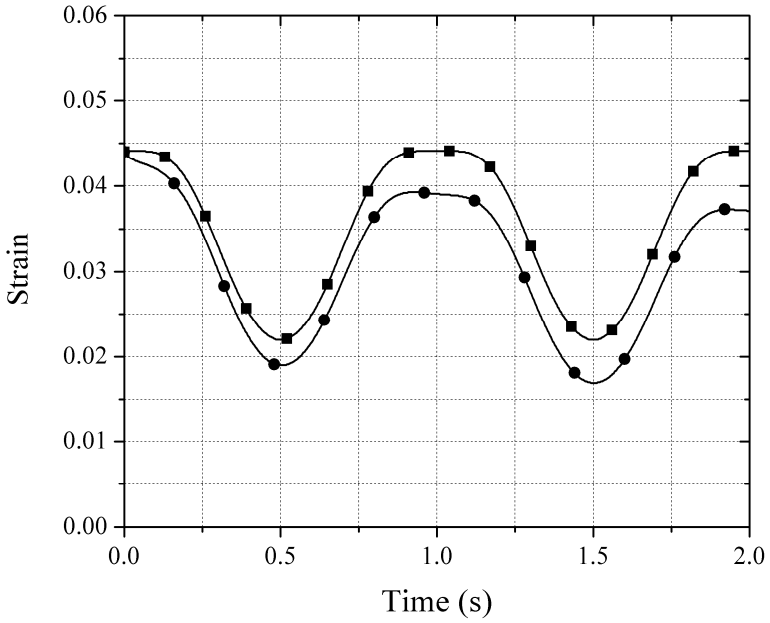

Figure 28 Axial strain at the midpoint for MCL
(—●—ECF, —■—ECCF)

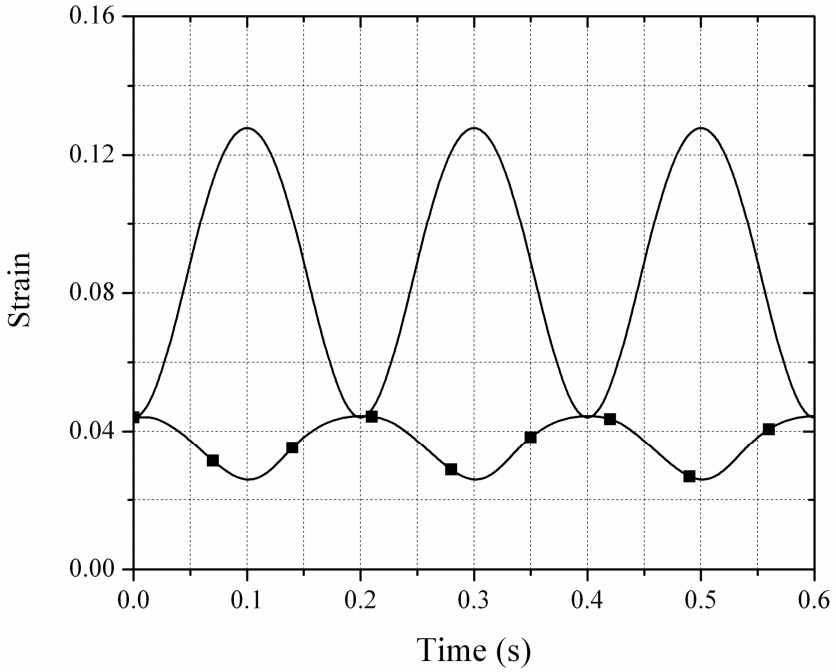

Figure 29 Axial strain at the midpoint for MCL
(Ƶ previous knee model,—■— current knee model)

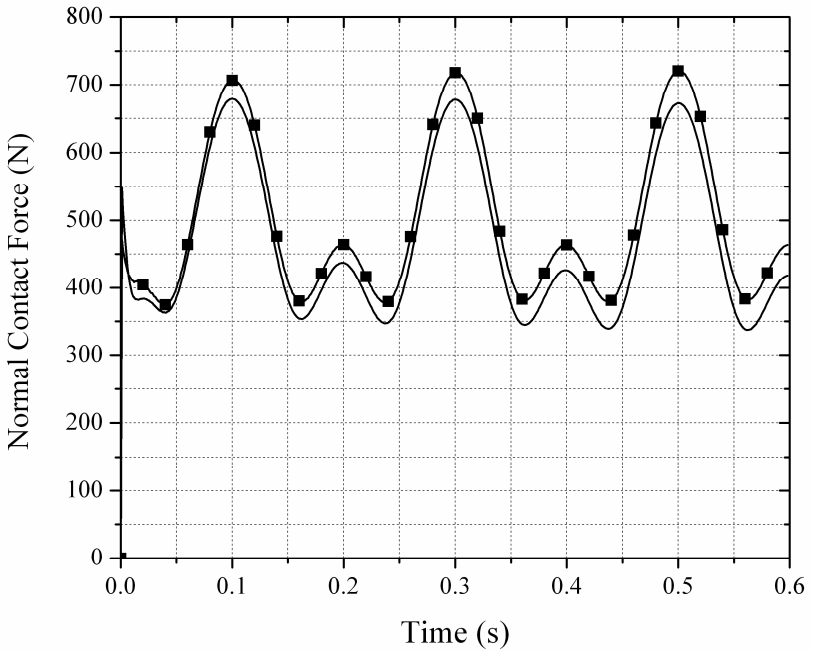

Figure 30 Normal contact force for the knee lateral side
(Ƶ ECF, —■— ECCF)

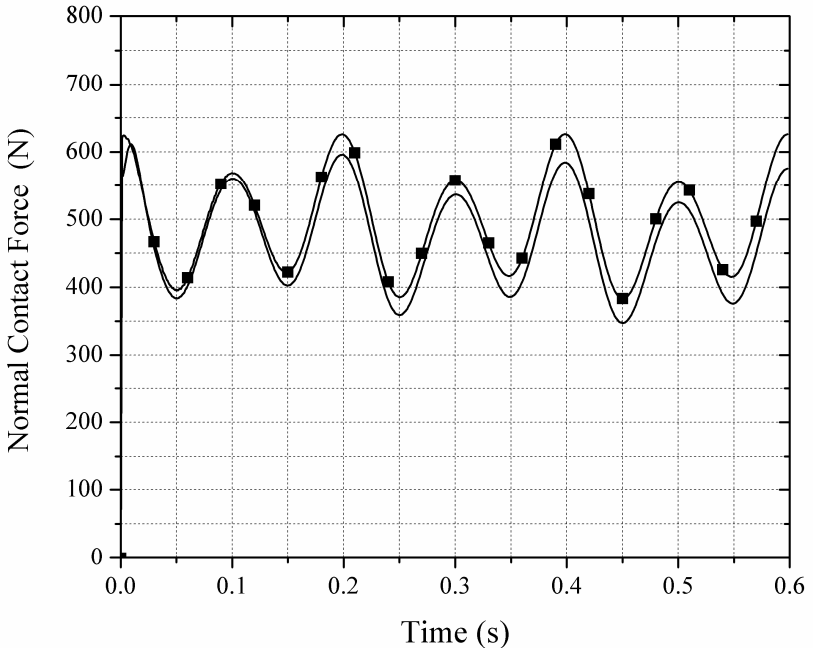

Figure 31 Normal contact force for the knee medial side
(Ƶ ECF, —■— ECCF)

3.8. Concluding Remarks

The main contribution of this chapter is to introduce a new unified approach for modeling the contact geometry and ligament deformation in bio-mechanics applications using ANCF finite elements. In this unified computational environment, one method was used for the development of accurate geometry as well as for performing the analysis. The main features that characterize and distinguish the model proposed here are: a) ANCF geometry and analysis are integrated to study the femur/tibia contact and large ligament displacements, b) the methods used are general and can be applied to other biomechanics systems, c) the model is dynamic and is more appropriate for studying human activities as compared to the static models, d) this model relates the knee mechanical properties and the contact forces produced, e) the model is simple and easy to implement in other types of biomechanical systems. The model considered in this investigation demonstrated the importance of the integration of geometry, FE, and MBS algorithms.

The previous chapter did not consider the geometry of the contact between the femur and the tibia of the knee joint. Two general formulations based on ANCF finite elements for modeling the contact in bio-mechanics applications are presented. In one method, ANCF volume geometry is converted to surface geometry using a parametric relationship that reduces the number of independent coordinate lines. In the second method, ANCF surfaces can be directly used without the need for using the parametric relationship. Each contact surface is described in a parametric form using two surface parameters that enter into the ANCF finite element geometric description. In addition to the geometry description of the femur and tibia surfaces, ANCF finite

elements are used in modeling the LCL and MCL large displacements. Both ligaments are assumed to have distributed inertia and elasticity.

Two formulations, the elastic and constraint, are used in this thesis to predict the femur/tibia contact forces. A set of nonlinear algebraic equations that depend on the surface parameters is developed and used to determine the location of the contact points. In both methods, the assumptions of non-conformal contact are used. In the constraint method, if no degrees of freedom are specified, the femur has five degrees of freedom with respect to the tibia, and the normal contact forces are obtained as reaction forces using the technique of Lagrange multipliers. In the elastic contact formulation, penetration between the bodies is allowed; this penetration and its derivative enter into the calculation of the contact forces. In the elastic contact formulation, if no degrees of freedom are specified, the femur has six degrees of freedom with respect to the tibia. The numerical results obtained in this chapter show, in general, a good agreement between the results obtained using the constraint and elastic contact formulations.

CHAPTER 4

BONE/LIGAMENT INSERTION SITE CONSTRAINTS

Because the absolute nodal coordinate formulation (ANCF) allows for capturing the cross section deformation, different sets of clamped end conditions can be formulated. As discussed in Chapter 2, these include fully clamped joint and partially clamped joint. A *partially clamped joint* eliminates only the translations and rotations at the joint definition point, allowing for the cross section stretch and shears. The fully *clamped joint*, on the other hand, eliminates all the translations, rotations, and deformation degrees of freedom of the cross section at the joint definition point. In addition, in the case of partially clamped joint, the gradient vectors do not always define a set of orthogonal unit vectors at the joint node when the body deforms. The formulation of the partially clamped joint depends on the joint coordinate system selected. Different choices for this coordinate system, including the *tangent* and the *cross section frames*, can be made. This chapter is focused on examining the effect of the choice of the joint coordinate system on the formulation of the clamped joint boundary conditions. To this end the tangent and cross section frames are used. The *tangent frame* is a coordinate system selected such that one of its axes is tangent to the space curve defined by the beam centerline, while in the *cross section frame* the coordinate system is selected such that two of its axes lie in the plane that defines the beam cross section. In order to examine the effect of using these two frames on the formulation of the boundary conditions, the knee joint model from previous chapter will be used. This model consists of the femur, tibia, fibula which are modeled as rigid bodies; with the lateral and medial ligaments modeled using the large displacement ANCF finite elements. The contact constraint

formulation is used in this investigation to predict the femur/tibia contact forces. The numerical results obtained show that, while the type of frame does not significantly affect the motion, the cross section frame has a better convergence characteristics than the tangent frame for the knee joint example considered in this chapter.

4.1. Clamped Joint Formulation

One of the important joints that are widely used in various types of physics and engineering system models is the clamped joint. When fully parameterized ANCF finite elements are used, different clamped joint models can be defined. In this section, as previously discussed in the thesis, the formulation of the partially clamped joints is discussed. Fully parameterized planar and spatial ANCF finite elements are based on the general continuum mechanics theory. The elimination of the relative translations and rotations at a point in the ANCF finite element does not necessarily define a fully clamped joint, particularly in the case of fully parameterized ANCF finite elements.

The *partially clamped joint*, which can be used to connect rigid, flexible, and very flexible bodies, eliminates six degrees of freedom, and therefore, it requires six constraint equations. The degrees of freedom eliminated are three relative translation coordinates and three relative rotations between two coordinate systems on the two bodies connected by the joint. Therefore, in the case of very flexible bodies modeled using the fully parameterized ANCF finite elements, the partially clamped joint does not eliminate all the degrees of freedom at the joint node, allowing the finite element to deform at this node. Recall that ANCF gradient vectors do not always define a set of orthogonal unit vectors at the joint node when the body deforms.

Nonetheless, by using the gradient vectors, one can always define a set of orthonormal vectors at arbitrary points on the finite element (Sugiyama et al., 2003).

Different sets of orthonormal vectors can be defined. In this investigation, two different sets of orthonormal vectors that define two different frames are presented in the case of *partially clamped joint*. The first set defines the *tangent frame,* while the second defines the *cross section frame*. The knee joint model presented in Chapter 3 is used in this investigation to examine the behavior of these two frames. In this model, shown in Figure 1 the very flexible ligaments LCL and MCL can be effectively modeled using ANCF finite elements, while the tibia and femur can be modeled as rigid bodies. The partially clamped joint formulation requires the formulation of the constraint equations of the spherical joint in which the relative translation between two bodies is eliminated in three perpendicular directions. The constraint equations of the spherical joint which eliminate the relative translational displacement between bodies i and j at a joint definition point P or a node can be written as

$$\mathbf{C}(\mathbf{q}^i, \mathbf{q}^j) = \mathbf{r}_P^i - \mathbf{r}_P^j = \mathbf{0} \tag{4.1}$$

where $\mathbf{q}^i$ and $\mathbf{q}^j$ are the generalized coordinates used to model bodies i and j, respectively; and $\mathbf{r}_P^i$ and $\mathbf{r}_P^j$ are the global position vectors of point P on bodies i and j, respectively. In the case of the floating frame of reference (FFR) formulation, the vector $\mathbf{r}_P^k$, $k = i, j$, can be written as

$$\mathbf{r}_P^k = \mathbf{R}^k + \mathbf{A}^k \overline{\mathbf{u}}_P^k, \qquad k = i, j \tag{4.2}$$

In this equation, $\mathbf{R}^k$ is the global position vector of the reference point of body k coordinate system, $\mathbf{A}^k$ is the transformation matrix that defines the orientation of this coordinate system

with respect to the global system, and $\bar{\mathbf{u}}_P^k$ is the local position vector of the joint definition point with respect to body k coordinate system.

Three degrees of relative rotation must also be constrained in addition to the conditions of Equation 4.1. Let $\mathbf{v}^i$ and $\mathbf{v}^j$ be two vectors defined along a selected joint axis on body i and body j, respectively. These two vectors must remain parallel to each other. The condition that the two vectors must remain parallel is equivalent to the condition $\mathbf{v}^i \times \mathbf{v}^j = \mathbf{0}$, which can alternatively be written using two independent dot product equations (Shabana, 2001). Therefore, the orientation constraint equations in the partially clamped joint can be written using the dot product as

$$\mathbf{v}^{i^{\mathrm{T}}} \mathbf{v}_1^j = 0, \quad \mathbf{v}^{i^{\mathrm{T}}} \mathbf{v}_2^j = 0, \quad \mathbf{v}_2^{i^{\mathrm{T}}} \mathbf{v}_1^j = 0 \tag{4.3}$$

where $\mathbf{v}_1^j$ and $\mathbf{v}_2^j$ are two orthogonal vectors that are orthogonal to $\mathbf{v}^j$, and $\mathbf{v}_2^i$ is a vector defined on body i that is perpendicular to $\mathbf{v}^i$ and must remain perpendicular to $\mathbf{v}_1^j$. The conditions of Equation 4.3 eliminate all the rigid body rotation degrees of freedom of body i with respect to body j. In the case of the FFR formulation, the vectors that appear in Equation 4.3 can be written in terms of vectors defined in their respective body coordinates.The six constraint equations of the partially clamped joint can then be written as follows:

$$\mathbf{C}(\mathbf{q}^i, \mathbf{q}^j) = \begin{bmatrix} \mathbf{r}_P^i - \mathbf{r}_P^j \\ \mathbf{v}^{i^{\mathrm{T}}} \mathbf{v}_1^j \\ \mathbf{v}^{i^{\mathrm{T}}} \mathbf{v}_2^j \\ \mathbf{v}_2^{i^{\mathrm{T}}} \mathbf{v}_1^j \end{bmatrix} = \mathbf{0} \tag{4.4}$$

where $\mathbf{q}^i$ and $\mathbf{q}^j$ are the position coordinates of the bodies connected by the joint. The constraint Jacobian matrix of the partially clamped joint as defined by Equation 4.4 is:

$$\mathbf{C}_{\mathbf{q}} = [\mathbf{C}_{\mathbf{q}^i} \quad \mathbf{C}_{\mathbf{q}^j}] = \begin{bmatrix} \partial \mathbf{r}_p^i / \partial \mathbf{q}^i & -\partial \mathbf{r}_p^j / \partial \mathbf{q}^j \\ \mathbf{v}^{i^{\mathrm{T}}} \left(\partial \mathbf{v}_1^j / \partial \mathbf{q}^j \right) & \mathbf{v}_1^{j^{\mathrm{T}}} \left(\partial \mathbf{v}^i / \partial \mathbf{q}^i \right) \\ \mathbf{v}^{i^{\mathrm{T}}} \left(\partial \mathbf{v}_2^j / \partial \mathbf{q}^j \right) & \mathbf{v}_2^{j^{\mathrm{T}}} \left(\partial \mathbf{v}^i / \partial \mathbf{q}^i \right) \\ \mathbf{v}_2^{i^{\mathrm{T}}} \left(\partial \mathbf{v}_1^j / \partial \mathbf{q}^j \right) & \mathbf{v}_1^{j^{\mathrm{T}}} \left(\partial \mathbf{v}_2^i / \partial \mathbf{q}^i \right) \end{bmatrix} = \mathbf{0} \tag{4.5}$$

The number and type of generalized coordinates of the two bodies used in this equation depends on the type of formulation (Rigid, FFR, or ANCF) used to model the bodies connected by the joint. A fundamental difference in the case of the *partially clamped joint* formulation is that the gradient vectors on the ANCF body do not remain orthogonal unit vectors, and therefore, shear deformation and stretch of the cross section at the joint node are allowed.

4.2. Joint Frames

In the absolute nodal coordinate formulation, the orientation and shape of the cross section is defined using three independent vectors $\mathbf{r}_x^{ie}, \mathbf{r}_y^{ie}, \mathbf{r}_z^{ie}$, where subscript x, y, z indicate partial derivatives of the vector $\mathbf{r}$. These vectors define nonorthogonal basis vectors at the deformed configuration. Different frames can be defined using these vectors, the cross section frame and the tangent frame (Sugiyama et al., 2003).

4.2.1. Tangent Frame

The tangent frame is a coordinate system selected such that one of its axes is tangent to the space curve defined by the beam centerline. The normal plane of the tangent frame is always perpendicular to the tangent vector but does not coincide with the beam cross section, as shown in Figure 4b. Let $\mathbf{t}_t^{ie}, \mathbf{n}_t^{ie}$ and $\mathbf{b}_t^{ie}$ be three orthogonal vectors defined at an arbitrary point on the beam centerline of an element *e* on a body i. The vector tangent to the beam centerline can be defined as

$$\mathbf{t}_t^{ie} = \frac{\mathbf{r}_x^{ie}}{\left|\mathbf{r}_x^{ie}\right|}, \tag{4.6}$$

where $\mathbf{r}_x^{ie} = \partial \mathbf{r}^{ie} / \partial x^{ie}$ is the tangent to the centerline, and $\left|\mathbf{r}_x^{ie}\right|$ is the Euclidian norm of $\mathbf{r}_x^{ie}$ defined by $\sqrt{\mathbf{r}_x^{ie^{\mathrm{T}}} \mathbf{r}_x^{ie}}$. A unit vector $\mathbf{b}_t^{ie}$ normal to both $\mathbf{t}_t^{ie}$ and $\partial \mathbf{r}^{ie} / \partial y^{ie}$ can be defined as

$$\mathbf{b}_t^{ie} = \frac{\mathbf{t}_t^{ie} \times \mathbf{r}_y^{ie}}{\left|\mathbf{t}_t^{ie} \times \mathbf{r}_y^{ie}\right|}, \tag{4.7}$$

where $\mathbf{r}_y^{ie} = \partial \mathbf{r}^{ie} / \partial y^{ie}$. A unit vector $\mathbf{n}_t^{ie}$ that completes the tangential frame triad can then be defined as

$$\mathbf{n}_t^{ie} = \mathbf{b}_t^{ie} \times \mathbf{t}_t^{ie}. \tag{4.8}$$

Because the vector $\mathbf{b}_t^{ie}$ is derived using the vector $\mathbf{r}_y^{ie}$, $\mathbf{b}_t^{ie}$ is always perpendicular to $\mathbf{r}_y^{ie}$ but not necessarily to vector $\mathbf{r}_z^{ie}$. The tangent frame can also be defined using the vector $\mathbf{r}_z^{ie}$. This frame is independent of the vector $\mathbf{r}_y^{ie}$ and is defined as follows (Dufva et al., 2006)

$$\mathbf{t}_{t1}^{ie} = \frac{\mathbf{r}_x^{ie}}{\left|\mathbf{r}_x^{ie}\right|},\ \mathbf{n}_{t1}^{ie} = \frac{\mathbf{r}_z^{ei} \times \mathbf{t}_{t1}^{ie}}{\left|\mathbf{r}_z^{ei} \times \mathbf{t}_{t1}^{ie}\right|},\ \mathbf{b}_{t1}^{ie} = \mathbf{t}_{t1}^{ie} \times \mathbf{n}_{t1}^{ie} \tag{4.9}$$

The orthogonal triad $\mathbf{t}_t^{ie}, \mathbf{n}_t^{ie}$ and $\mathbf{b}_t^{ie}$ can be used to define the orthogonal transformation matrix $\mathbf{A}_t^{ie}$ as follows:

$$\mathbf{A}_t^{ie} = \left[\mathbf{t}_t^{ie} \quad \mathbf{n}_t^{ie} \quad \mathbf{b}_t^{ie}\right] \tag{4.10}$$

The matrix of the position vector gradients **J** can be expresses as follows:

$$\mathbf{J}_t = \mathbf{A}_t^{ie}\mathbf{U}_t, \mathbf{J}_t = \frac{\partial \mathbf{r}^{ie}}{\partial \mathbf{x}} = \left[\mathbf{r}_x^{ie} \ \mathbf{r}_y^{ie} \ \mathbf{r}_z^{ie}\right] \tag{4.11}$$

$$\mathbf{U}_t = \left(\mathbf{A}_t^{ie}\right)^T \mathbf{J}_t = \begin{bmatrix} \left(\mathbf{t}_t^{ie}\right)^T \mathbf{r}_x^{ie} & \left(\mathbf{t}_t^{ie}\right)^T \mathbf{r}_y^{ie} & \left(\mathbf{t}_t^{ie}\right)^T \mathbf{r}_z^{ie} \\ 0 & \left(\mathbf{n}_t^{ie}\right)^T \mathbf{r}_y^{ie} & \left(\mathbf{n}_t^{ie}\right)^T \mathbf{r}_z^{ie} \\ 0 & 0 & \left(\mathbf{b}_t^{ie}\right)^T \mathbf{r}_z^{ie} \end{bmatrix} \tag{4.12}$$

where $\left(\mathbf{n}_t^{ie}\right)^T \mathbf{r}_x^{ie} = 0, \left(\mathbf{b}_t^{ie}\right)^T \mathbf{r}_x^{ie} = 0, \left(\mathbf{b}_t^{ie}\right)^T \mathbf{r}_y^{ie} = 0$. It is clear from the Equation 4.12, that on the centerline of the beam, one has the following decomposition for the matrix of the position vector gradients:

$$\mathbf{J}_t = \mathbf{A}_t^{ie}\mathbf{U}_t, \tag{4.13}$$

where **U** is an upper triangular matrix that enter into the formulation of the Lagrangian strains Tensor:

$$\boldsymbol{\varepsilon} = 1/2\left(\mathbf{J}_t^T\mathbf{J}_t - \mathbf{I}\right) = 1/2\left(\mathbf{U}_t^T\mathbf{U}_t - \mathbf{I}\right) \tag{4.14}$$

The matrix $\mathbf{U}_t$ can be written as

$$\mathbf{U}_t = \begin{bmatrix} \dfrac{\left(\mathbf{r}_x^{ie}\right)^T \mathbf{r}_x^{ie}}{\left|\mathbf{r}_x^{ie}\right|} & \dfrac{\varepsilon_{xy}}{\left|\mathbf{r}_x^{ie}\right|} & \dfrac{\varepsilon_{xz}}{\left|\mathbf{r}_x^{ie}\right|} \\ 0 & \dfrac{\left(\mathbf{r}_x^{ie}\right)^T \mathbf{r}_x^{ie}\left(\mathbf{r}_y^{ie}\right)^T \mathbf{r}_y^{ie} - \varepsilon_{xy}\varepsilon_{xy}}{\left|\mathbf{r}_x^{ie} \times \mathbf{r}_y^{ie}\right|\left|\mathbf{r}_x^{ie}\right|} & \dfrac{\left(\mathbf{r}_x^{ie}\right)^T \mathbf{r}_x^{ie}\varepsilon_{yz} - \varepsilon_{xy}\varepsilon_{xz}}{\left|\mathbf{r}_x^{ie} \times \mathbf{r}_y^{ie}\right|\left|\mathbf{r}_x^{ie}\right|} \\ 0 & 0 & \dfrac{\mathbf{J}}{\left|\mathbf{r}_x^{ie} \times \mathbf{r}_y^{ie}\right|} \end{bmatrix} \tag{4.15}$$

The decomposition of Equation 4.11 is the QR decomposition of the matrix of the position vector gradients defined on the beam centerline, with $\mathbf{Q} = \mathbf{A}_t^{ie}$ and $\mathbf{R} = \mathbf{U}_t$. The use of the decomposition leads to the same definition of the Lagrangian strain components. The proof that the use of tangent frame leads to the QR decomposition is presented in the literature (Sugiyama et al., 2006). Note that the elements of the upper- triangular matrix U defines components that can be related to the stretch and shear deformation on the beam centerline.

4.2.2. Cross Section Frame

As previously mentioned in Chapter 2 of the thesis, another possible choice for the coordinate system is to use the cross section frame that describes the orientation of a joint coordinate system that is rigidly attached to the beam centerline, Figure 4c. In the three-dimensional two nodes ANCF beam element, the cross section deforms but remains planar due to the use of linear polynomials in *y* and *z*. It can be shown that an arbitrary vector drawn on the cross section can be expressed as a linear combination of the two vectors $\mathbf{r}_y^{ie}$ and $\mathbf{r}_z^{ie}$ (Sugiyama et al., 2003). Let $\mathbf{t}_s^{ie}, \mathbf{n}_s^{ie}$ and $\mathbf{b}_s^{ie}$ be three orthogonal vectors defined at an arbitrary point on the beam

centerline of an element *e* on a body i. A vector on the cross section of the beam can be defined as

$$\mathbf{n}_s^{ie} = \frac{\mathbf{r}_y^{ie}}{\left|\mathbf{r}_y^{ie}\right|}, \tag{4.16}$$

where $\mathbf{r}_y^{ie} = \partial \mathbf{r}^{ie} / \partial y^{ie}$, and $\left|\mathbf{r}_y^{ie}\right|$ is the Euclidian norm of $\mathbf{r}_y^{ie}$ defined as $\sqrt{\mathbf{r}_y^{ie^{\mathrm{T}}} \mathbf{r}_y^{ie}}$. A unit vector $\mathbf{t}_s^{ie}$ normal to both $\mathbf{n}_s^{ie}$ and $\partial \mathbf{r}^{ie} / \partial z^{ie}$ can be defined as

$$\mathbf{t}_s^{ie} = \frac{\mathbf{n}_s^{ie} \times \mathbf{r}_z^{ie}}{\left|\mathbf{n}_s^{ie} \times \mathbf{r}_z^{ie}\right|} \tag{4.17}$$

where $\mathbf{r}_z^{ie} = \partial \mathbf{r}^{ie} / \partial z^{ie}$. A unit vector $\mathbf{b}_s^{ie}$ can then be defined as

$$\mathbf{b}_s^{ie} = \mathbf{t}_s^{ie} \times \mathbf{n}_s^{ie} \tag{4.18}$$

One can show that the unit vector $\mathbf{b}_s^{ie}$ lies in the cross section plane that contains the gradient vectors $\mathbf{r}_y^{ie}$ and $\mathbf{r}_z^{ie}$. In the case of the cross section frame, the orientation of the joint coordinate system at an arbitrary point on an element can be defined using the following orthogonal transformation matrix:

$$\mathbf{A}_s^{ie} = \left[\mathbf{t}_s^{ie} \quad \mathbf{n}_s^{ie} \quad \mathbf{b}_s^{ie} \right] \tag{4.19}$$

Note that in the deformed configuration, the cross section frame is not in general the same as the tangent frame previously discussed in this section, and they differ due the rotation of the cross section as the result of the shear effect.

The matrix of the position vector gradients **J** can be expresses as follows:

$$\mathbf{J}_s = \mathbf{A}_s^{ie} \mathbf{U}_s, \quad \mathbf{J}_s = \frac{\partial \mathbf{r}^{ie}}{\partial \mathbf{x}} = \left[\mathbf{r}_x^{ie} \ \ \mathbf{r}_y^{ie} \ \ \mathbf{r}_z^{ie} \right] \tag{4.20}$$

$$\mathbf{U}_s = \left(\mathbf{A}_s^{ie}\right)^T \mathbf{J}_s = \begin{bmatrix} \left(\mathbf{t}_s^{ie}\right)^T \mathbf{r}_x^{ie} & 0 & 0 \\ \left(\mathbf{n}_s^{ie}\right)^T \mathbf{r}_x^{ie} & \left(\mathbf{n}_s^{ie}\right)^T \mathbf{r}_y^{ie} & \left(\mathbf{n}_s^{ie}\right)^T \mathbf{r}_z^{ie} \\ \left(\mathbf{b}_s^{ie}\right)^T \mathbf{r}_x^{ie} & 0 & \left(\mathbf{b}_s^{ie}\right)^T \mathbf{r}_z^{ie} \end{bmatrix} \tag{4.21}$$

where $\left(\mathbf{t}_s^{ie}\right)^T \mathbf{r}_y^{ie} = 0, \left(\mathbf{t}_s^{ie}\right)^T \mathbf{r}_z^{ie} = 0, \left(\mathbf{b}_s^{ie}\right)^T \mathbf{r}_y^{ie} = 0$. It is clear from Equation 4.16, that on the centerline of the beam, one has the following decomposition for the matrix of the position vector gradients:

$$\mathbf{J}_s = \mathbf{A}_s^{ie} \mathbf{U}_s, \tag{4.22}$$

where $\mathbf{U}$ is an upper triangular matrix that depends on the strains.

$$\boldsymbol{\varepsilon} = 1/2\left(\mathbf{J}_s^T \mathbf{J}_s - \mathbf{I}\right) = 1/2\left(\mathbf{U}_s^T \mathbf{A}_s^T \mathbf{A}_s \mathbf{U}_s - \mathbf{I}\right) = 1/2\left(\mathbf{U}_s^T \mathbf{U}_s - \mathbf{I}\right) \tag{4.23}$$

The matrix $\mathbf{U}_s$ can be written as

$$\mathbf{U}_s = \begin{bmatrix} \dfrac{\mathbf{J}}{\left|\mathbf{r}_y^{ie} \times \mathbf{r}_z^{ie}\right|} & 0 & 0 \\ \dfrac{\varepsilon_{xy}}{\left|\mathbf{r}_y^{ie}\right|} & \dfrac{\left(\mathbf{r}_y^{ie}\right)^T \mathbf{r}_y^{ie}}{\left|\mathbf{r}_y^{ie}\right|} & \dfrac{\varepsilon_{yz}}{\left|\mathbf{r}_y^{ie}\right|} \\ \dfrac{\left(\mathbf{r}_y^{ie}\right)^T \mathbf{r}_y^{ie} \varepsilon_{xz} - \varepsilon_{yz}\varepsilon_{xy}}{\left|\mathbf{r}_y^{ie} \times \mathbf{r}_z^{ie}\right| \left|\mathbf{r}_y^{ie}\right|} & 0 & \dfrac{\left(\mathbf{r}_y^{ie}\right)^T \mathbf{r}_y^{ie} \left(\mathbf{r}_z^{ie}\right)^T \mathbf{r}_z^{ie} - \varepsilon_{yz}\varepsilon_{yz}}{\left|\mathbf{r}_y^{ie} \times \mathbf{r}_z^{ie}\right| \left|\mathbf{r}_y^{ie}\right|} \end{bmatrix} \tag{4.24}$$

4.3. Relation between Joint Frames

Consider the case of the two coordinate systems (*tangent* and *cross section frame*) discussed in the preceding section; these two coordinate systems have two different orientations. Let $\mathbf{A}_s^{ie}$ be the transformation matrix that defines the orientation of the coordinate system defined by the cross section frame with respect to the global coordinate system, and $\mathbf{A}_t^{ie}$ be the transformation matrix that defines the orientation of the coordinate system defined by the tangent frame with respect to the global coordinate system. Let $\mathbf{u}$ be a vector defined in the global coordinate system, $\mathbf{u}_s$ a vector defined in the cross section coordinate system, and $\mathbf{u}_t$ a vector defined in the tangent coordinate system, then $\mathbf{u}$ can be defined as $\mathbf{u} = \mathbf{A}_s^{ie}\mathbf{u}_s = \mathbf{A}_t^{ie}\mathbf{u}_t$ and $\mathbf{u}_s = \mathbf{T}_{st}^{ie}\mathbf{u}_t$. Using the formulas for the tangent and cross section frames presented in the preceding section, one can obtain the transformation matrix the defines the orientation of the tangent frame with respect to the cross section frame as

$$\mathbf{T}_{st}^{ie} = \left(\mathbf{A}_t^{ie}\right)^T \mathbf{A}_s^{ie} = \left[\mathbf{t}_t^{ie} \quad \mathbf{n}_t^{ie} \quad \mathbf{b}_t^{ie}\right]^T \left[\mathbf{t}_s^{ie} \quad \mathbf{n}_s^{ie} \quad \mathbf{b}_s^{ie}\right] \tag{4.25}$$

This transformation can be written in a more explicit form as

$$\mathbf{T}_{st}^{ie} = \begin{bmatrix} \dfrac{J}{\left|\mathbf{r}_x^{ie}\right|\left|\mathbf{r}_y^{ie} \times \mathbf{r}_z^{ie}\right|} & \dfrac{\varepsilon_{xy}}{\left|\mathbf{r}_x^{ie}\right|\left|\mathbf{r}_y^{ie}\right|} & \dfrac{\varepsilon_{xz}\left(\mathbf{r}_y^{ie}\right)^T \mathbf{r}_y^{ie} - \varepsilon_{xy}\varepsilon_{yz}}{\left|\mathbf{r}_x^{ie}\right|\left|\mathbf{r}_y^{ie} \times \mathbf{r}_z^{ie}\right|\left|\mathbf{r}_y^{ie}\right|} \\ \dfrac{-\varepsilon_{xy}J}{\left|\mathbf{r}_x^{ie} \times \mathbf{r}_y^{ie}\right|\left|\mathbf{r}_x^{ie}\right|\left|\mathbf{r}_y^{ie} \times \mathbf{r}_z^{ie}\right|} & \dfrac{\left(\mathbf{r}_x^{ie}\right)^T \mathbf{r}_x^{ie}\left(\mathbf{r}_y^{ie}\right)^T \mathbf{r}_y^{ie} - \varepsilon_{xy}\varepsilon_{xy}}{\left|\mathbf{r}_x^{ie} \times \mathbf{r}_y^{ie}\right|\left|\mathbf{r}_x^{ie}\right|\left|\mathbf{r}_y^{ie}\right|} & \dfrac{\varepsilon_{xy}\varepsilon_{xy}\varepsilon_{yz} - \left(\left(\mathbf{r}_y^{ie}\right)^T \mathbf{r}_y^{ie}\right)\varepsilon_{xy}\varepsilon_{xz}}{\left|\mathbf{r}_x^{ie} \times \mathbf{r}_y^{ie}\right|\left|\mathbf{r}_x^{ie}\right|\left|\mathbf{r}_y^{ie} \times \mathbf{r}_z^{ie}\right|\left|\mathbf{r}_y^{ie}\right|} \\ \dfrac{\varepsilon_{xy}\varepsilon_{yz} - \left(\mathbf{r}_y^{ie}\right)^T \mathbf{r}_y^{ie}\varepsilon_{xz}}{\left|\mathbf{r}_x^{ie} \times \mathbf{r}_y^{ie}\right|\left|\mathbf{r}_y^{ie} \times \mathbf{r}_z^{ie}\right|} & 0 & \dfrac{J\left(\mathbf{r}_y^{ie}\right)^T \mathbf{r}_y^{ie}}{\left|\mathbf{r}_x^{ie} \times \mathbf{r}_y^{ie}\right|\left|\mathbf{r}_y^{ie} \times \mathbf{r}_z^{ie}\right|\left|\mathbf{r}_y^{ie}\right|} \end{bmatrix} \tag{4.26}$$

where $J = \mathbf{r}_x^{ie}\left(\mathbf{r}_y^{ie} \times \mathbf{r}_z^{ie}\right)$, $\varepsilon_{xy} = \left(\mathbf{r}_x^{ie}\right)^T \mathbf{r}_y^{ie}$, $\varepsilon_{xz} = \left(\mathbf{r}_x^{ie}\right)^T \mathbf{r}_z^{ie}$, $\varepsilon_{yz} = \left(\mathbf{r}_y^{ie}\right)^T \mathbf{r}_z^{ie}$. In the knee joint model used in this investigation, the ligaments don't experience a planar motion and the constitutive model used for modeling the ligaments is nearly incompressible.

4.4. Constraint Contact Formulation

In the second chapter, a kinematic revolute joint was used to model the sliding between the femur and tibia. Only two lateral ligaments were providing stability for the knee: LCL and MCL. In the third chapter, two contact formulations were used to model the tibia/femur contact of the knee joint: the *elastic contact formulation* and the *constraint contact formulations*. The effects of the meniscus and two other ligaments were taken into consideration. The two contact formulations were successfully implemented in a general MBS algorithm that allows for modeling rigid and flexible body dynamics. In this chapter, the constraint contact formulation is used to predict the femur/tibia contact forces. First, the contact points on the surfaces must coincide, and second, the two surfaces must have the same tangent planes at the contact point. No penetrations and separations are allowed in this formulation and the non-conformal contact conditions are imposed as constraints equations. As shown in the preceding chapter, the following five constraint equations are required to describe the non-conformal contact between the two bodies.

$$\mathbf{t}_1^t \cdot \left(\mathbf{r}^f - \mathbf{r}^t\right) = 0,\ \mathbf{t}_2^t \cdot \left(\mathbf{r}^f - \mathbf{r}^t\right) = 0,\ \mathbf{t}_1^f \cdot \mathbf{n}^t = 0,\ \mathbf{t}_2^f \cdot \mathbf{n}^t = 0,\ \mathbf{n}^t \cdot \left(\mathbf{r}^f - \mathbf{r}^t\right) = 0 \tag{4.27}$$

where $\mathbf{t}_1^k$ and $\mathbf{t}_2^k$, $k = f, t$, are respectively, the tangents to the tibia and the femur surfaces at the potential contact point, $\mathbf{r}^{ft} = \mathbf{r}^f - \mathbf{r}^t$ is the vector that defines the relative position of the point on

the femur with respect to the point on the tibia; and $\mathbf{n}^t$ is the normal to the tibia surface at the potential contact point.

4.5. Change in Area

As previously mentioned, the partially clamped joint allows for the deformation of the cross section. In the case of the fully clamped joint, the gradient vectors are constrained to be orthogonal unit vectors, and therefore, the cross section area remains the same in both configurations: reference and current configurations. Nansonôs formula, which defines the relationship between the areas in the undeformed and deformed (or reference and current) states can be used to calculate the cross section deformation in the two cases of the partially clamped joint (*tangent frame* and *cross section frame*) (Ogden, 1984; Shabana, 2008). This formula as shown in Chapter 2 of the thesis is given by

$$\frac{ds}{dS} = \frac{J}{\left(\mathbf{n}^T \mathbf{J}\mathbf{J}^T \mathbf{n}\right)^{1/2}} \tag{4.28}$$

In this equation, dS and ds are the areas of an infinitesimal surface in the reference and current configurations, respectively; $\mathbf{n}$ is a unit vector normal to the area in the current configuration; and $J = |\mathbf{J}|$ is the determinant of the matrix of position vector gradients. (Hussein et al., 2009)

In this chapter, as previously pointed out, the cross section frame and the tangent frame are used for the ANCF bodies. As a consequence, the unit vector normal to the cross section surface is defined by the following equation:

$$\mathbf{n} = \frac{\mathbf{r}_y^{ie} \times \mathbf{r}_z^{ie}}{\left|\mathbf{r}_y^{ie} \times \mathbf{r}_z^{ie}\right|} \tag{4.29}$$

The matrix of position vector gradients is

$$\mathbf{J} = \begin{bmatrix} \mathbf{r}_x & \mathbf{r}_y & \mathbf{r}_z \end{bmatrix} \tag{4.30}$$

Using Equation 4.21, one obtains for cross section and tangent frame:

$$\frac{ds}{dS} = \left| \mathbf{r}_y^{ie} \times \mathbf{r}_z^{ie} \right| \tag{4.31}$$

These simple formulas are used in this investigation to obtain the ratio of the cross section area in the current and reference configurations for the tangent and cross section frames.

4.6. Constrained MBS Equations

Nonlinear finite element formulations can be integrated with the computational multibody system algorithms that are designed to solve the differential and the algebraic equations of complex systems. In order to be able to solve the resulting nonlinear dynamic equations, a multi-formulation approach will be used. The tibia and the femur are modeled as rigid bodies. On the other hand, the very flexible bodies (ligaments) will be modeled using the large deformation ANCF finite elements. Joint constraints that describe insertion site conditions and specified motion trajectories are being formulated using a set of nonlinear algebraic constraints equations that are adjoined to the system differential equations of motion using the technique of Lagrange multipliers. The augmented form of the equations of motion is used to obtain the vector of reference, elastic, and absolute accelerations.

Lagrange multipliers are used to determine the generalized constraint forces associated with the reference, elastic and absolute nodal coordinate formulation. The algorithm is based on a sparse matrix structure of the augmented Lagrangian form of the equation of motion and has

been discussed in several previous publications (Yakoub et al., 1999). As previously mentioned in this thesis, the augmented form of the equations of motion can be written as (Shabana, 2005):

$$\begin{bmatrix} \mathbf{m}_{rr} & \mathbf{m}_{rf} & \mathbf{0} & \mathbf{C}_{\mathbf{q}_r}^{\mathrm{T}} \\ \mathbf{m}_{fr} & \mathbf{m}_{ff} & \mathbf{0} & \mathbf{C}_{\mathbf{q}_f}^{\mathrm{T}} \\ \mathbf{0} & \mathbf{0} & \mathbf{m}_{aa} & \mathbf{C}_{\mathbf{q}_a}^{\mathrm{T}} \\ \mathbf{C}_{\mathbf{q}_r} & \mathbf{C}_{\mathbf{q}_f} & \mathbf{C}_{\mathbf{q}_a} & \mathbf{0} \end{bmatrix} \begin{bmatrix} \ddot{\mathbf{q}}_r \\ \ddot{\mathbf{q}}_f \\ \ddot{\mathbf{q}}_a \\ \boldsymbol{\lambda} \end{bmatrix} = \begin{bmatrix} \mathbf{Q}_r \\ \mathbf{Q}_f \\ \mathbf{Q}_a \\ \mathbf{Q}_c \end{bmatrix} \tag{4.32}$$

where the subscripts *r*, *f* and *a* refer respectively, to reference, elastic and absolute nodal coordinates; $\mathbf{m}_{rr}$, $\mathbf{m}_{rf}$, $\mathbf{m}_{fr}$, $\mathbf{m}_{ff}$ are the inertia sub-matrices that appear in the FFR formulation; $\mathbf{m}_{aa}$ is the constant symmetric mass matrix associated with the absolute nodal coordinate formulation and it is the identity matrix when Cholesky coordinates, $\mathbf{q}_a$, are used; $\mathbf{C}_{\mathbf{q}_r}$, $\mathbf{C}_{\mathbf{q}_f}$, and $\mathbf{C}_{\mathbf{q}_a}$ are the Jacobian matrices of the constraint equations associated, respectively, with the reference, elastic, and ANCF coordinates, $\boldsymbol{\lambda}$ is the vector of Lagrange multipliers, and $\mathbf{Q}_c$ is the quadratic velocity vector that results from the differentiation of the constraint equations twice with respect to time. The generalized coordinates, $\mathbf{q}_r$ and $\mathbf{q}_f$, are the coordinates used in the FFR formulation to describe the motion of rigid and flexible bodies that experience small deformation. The vector $\mathbf{q}_a$ is the vector of absolute nodal coordinate formulation used to describe the motion of flexible bodies that may experience large displacement, deformations, and change in the cross section. Knowing the independent coordinates, the nonlinear kinematic constraint equations can be solved for the dependent coordinates using an iterative Newton-Raphson algorithm.

4.7. Numerical Results

In the numerical study presented in this section, two different joint frames are used to impose the partially clamped joint constraints: *tangent* and *cross section frame*. The goal of this chapter is to examine the effect of using different frames to formulate the partially clamped joints. In order to focus on the frames discussed in this chapter, the newly developed framework is applied to a simplified knee model (Chapter 3). The lateral ligaments LCL and MCL and the contact surface geometry of the femur and tibia are modeled using three dimensional ANCF beam elements. In this numerical study, the fibula, assumed rigid, is connected to the tibia using rigid joint, constraining all the translations and rotations of the fibula with respect to the tibia; also the constraint contact formulation is used to predict the femur/tibia contact forces. The tibia and the femur are also considered as rigid bodies and the cruciate ligaments ACL and PCL are modeled using spring damper elements. All the ligaments are assumed to have pretension.

The results from this section are based on the knee joint example used in Chapter 3 of this thesis. For completeness the important details of the knee model are presented again. The LCL is assumed clamped to the fibula and femur. This ligament is positioned vertically lengthwise and rotated 19 degrees from the vertical axis of the femur. It has a length of 66.6 mm and elliptical cross-section radii of 3.4 mm and 2.3 mm. The LCL femoral insertion site is 19.5 mm above the inferior tip of the femur with the fibular insertion site located 43.5 mm below the tibial plateau (LaPrade et al., 2007). The anterior fibers of the MCL are clamped to the femur and tibia. This ligament has a length of 94.8 mm with cross-section radii of 7 mm and 2.3 mm; and it is attached vertically and lengthwise to the femur 32.8 mm above the inferior tip of the femur. Its tibial attachment is 62 mm below the tibial plateau (Meister et al., 2000). Table I shows other

dimensions and inertia properties of the femur and tibia; Table II shows the values of the ligament material coefficients used in this investigation; while Table III presents the physical properties of the ligaments. The MCL and LCL are exposed to residual stresses as all biological soft tissues. The residual longitudinal strain in the MCL and LCL is assumed to be 0.04 (Weed et al., 2008) and for ACL and PCL is assumed to be 0.05 (Song et al, 2004).

The result of the *X*-displacement of the femur center of mass is presented in Figure 32, while the magnitudes of the two contact forces obtained using the constraint contact formulation for both cases tangent and cross section frames are shown in Figures 33-34. Previous knee model used in Chapter 3 showed the magnitudes of the contact forces depend on the length and insertion site of the cruciate ligaments.

As previously mentioned in this chapter, the fully clamped joint eliminates all the translation, rotation and deformations degrees of freedom of the cross section at the ligament/ bone insertion site; the gradient vectors do not change their length and orientation, and at the joint node remain orthogonal unit vectors. Figure 35 illustrates the differences between the axial strains in the case of fully clamped joint and partially clamped joint for the MCL. The axial strain at the midpoint in the case of fully clamped joint is smaller since the deformation of the material is fully constrained at the ligament ends and in this special case the material will deform more at the middle.

The partially clamped joint is not a fully constrained connection; the cross section of the joint has the freedom to deform at the joint node. Numerical results using the Neo-Hookean material model are obtained for the partially clamped joint models in both cases, based on the fully parameterized ANCF beam elements. The convergence the fully parameterized ANCF

beam element models is examined by comparing 8 and 12 elements models. Using this convergence results, all the other figures are produced using the 8 beam element model. Figure 36 shows the axial strain at the LCL/femur insertion site, while Figure 37 shows the axial strain of the MCL midpoint. The LCL axial strain of the fibula insertion site is presented in Figure 38. Figures 39-40 show the change in the cross sections at the midpoints of the MCL and LCL using Nansonôs formula. In Figures 41-44 shear strain at LCL/MCL femur insertion site are presented; it can be seen that ε_{yz} is equal to zero only in the case of the tangent frame in this knee joint example. These figures show a good agreement between the two frames. The results presented for the tangent frame show that the maximum strain appears at the ligaments/femur insertion site for both the LCL and MCL.

The results also indicated the strain is different in different regions of the two lateral ligaments and the distribution of the strain changes with flexion angle. The highest strain in the MCL and LCL were found at the ligament/femur insertion site at full extension. Maximum strains in this example are slightly lower than the ones presented in the literature (Weiss et al., 2001). From the results presented in these figures, it can be seen that the tangent frame has a better convergence than the cross section frame in the case of axial strains.

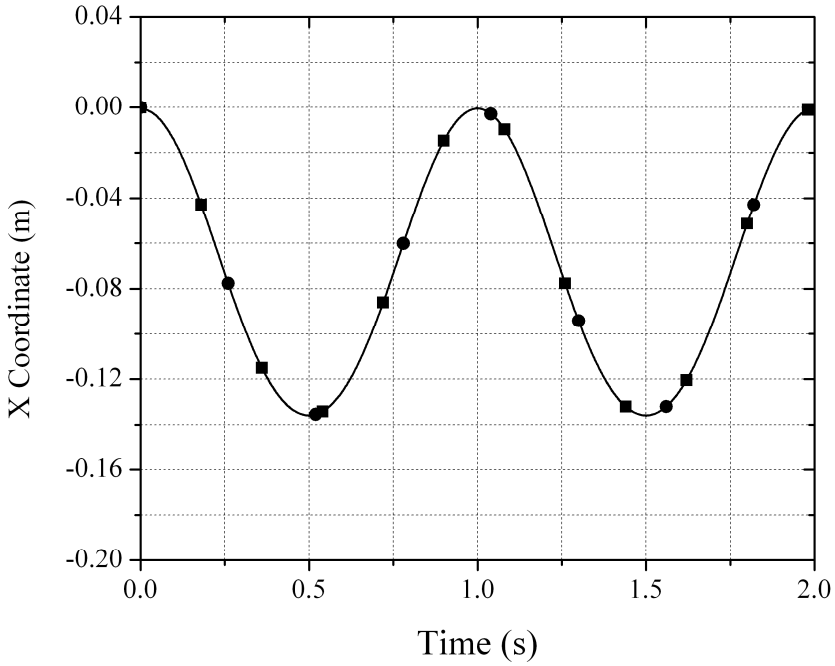

Figure 32 X Coordinate of center of mass of the femur
(—■— Cross section frame, —●— Tangent frame)

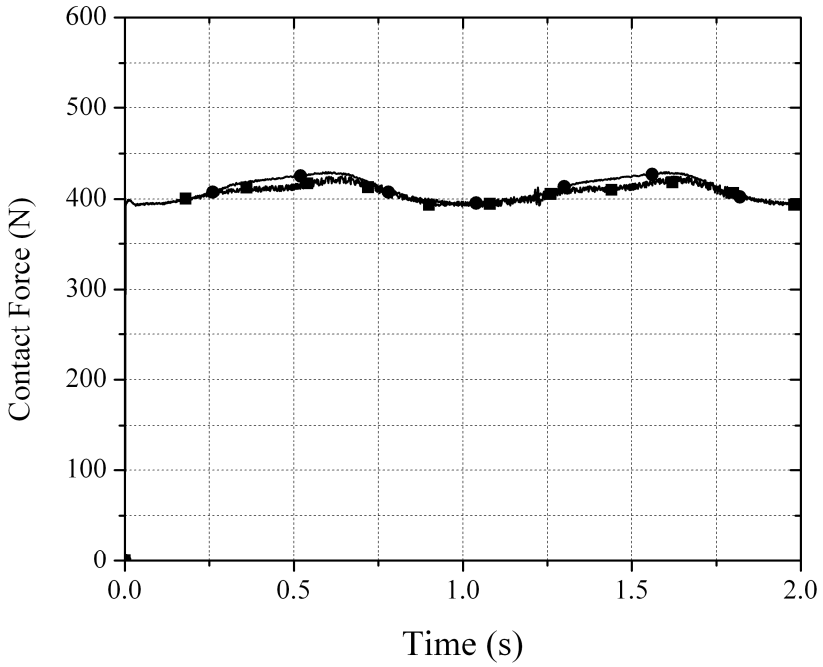

Figure 33 Normal contact forces for contact 1
(—■— Cross section frame, —●— Tangent frame)

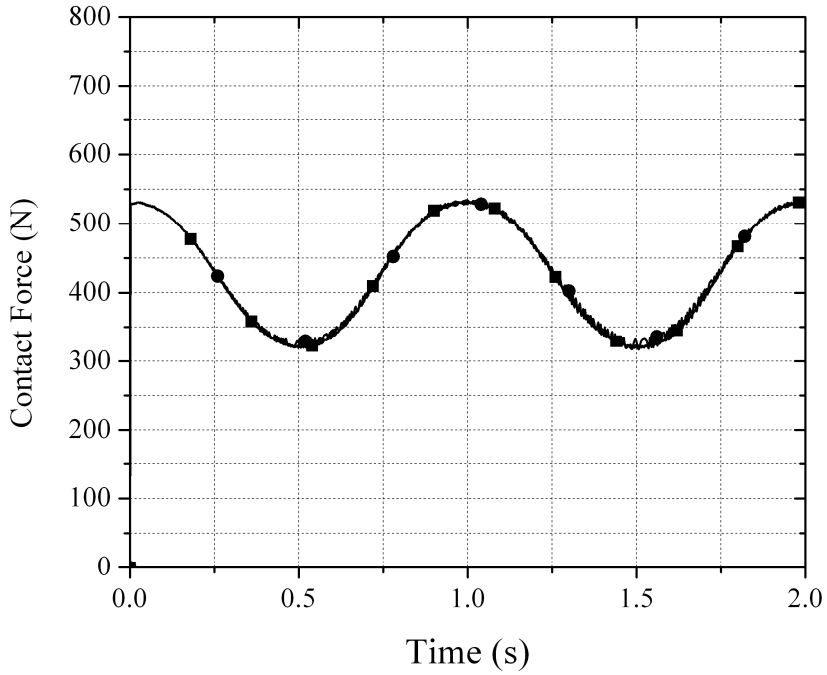

Figure 34 Normal contact forces for contact 2
(—■— Cross section frame, —●— Tangent frame)

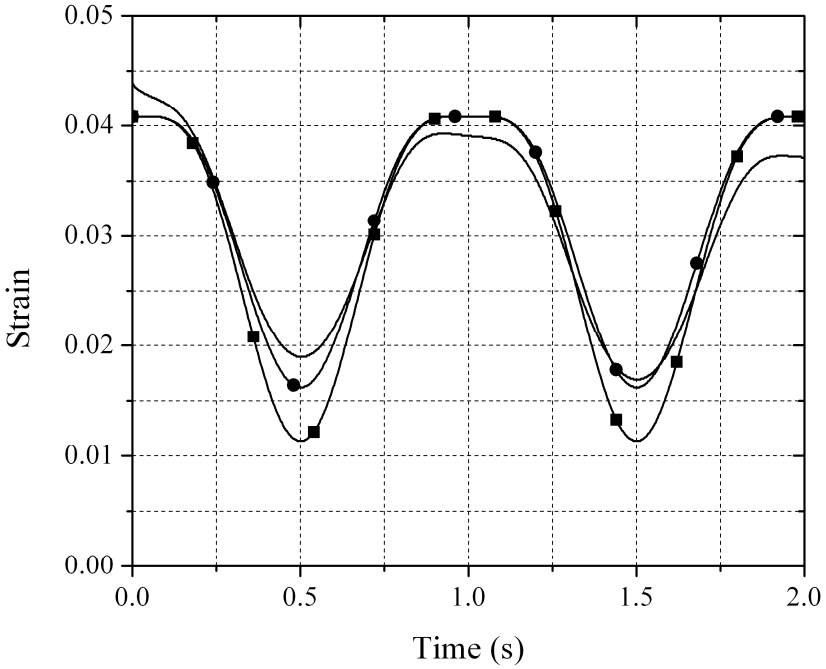

Figure 35 Axial strain of the MCL midpoint
(—■— cross section frame, —●— tangent frame, Ƶ fully clamped)

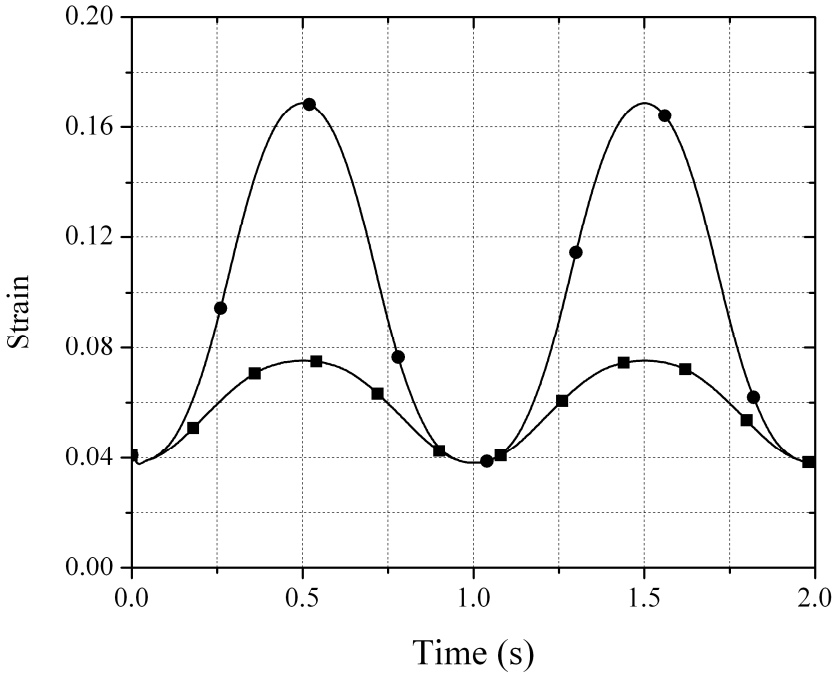

Figure 36 Axial strain of the LCL / femur insertion site
(—■— LCL tangent frame, —●— LCL cross section frame)

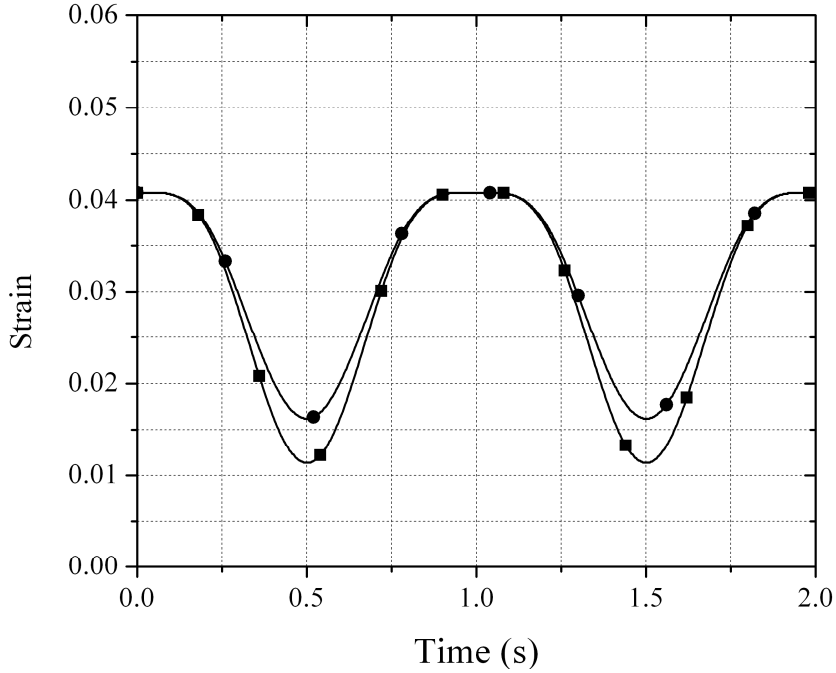

Figure 37 Axial strain of the MCL midpoint
(—■— MCL cross section frame, —●— MCL tangent frame)

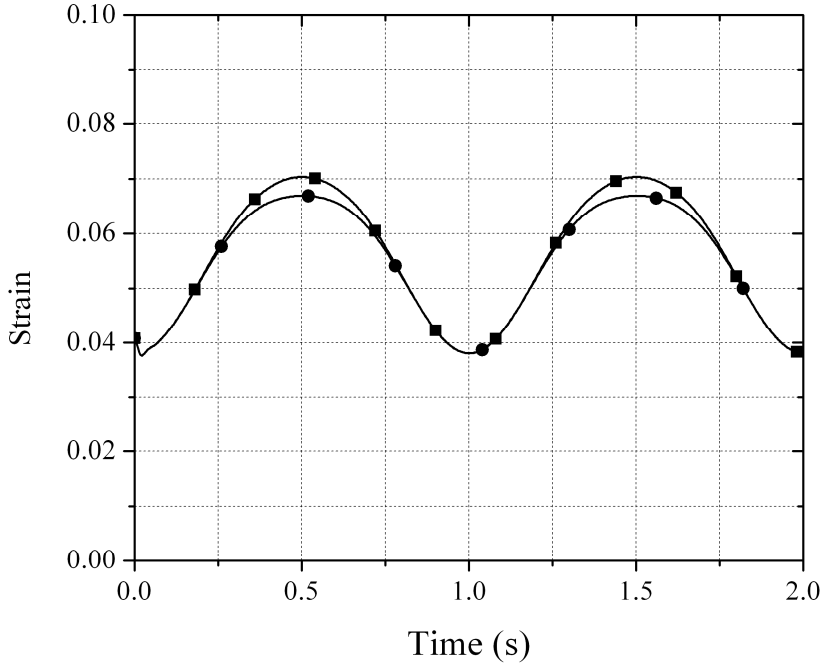

Figure 38 Axial strain of the LCL/fibula insertion site
(—■— LCL cross section frame, —●— LCL tangent frame)

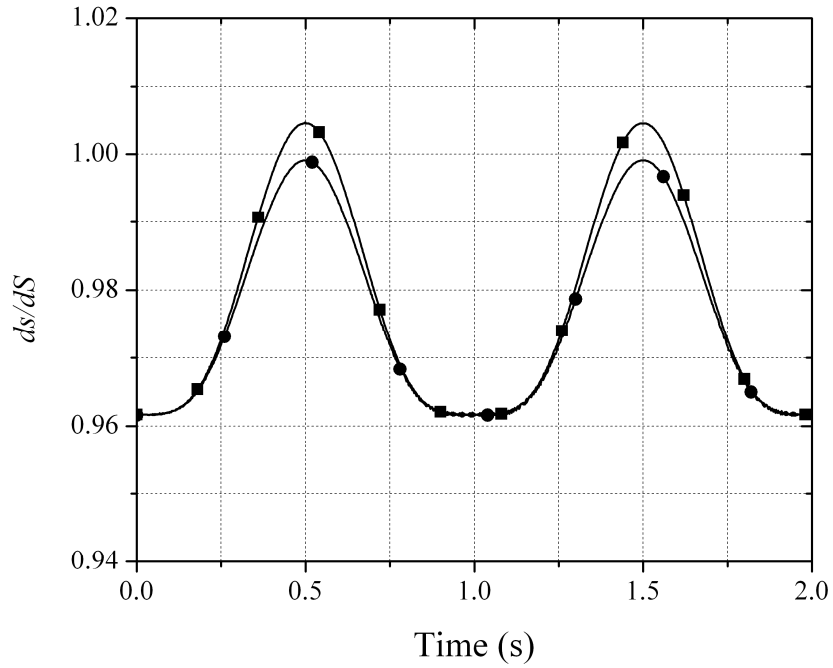

Figure 39 Deformation of the cross section area at the midpoint
(—■—MCL cross section frame, —●— MCL tangent frame)

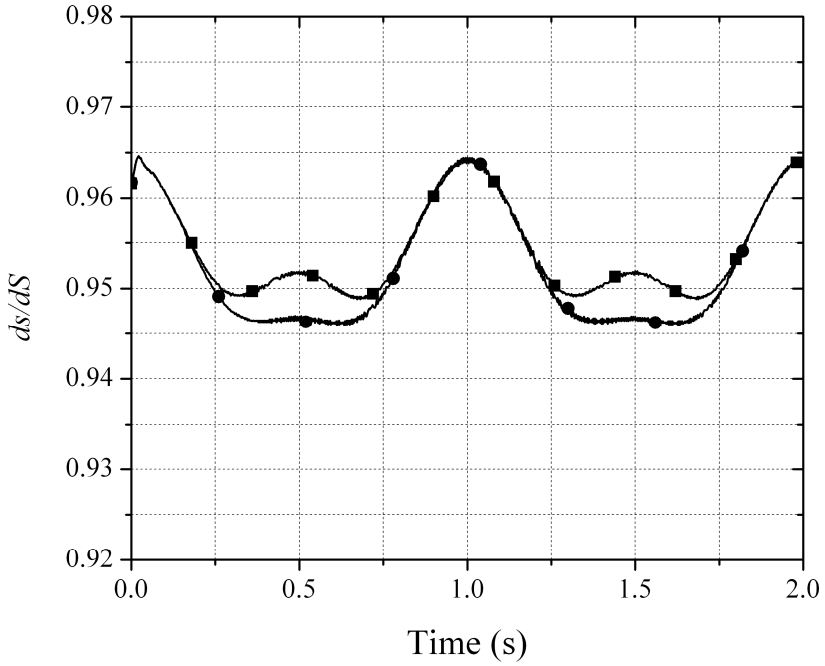

Figure 40 Deformation of the cross section area at the midpoint
(—■—LCL cross section frame, —●— LCL tangent frame)

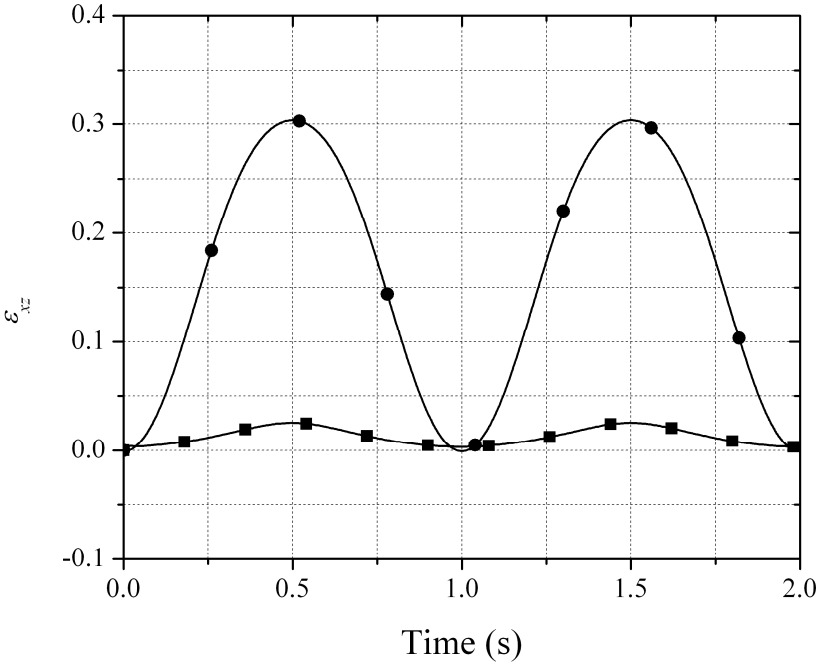

Figure 41 Shear strain $\mathcal{E}_{xz}$ at LCL femur insertion site
(—■—LCL cross section frame, —●— LCL tangent frame)

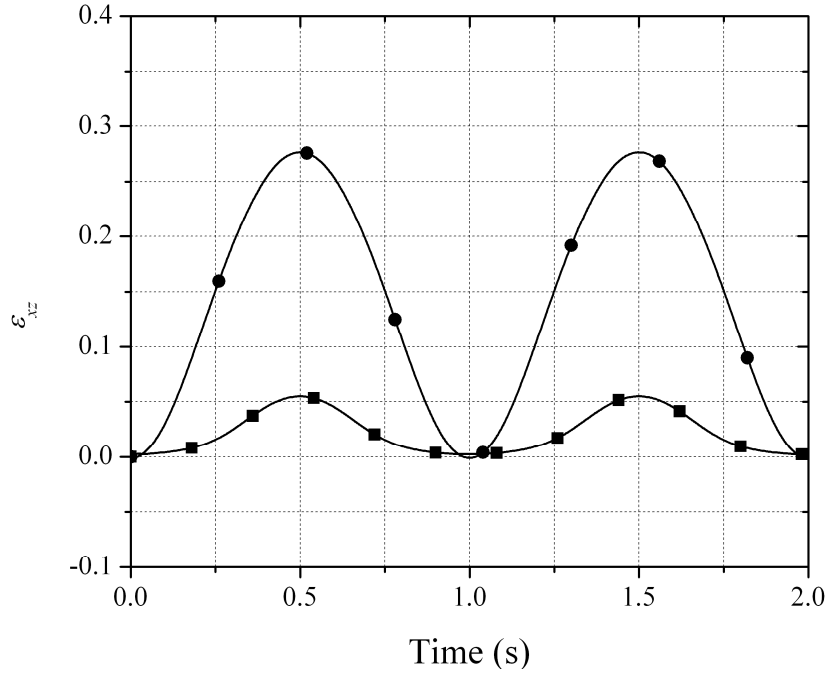

Figure 42 Shear strain $\mathcal{E}_{xz}$ at MCL femur insertion site
(—■—MCL cross section frame, —●— MCL tangent frame)

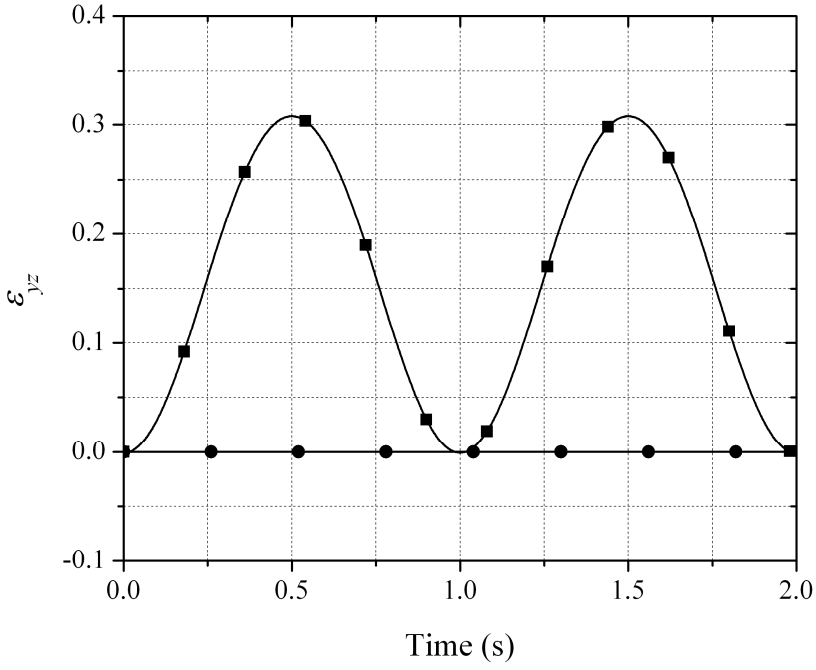

Figure 43 Shear strain $\mathcal{E}_{yz}$ at LCL femur insertion site
(—■—LCL cross section frame, —●— LCL tangent frame)

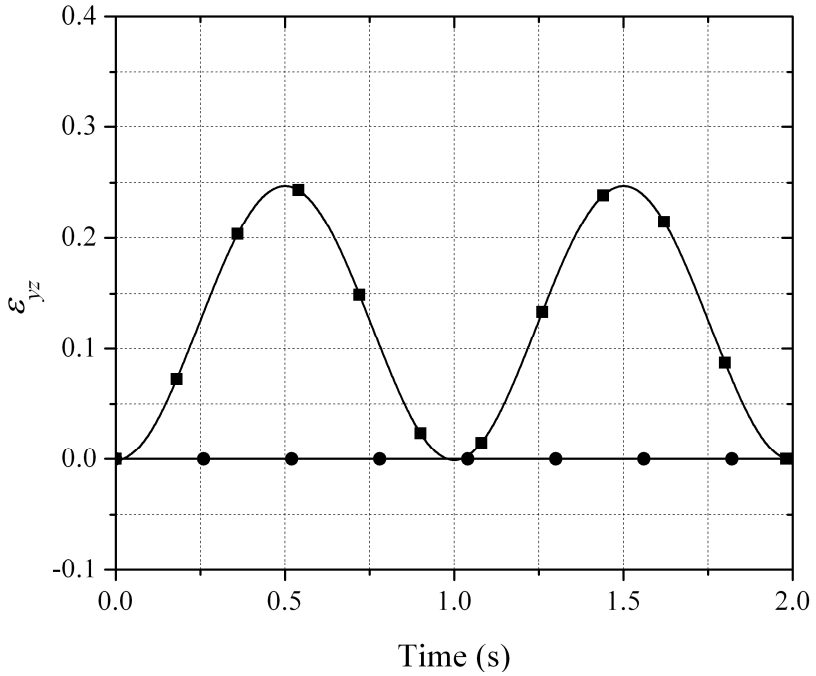

Figure 44 Shear strain $\mathcal{E}_{yz}$ at MCL femur insertion site
(—■—MCL cross section frame, —●— MCL tangent frame)

4.8. Concluding Remarks

In this chapter, the formulation of the boundary conditions of the partially clamped joint is investigated using two different models that employ the cross section and the tangent frames. The fully parameterized ANCF beam element, which allows for the deformation of the cross section, is employed in this investigation with the human knee joint as an example. The fully clamped joint does not allow for the cross section deformation, while the partially clamped joint allows for the cross section deformation at the ligament/bone insertion site. This cross section deformation can be measured using Nansonôs formula. The numerical results demonstrate that the new computational finite element/multibody system framework using the simplified knee model with either the cross section frame or tangent frame can yield useful data in regard to the change in length and strains of either the LCL or MCL. The data shows higher strains for both ligaments than the quasi-static finite element models reported in the literature (Weiss et al., 2001; Peña et al., 2006). The higher strains are the result of the integration of the fully parameterized ANCF beam finite element model and contact constraint formulation into a dynamic multibody computational framework that captures the large displacement and change in the ligament cross section resulting from the prescribed cyclic motion. Also, the use of the constraint contact formulation, the pretension in the cruciate ligaments and the fact that the knee joint model used in this study is not symmetric, have an important effect on the strains obtained in this chapter.

In general, the tangent frame and the cross-section frame are not the same and they differ due to the rotation of the cross-section as the result of the shear and torsion effects. In most applications, the difference is small, permitting without producing significant errors the use of

either frame. Nonetheless, the results of the example used in this investigation show that the cross section frame has a better convergence characteristics as compared to the tangent frame.

CHAPTER 5

CROSS SECTION DEFORMATION

Most existing beam formulations assume that the cross section of the beam remains rigid regardless of the amplitude of the displacement. The *absolute nodal coordinate formulation* (ANCF), however, allows for the deformation of the cross section and leads to a more general beam models that capture the coupling between different modes of displacement. This chapter examines the effect of the order of interpolation on the modes of deformation of the beam cross section using ANCF finite elements. To this end, a new two-dimensional shear deformable ANCF beam element is developed. The new finite element employs a higher order of interpolation, and allows for new cross section deformation modes that cannot be captured using previously developed shear deformable ANCF beam elements. The element developed in this study relaxes the assumption of planar cross section; thereby allowing for including the effect of warping as well as for different stretch values at different points on the element cross section. The displacement field of the new element is assumed to be cubic in the axial direction and quadratic in the transverse direction. Using this displacement field, more expressions for the element extension, shear and the cross section stretch can be systematically defined. Measures of the shear angle, extension, and cross section stretch can also be systematically defined using coordinate systems defined at the element material points. Using these local coordinate systems, expressions for a nominal shear angle are obtained. The differences between the cross section deformation modes obtained using the new higher order element and those obtained using the previously developed lower order elements are highlighted. Numerical examples are presented in

order to compare the results obtained using the new finite element and the results obtained using previously developed ANCF finite elements.

5.1. Background

Before introducing the higher order TDBE16, the TDBE12 that will be used in the comparative study presented in this chapter is first reviewed in this section.

5.1.2. TDBE12 Displacement Field

The planar shear deformable TDBE12 displacement field is cubic in the longitudinal coordinate x and linear in the transverse coordinate y. The displacement field of this ANCF finite element is defined as (Omar and Shabana, 2001; Shabana, 2008)

$$\mathbf{r} = \begin{bmatrix} a_0 + a_1 x + a_2 y + a_3 xy + a_4 x^2 + a_5 x^3 \\ b_0 + b_1 x + b_2 y + b_3 xy + b_4 x^2 + b_5 x^3 \end{bmatrix} \tag{5.1}$$

where $\mathbf{r}$ is the global position vector of an arbitrary point on the finite element, a_i and b_i (i=0,1,é ,5) are the polynomial coefficients, and x and y are the coordinates defined in the beam coordinate system. The coordinates of each node of this shear deformable element consist of one position vector and two gradient vectors. For node k, these coordinates are defined as

$$\mathbf{e}^k = \left[\left(\mathbf{r}^k\right)^T \ \left(\mathbf{r}_{,x}^k\right)^T \ \left(\mathbf{r}_{,y}^k\right)^T \right]^T \tag{5.2}$$

where $\mathbf{e}^k$ is the nodal coordinate vector at node k, $\mathbf{r}^k$ is the global position vector of node k and $\mathbf{r}_{,x}^k = \partial \mathbf{r}^k / \partial x$ and $\mathbf{r}_{,y}^k = \partial \mathbf{r}^k / \partial y$ define the position vector gradients. Using the preceding two equations, one can write the global position vector as $\mathbf{r} = \mathbf{S}(x, y)\mathbf{e}(t)$; where

$\mathbf{e} = \left[(\mathbf{e}^k)^T \quad (\mathbf{e}^{(k+1)})^T \right]^T$ is the vector of the element nodal coordinates, t is time, and $\mathbf{S}$ is the element shape function matrix defined as

$$\mathbf{S} = \left[s_1\mathbf{I} \quad s_2\mathbf{I} \quad s_3\mathbf{I} \quad s_4\mathbf{I} \quad s_5\mathbf{I} \quad s_6\mathbf{I} \right] \tag{5.3}$$

where $\mathbf{I}$ is a 2×2 identity matrix, and the shape functions s_i (i=1,2,é ,6) are defined as

$$\left.\begin{array}{lll} s_1 = 1-3\xi^2+2\xi^3 & s_2 = l(\xi-2\xi^2+\xi^3) & s_3 = l(\eta-\xi\eta) \\ s_4 = 3\xi^2-2\xi^3 & s_5 = l(-\xi^2+\xi^3) & s_6 = l\xi\eta \end{array}\right\} \tag{5.4}$$

and, $\xi = x/l, \eta = y/l$, l is the length of the element in the reference configuration (Omar and Shabana, 2001).

5.1.3. Gradients and Element Cross Section

As previously mentioned, the TDBE12 displacement field is linear in the transverse coordinate y, and consequently, the gradient vector $\mathbf{r}_{,y}$ defines the orientation of the element cross section. Furthermore, the cross section remains planar despite the fact that the element displacement allows for the cross section stretch. Nonetheless, this stretch does not depend on the location of the material points on the cross section. The TDBE gradient vectors are defined as

$$\begin{aligned} \mathbf{r}_{,x} &= \begin{bmatrix} a_1 + a_3 y + 2a_4 x + 3a_5 x^2 \\ b_1 + b_3 y + 2b_4 x + 3b_5 x^2 \end{bmatrix} \\ &= \left[s_{1,x}\mathbf{I} \quad s_{2,x}\mathbf{I} \quad s_{3,x}\mathbf{I} \quad s_{4,x}\mathbf{I} \quad s_{5,x}\mathbf{I} \quad s_{6,x}\mathbf{I} \right]\mathbf{e} \end{aligned} \tag{5.5}$$

and

$$\mathbf{r}_{,y} = \begin{bmatrix} a_2 + a_3 x \\ b_2 + b_3 x \end{bmatrix} = \left[\mathbf{0} \quad \mathbf{0} \quad s_{3,y}\mathbf{I} \quad \mathbf{0} \quad \mathbf{0} \quad s_{6,y}\mathbf{I} \right]\mathbf{e} \tag{5.6}$$

It is clear from these two equations that the TDBE12 gradient vector $\mathbf{r}_{,x}$ is linear in the transverse coordinate y, and since the position vector can be written as $\mathbf{r} = (\mathbf{r})_c + y\mathbf{r}_{,y}$, the gradient $\mathbf{r}_{,y}$ defines the TDBE12 cross section, where $(\mathbf{r})_c = \mathbf{r}(y=0)$. The gradient vector $\mathbf{r}_{,y}$ enters into the definition of the matrix of position vector gradients and the Green-Lagrange strain tensor. Therefore, the order of interpolation of this gradient vector will have an effect on various strain measures as will be discussed in this section.

5.1.4. Local Measures and Comparison with Timoshenko Beam

In Timoshenko beam theory, the cross section remains rigid and planar, that is, cross section stretch is not allowed. The rotation of the cross section α with respect to a line perpendicular to the centerline defines the shear angle. Using TDBE12 gradients, the shear angle of Timoshenko beam theory at an arbitrary point x on the element centerline is defined as $\alpha(x) = -\sin^{-1}\left(\left(\check{\mathbf{E}}_{,x}^T\right)_c \check{\mathbf{E}}_{,y}\right)$, where $(\ )_c$ implies points at the element centerline $(y=0)$. This equation shows that the shear in Timoshenko beam theory is independent of the transverse coordinate y. When ANCF TDBE12 is used, the shear measure is defined in terms of $\check{\mathbf{E}}_{,x}^T\check{\mathbf{E}}_{,y}$ which is function of y as well as x; and different point on the cross section have different shear values.

The assumption of the cross section rigidity in Timoshenko beam theory does not allow for stretch in the direction of the y coordinate. This stretch effect can be captured by ANCF finite elements. In the case of ANCF finite elements, the stretch measure is function of $\mathbf{r}_{,y}^T\mathbf{r}_{,y}$ which is the square of the magnitude of the gradient vector $\mathbf{r}_{,y}$. Nonetheless, for the TDBE12,

this stretch measure for a given x is constant along cross section lines and it is independent of y.

As previously mentioned in this thesis, ANCF finite elements can also capture the change in the cross section area as defined by Nansonôs formula given by

$$da = \frac{J}{(\mathbf{n}^T \mathbf{J}\mathbf{J}^T \mathbf{n})^{1/2}} dA \tag{5.7}$$

where dA and da are the areas of an infinitesimal surface in the reference and current configurations, respectively; $\mathbf{n}$ is a unit normal to the surface; $\mathbf{J} = \begin{bmatrix} \mathbf{r}_{,x} & \mathbf{r}_{,y} \end{bmatrix}$ is the matrix of position vector gradients; and J is the determinant of $\mathbf{J}$. Since the TDBE12 cross section remains planar, $\mathbf{n}$ is independent of y, and $\mathbf{J}^T\mathbf{n}$ is linear in y; da/dA is independent of y in the case of TDBE12; that is, area ratios at all points of a cross section at fixed longitudinal coordinate x are the same. This fact is proved in Appendix B of the thesis.

5.2. Proposed New Shear Deformable Element

In this section, a new shear deformable ANCF finite beam element, TDBE16, is introduced. This element allows for the variation of the stretch along cross section lines, capturing warping modes of deformation, and allows for a more general description for the change of the cross section area. The results obtained using the proposed element will be compared with the results obtained using TDBE12 in order to validate the new element and also in order to demonstrate the fundamental difference between the TDBE12 and TDBE16.

5.2.1. TDBE16 Displacement Field

In order to allow for warping of the cross section and for the variation of the stretch along cross section lines, the use of the following displacement field is proposed:

$$\mathbf{r} = \begin{bmatrix} a_0 + a_1 x + a_2 y + a_3 xy + a_4 x^2 + a_5 x^3 + a_6 x^2 (y - 3y^2) + a_7 x^3 y \\ b_0 + b_1 x + b_2 y + b_3 xy + b_4 x^2 + b_5 x^3 + b_6 x^2 (y - 3y^2) + b_7 x^3 y \end{bmatrix} \tag{5.8}$$

where $\mathbf{r}$ is the global position vector of an arbitrary point P on the element as shown in Figure 45, a_i and b_i (i=0,1,é ,7) are the polynomial coefficients. For this element, the following vector of nodal coordinates $\mathbf{e}^k$ is used at node k:

$$\mathbf{e}^k = \left[\left(\mathbf{r}^k\right)^T \ \left(\mathbf{r}^k_{,x}\right)^T \ \left(\mathbf{r}^k_{,y}\right)^T \ \left(\mathbf{r}^k_{,xy}\right)^T \right]^T \tag{5.9}$$

where, as in the TDBE12 model, $\mathbf{r}^k$ is the global position vector of node k, and $\mathbf{r}^k_{,x} = \partial \mathbf{r}^k / \partial x$, $\mathbf{r}^k_{,y} = \partial \mathbf{r}^k / \partial y$ and $\mathbf{r}^k_{,xy} = \partial^2 \mathbf{r}^k / \partial x \partial y$ define the position vector gradients at node k.

The TDBE16 has additional vector, $\mathbf{r}^k_{,xy}$, in the nodal coordinates since higher order of interpolation is used. Using the two preceding equations, the element shape function matrix $\mathbf{S}$ can be defined as

$$\mathbf{S} = \begin{bmatrix} s_1 \mathbf{I} & s_2 \mathbf{I} & s_3 \mathbf{I} & s_4 \mathbf{I} & s_5 \mathbf{I} & s_6 \mathbf{I} & s_7 \mathbf{I} & s_8 \mathbf{I} \end{bmatrix} \tag{5.10}$$

where, the shape functions s_i (i=1,2,é ,8) can be written as

$$\left.\begin{array}{ll} s_1 = 1 - 3\xi^2 + 2\xi^3 & s_2 = l(\xi - 2\xi^2 + \xi^3) \\ s_3 = l(\eta - 3\xi^2\eta + 9l\xi^2\eta^2 + 2\xi^3\eta) & s_4 = l^2(\xi\eta - 2\xi^2\eta + 6l\xi^2\eta^2 + \xi^3\eta) \\ s_5 = 3\xi^2 - 2\xi^3 & s_6 = l(-\xi^2 + \xi^3) \\ s_7 = l(3\xi^2\eta - 9l\xi^2\eta^2 - 2\xi^3\eta) & s_8 = l^2(-\xi^2\eta + 3l\xi^2\eta^2 + \xi^3\eta) \end{array}\right\} \tag{5.11}$$

Note that s_1, s_2, s_5 and s_6 are the same as those of the TDBE12. Nonetheless, some of the TDBE16 shape functions such as s_3, s_4, s_7, and s_8 are quadratic in η, while TDBE12 shape functions are only linear in η. It follows that the TDBE16 transverse gradient vector $\mathbf{r}_{,y}$ can capture quadratic cross section strain variations. It is also important to mention that a standard finite element assembly process will ensure continuity of the curvature vector $\mathbf{r}_{,xy}$ for the TDBE16, while this continuity is not guaranteed in the case of the TDBE12 models.

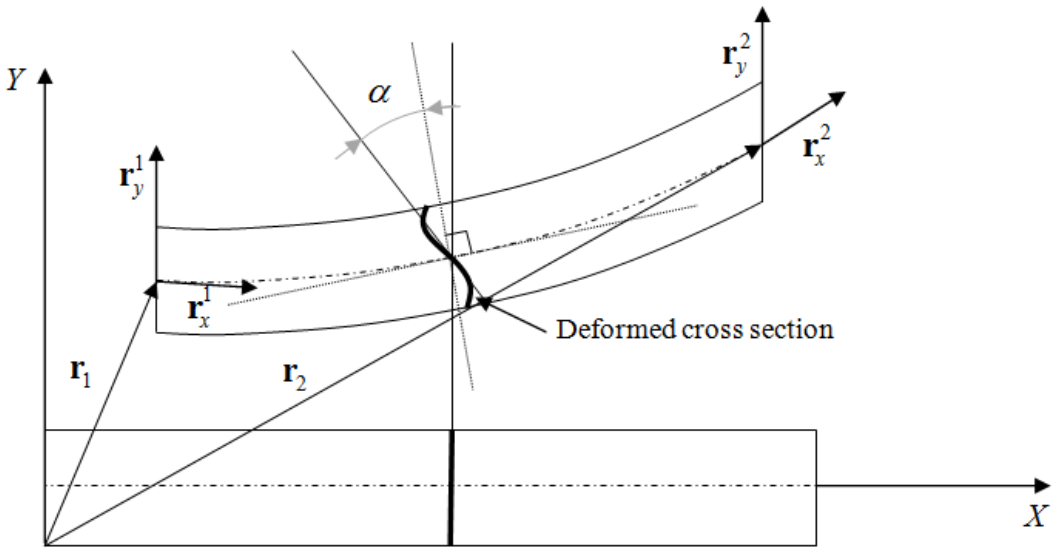

Figure 45 Undeformed and deformed beam configurations

5.2.2. TDBE16 Gradient Vectors

As previously mentioned, the proposed new ANCF finite element is cubic in x and quadratic in y. The gradient vectors of the element are defined as

$$\begin{aligned}\mathbf{r}_{,x} &= \begin{bmatrix} a_1 + a_3 y + 2a_4 x + 3a_5 x^2 + 2a_6 x(y - 3y^2) + 3a_7 x^2 y \\ b_1 + b_3 y + 2b_4 x + 3b_5 x^2 + 2b_6 x(y - 3y^2) + 3b_7 x^2 y \end{bmatrix} \\ &= \begin{bmatrix} s_{1,x}\mathbf{I} & s_{2,x}\mathbf{I} & s_{3,x}\mathbf{I} & s_{4,x}\mathbf{I} & s_{5,x}\mathbf{I} & s_{6,x}\mathbf{I} & s_{7,x}\mathbf{I} & s_{8,x}\mathbf{I} \end{bmatrix} \mathbf{e}\end{aligned} \tag{5.12}$$

and

$$\begin{aligned}\mathbf{r}_{,y} &= \begin{bmatrix} a_2 + a_3 x + a_6 x^2 (1 - 6y) + a_7 x^3 \\ b_2 + b_3 x + b_6 x^2 (1 - 6y) + b_7 x^3 \end{bmatrix} \\ &= \begin{bmatrix} \mathbf{0} & \mathbf{0} & s_{3,y}\mathbf{I} & s_{4,y}\mathbf{I} & \mathbf{0} & \mathbf{0} & s_{7,y}\mathbf{I} & s_{8,y}\mathbf{I} \end{bmatrix} \mathbf{e}\end{aligned} \tag{5.13}$$

The derivatives of the shape functions that appear in the preceding two equations are

$$\left.\begin{aligned} &s_{1,x} = 6l^{-1}\left(-\xi + \xi^2\right), \quad s_{2,x} = 1 - 4\xi + 3\xi^2, \quad s_{3,x} = -6\xi\eta + 18l\xi\eta^2 + 6\xi^2\eta \\ &s_{4,x} = l\eta - 4l\xi\eta + 12l^2\xi\eta^2 + 3l\xi^2\eta, \quad s_{5,x} = 6l^{-1}\left(\xi - \xi^2\right), \quad s_{6,x} = -2\xi + 3\xi^2 \\ &s_{7,x} = 6\xi\eta - 18l\xi\eta^2 - 6\xi^2\eta, \qquad s_{8,x} = -2l\xi\eta + 6l^2\xi\eta^2 + 3l\xi^2\eta \\ &s_{3,y} = 1 - 3\xi^2 + 18l\xi^2\eta + 2\xi^3, \qquad s_{4,y} = l\xi - 2l\xi^2 + 12l^2\xi^2\eta + l\xi^3 \\ &s_{7,y} = 3\xi^2 - 18l\xi^2\eta - 2\xi^3, \qquad s_{8,y} = -l\xi^2 + 6l^2\xi^2\eta + l\xi^3 \end{aligned}\right\} \tag{5.14}$$

Note that in the case of the TDBE16 model, $\mathbf{r}_{,y}$ becomes dependent on the transverse coordinate y and is quadratic in the longitudinal coordinate x.

5.2.3. Local Measures and Comparison with TDBE12

The fact that the TDBE16 gradient vector $\mathbf{r}_{,y}$ can vary linearly with respect to y and quadratic with respect to x regardless of the load applied makes the new element fundamentally different from TDBE12. The TDBE16 cross section is no longer defined by the vector $\mathbf{r}_{,y}$ because of the warping effect, the stretch of the TDBE16 is no longer constant along the cross section lines, and Nansonôs formula leads to different area ratios for different values for the TDBE16 transverse coordinate y. The global position of an arbitrary point on the TDBE16 can be written as $\mathbf{r} = (\mathbf{r})_c + y\mathbf{r}_{,y} + \mathbf{h}$, where $(\mathbf{r})_c = \mathbf{r}(y=0)$, and $\mathbf{h} = 3x^2y^2 \begin{bmatrix} a_6 & b_6 \end{bmatrix}^T$. Because of the TDBE16 kinematic description, the definition of the shear angle used in Timoshenko beam theory is not straight forward as in the case of the TDBE12 element in which the cross section remains planar.

5.3. Average Measures

While a general continuum mechanics approach based on the Green-Lagrange strain tensor definition is used in this investigation to define the element elastic forces, it is sometimes convenient to introduce coordinate systems that can be used to define average kinematic measures, instead of the local measures. These coordinate systems, which do not affect the definition of the Green-Lagrange strains, can be used to define nominal cross section planes that can be used to define nominal measures. Furthermore, these coordinate systems enter into the formulation of the joints in multibody system (MBS) applications. Therefore, it is also important to understand the basic differences in the definitions of these frames when different finite elements are used. To this end, two different frames; the *tangent frame* and the *cross section*

frame; that are often used in flexible MBS applications are discussed in this section. The analysis presented in this section will also shed more light on the fundamental differences between the two ANCF elements considered in this investigation.

5.3.1. Tangent Frame

The axes of the tangent frame at an arbitrary point on the element centerline is defined by the columns of the transformation matrix $\mathbf{A}^t$. This matrix is the same as the orthogonal matrix $\mathbf{Q}$ that appears in the **QR** decomposition of the matrix of the position vector gradients $\mathbf{J}$, where $\mathbf{R}$ is an upper-triangular matrix (Sugiyama et al., 2006). Therefore, in the case of the tangent frame, $\mathbf{A}^t = \mathbf{Q}$. The vector tangent to the beam centerline can be defined as $\mathbf{i}^t = \begin{bmatrix} i_1^t & i_2^t \end{bmatrix}^T = \mathbf{r}_{,x} \big/ \left|\mathbf{r}_{,x}\right|$, while the vector normal to the beam centerline is $\mathbf{j}^t = \begin{bmatrix} -i_2^t & i_1^t \end{bmatrix}^T$. The two orthogonal vectors $\mathbf{i}^t$ and $\mathbf{j}^t$ define the columns of the transformation matrix $\mathbf{A}^t = \begin{bmatrix} \mathbf{i}^t & \mathbf{j}^t \end{bmatrix}$. The matrix of position vectors gradients can then be expressed as $\mathbf{J} = \mathbf{A}^t \mathbf{U}^t$, where $\mathbf{U}^t$ is an upper-triangular stretch matrix defined as

$$\mathbf{U}^t = \left(\mathbf{A}^t\right)^T \mathbf{J} = \begin{bmatrix} \mathbf{i}^{t^T} \\ \mathbf{j}^{t^T} \end{bmatrix} \begin{bmatrix} \mathbf{r}_{,x} & \mathbf{r}_{,y} \end{bmatrix} = \begin{bmatrix} \mathbf{i}^{t^T}\mathbf{r}_{,x} & \mathbf{i}^{t^T}\mathbf{r}_{,y} \\ 0 & \mathbf{j}^{t^T}\mathbf{r}_{,y} \end{bmatrix} \tag{5.15}$$

In the case of Euler-Bernoulli beam theory, $\mathbf{U}^t$ reduces to a diagonal matrix since the cross section remains orthogonal to the beam centerline. Note also that the Green-Lagrange strain tensor can still be expressed in terms of $\mathbf{U}^t$ as $\boldsymbol{\varepsilon} = \left(\mathbf{J}^T\mathbf{J} - \mathbf{I}\right)\big/2 = \left(\mathbf{U}^{t^T}\mathbf{U}^t - \mathbf{I}\right)\big/2$; and $\mathbf{U}^t$ reduces to the identity matrix in the case of rigid body motion.

In the case of Timoshenko beam theory, the off-diagonal upper-triangular element in $\mathbf{U}^t$ is $\mathbf{i}^{t^T}\mathbf{r}_{,y} = \cos\left(\alpha + (\pi/2)\right)$, where α is the shear angle; while the diagonal element $\mathbf{j}^{t^T}\mathbf{r}_{,y}$ is equal to one since the cross section remains rigid and planar. The diagonal element $\mathbf{i}^{t^T}\mathbf{r}_{,x}$, however, can be used to measure the extension of the beam and this element is equal to $\sqrt{2\varepsilon_{xx} - 1}$, where ε_{xx} is the normal Lagrangian strain associated with the longitudinal coordinate line.

In the case of the TDBE12, a measure of the Timoshenko shear angle α can be obtained using the equation $\mathbf{i}^{t^T}\check{\mathbf{E}}_{,y} = \cos\left(\alpha + (\pi/2)\right)$, where $\check{\mathbf{E}}_{,y}$ is a unit vector along $\mathbf{r}_{,y}$. In this case, the cross section remains planar and $\mathbf{r}_{,y}$ is independent of y. In the more general TDBE16 case, $\mathbf{r}_{,y}$ and $\check{\mathbf{E}}_{,y}$ depend on the transverse coordinate y, and therefore, one cannot in general determine an equivalent to the shear angle used in Timoshenko beam theory. For instance, $\mathbf{i}^{t^T}\left(\check{\mathbf{E}}_{,y}\right)_c = \cos\left(\alpha_c + (\pi/2)\right)$ defines a shear angle at the element centerline, where subscript c refers to variables and vectors at $y = 0$. Furthermore, the element $\mathbf{i}^{t^T}\check{\mathbf{E}}_{,y}$ of the matrix $\mathbf{U}^t$, as well as the Lagrangian shear strain ε_{xy}, remains the same for all values of the transverse coordinate y, while these terms do not remain constant in the more general TDBE16 model. Similar comments apply to the diagonal element $\mathbf{j}^{t^T}\mathbf{r}_{,y}$ of $\mathbf{U}^t$ and the normal Lagrangian strain ε_{yy}. Note that this component of normal strain cannot be captured by Timoshenko beam theory.

The TDBE12 and TDB16 axial strain distributions along the coordinate line y are different, and both are significantly different from the distribution used in Euler-Bernoulli and Timoshenko beam theories. This is clear from the definition of the displacement field of the two

ANCF finite elements and the diagonal element $\mathbf{i}^{t^T}\mathbf{r}_{,x}$ of the stretch matrix $\mathbf{U}^t$. This diagonal element defines the axial Lagrangian strain ε_{xx}. In both TDBE12 and TDBE16 models, ε_{xx} is not restricted to a linear strain distribution along y; it is quadratic in the TDBE12 case, and of fourth order in the TDBE16 case.

5.3.2. Cross Section Frame

In the case of the cross section frame, the transverse axis is defined as $\mathbf{j}^c = [j_1^c \quad j_2^c]^T = \left(\mathbf{r}_{,y}\right)_c \Big/ \left|\left(\mathbf{r}_{,y}\right)_c\right|$, and the vector normal to $\mathbf{j}^c$ is $\mathbf{i}^c = \begin{bmatrix} j_2^c & -j_1^c \end{bmatrix}$. The two orthogonal vectors $\mathbf{i}^c$ and $\mathbf{j}^c$ define the axes of a coordinates system called cross section frame. This frame is defined by the transformation matrix $\mathbf{A}^c = \begin{bmatrix} \mathbf{i}^c & \mathbf{j}^c \end{bmatrix}$. The matrix of position vectors gradients can be expressed as $\mathbf{J} = \mathbf{A}^c\mathbf{U}^c$, where

$$\mathbf{U}^c = \begin{bmatrix} \mathbf{i}^{cT}\mathbf{r}_{,x} & 0 \\ \mathbf{j}^{cT}\mathbf{r}_{,x} & \mathbf{j}^{cT}\mathbf{r}_{,y} \end{bmatrix} \tag{5.16}$$

In the TDBE12 model, as previously mentioned, $\mathbf{r}_{,y}$ is independent of y, and this gradient vector defines the element cross section. In this case, an angle equivalent to the shear angle used in Timoshenko beam theory can be defined using the equation $\mathbf{i}^{c^T}\left(\check{\mathbf{r}}_{,x}\right)_c = \cos\alpha_c$. Since in the TDBE16 model, $\left(\mathbf{r}_{,y}\right)_c$ does not define the element cross section, the shear angle α_c is not equivalent to that used in the Timoshenko beam theory. One can also use the elements of the stretch matrix $\mathbf{U}^c$ to demonstrate that the ANCF TDBE12 and TDBE16 models are more general as compared to the finite elements that are based on the Euler-Bernoulli and Timoshenko beam theories.

5.4. Equations of Motion and Warping

While TDBE12 and TDBE16 have two different displacement fields and employ different number of nodal coordinates, one can show that the two elements can correctly describe an arbitrary rigid body displacement. These displacement fields do not employ rotations as nodal coordinates, and therefore, can define a unique rotation field. The two elements also have a constant mass matrix, allow for the use of general constitutive equations and general continuum mechanics approach in formulating the elastic forces, and allow for capturing the coupling between the cross section deformation, and bending and extension of the finite element. Using the kinematic equations presented in this chapter, the equations of motion of the two finite elements can be written in the following form (Shabana, 2008):

$$\mathbf{M}\ddot{\mathbf{e}} = \mathbf{Q}_e \tag{5.17}$$

where $\mathbf{Q}_e$ is the element nodal force vector, $\mathbf{M} = \int_V \rho \mathbf{S}^T \mathbf{S} dV$ is the constant symmetric mass matrix, and ρ and V are, respectively, the element density and volume. The vector $\mathbf{Q}_e$ is a nonlinear function of the element nodal coordinates. In this chapter, a general continuum mechanics approach based on Green-Lagrange strain tensor and the second Piola-Kirchhoff stress tensor is used to formulate the generalized elastic forces associated with the finite element nodal coordinates. Because the mass matrix is constant, an LU factorization can be performed only once at the beginning of the simulation. Note that the dimensions of the vectors and mass matrix that appear in Equation 5.17 depend on the finite element used. Furthermore, because the two elements employ different order of interpolation along the y coordinates, exact integration in this direction requires the use of different numbers of integration points. Full integration is

used in the numerical results obtained using the two elements and presented in the following section. An explicit Adams predictor-corrector method with variable order and variable step size is used in the direct numerical integration of the system equations of motion.

The effect of warping is included in some of the existing FE formulations by adding a warping function (Tsai et al., 2004; Yu et al, 2005). The warping function in these investigations does not capture other modes of deformations of the cross section; in some of these formulations which are implemented in commercial finite element codes, ε_{yy} is identically equal to zero, and therefore, the stretch of the cross section is not captured. Another example is Timoshenkoôs work on warping which assumes that the cross section second moment of area does not change during the deformation; an assumption which is relaxed when fully parameterized ANCF finite elements are used. Furthermore, in most (not all) existing beam formulations a stretch of the finite element does not lead to a reduction in the dimension of the cross section; and such an important mode of deformation among others is not captured. As an example, the work by Yu et al. (2005) is based on the classical beam theory and assumes that one covariant vector can be determined from the other two by using the cross product. This assumption is not used in fully parameterized ANCF beam elements that employ independent gradient vectors as nodal coordinates.

Most planar beam elements implemented in commercial codes do not account for the cross section deformation. For the most part, warping is considered for spatial elements to account for the coupling between torsional and bending deformations. While, the new element developed in this investigation is a planar element; the results obtained using this element are compared in the following section with the results obtained using a spatial element that accounts for warping. This spatial element is implemented in the general purpose FE commercial code ANSYS.

5.5. Numerical Results

In this section, the results obtained using the shear deformable beam element TDBE16 model are validated and compared with the results obtained using the TDBE12 model for different simulation scenarios of a free falling flexible pendulum under the effect of its weight. The nonlinear Green-Lagrange strain and the second Piola-Kirchhoff stress tensor are used with the Gauss integration technique to evaluate the nonlinear elastic forces. The principle of virtual work is utilized to define the generalized forces associated with the nodal coordinates (Shabana, 2008). The free falling two-dimensional pendulum is shown in Figure 46. The beam, which is assumed to have a square cross section, is connected to the ground by a pin joint; and has length of 1.2 m, a mass density of 5540 kg/m^3, Youngôs modulus $E = 7\times10^6$ N/m^2, and Poisson's ratio of 0.3. Two different beam models were considered in this study; the first model has 0.04×0.04 m^2 cross section area, while the second model has 0.02×0.02 m^2 cross section area. The beam shown in Figure 46 is assumed to be initially straight and horizontal and has zero initial velocity. The gravity constant is assumed to be 9.81m/s^2.

In the first model, the cross section area of the pendulum beam is chosen to be 0.04×0.04m^2. Figures 47-48 show, respectively, the tip point vertical displacement and midpoint transverse deformation obtained using the TDBE12 and TDBE16 models. These figures show that the TDBE12 and TDBE16 results are in a good agreement. Figure 49 shows the energy balance results obtained using the TDBE16 model. These results clearly show that the new finite element does not lead to a violation of the principle of work and energy. As previously mentioned in this chapter, the area ratio predicted by Nansonôs formula in the TDBE12 case remains constant along the y coordinate. This is not, however, the case when the TDBE16

model is used as demonstrated by the results presented in Figure 50. The results of this figure show that TDBE12 and TDBE16 results are in a good agreement at the element centerline, while the TDBE16 model predicts significantly different results away from the centerline. This change cannot be captured using Timoshenko beam or the TDBE12 models. Similar behavior is observed with the transverse strain ε_{yy}, as shown in Figure 51. As previously discussed in this chapter, ε_{yy} remains constant along y in the TDBE12 case, while the TDBE16 model captures warping and allow for the change of ε_{yy} along the coordinate line y. Figure 52 shows the nominal shear angle α_c as predicted by the two element models using the cross section frame. The transverse deformation results are obtained using 6 and 8 finite elements. Figures 53 and 54 show that in both TDBE12 and TDBE16 models, the 8-element solution itôs a convergent solution. For the area ratio results, however, 16 finite elements were required in order to achieve convergence.

In the second model, the cross section area of the pendulum is changed to 0.02×0.02 m^2. The tip vertical displacement and midpoint transverse deformation for both elements are shown in Figures 55-56. The TDBE16 energy balance for this model is shown in Figure 57. The area ratio and the normal strain ε_{yy} are shown in Figures 58 and 59. It is clear from the results presented in these two figures that the TDBE16 model captures again the change in these two measures in the case of thinner beams. Figure 60 shows the nominal shear angle α_c predicted by the two element models using the cross section frame.

Commercial FE codes have only spatial elements that account for the effect of warping. Some of these elements include the effect of warping by adding a seventh degree of freedom at

the node. While these elements do not capture all the modes of deformations captured by ANCF finite elements, a comparison is made with the BEAM188 element implemented in ANSYS. This element can have six or seven degrees of freedom per node; the seventh degree of freedom accounts for warping. BEAM188 is based on first order shear deformation theory (Timoshenko Beam theory). Figure 61 shows the vertical displacement of the tip point obtained using TDBE12, TDBE16, and ANSYS-BEAM188 elements. The results presented in this figure show a good agreement. Figure 62 show also a good agreement between the midpoint transverse deformation results obtained using the TDBE12, TDBE16 and ANSYS-BEAM188 models. It is important, however, to point out that the ANSYS-BEAM188 element, while it accounts for warping, does not capture the stretch of the cross section, and therefore, $\varepsilon_{yy} = 0$ for this element.

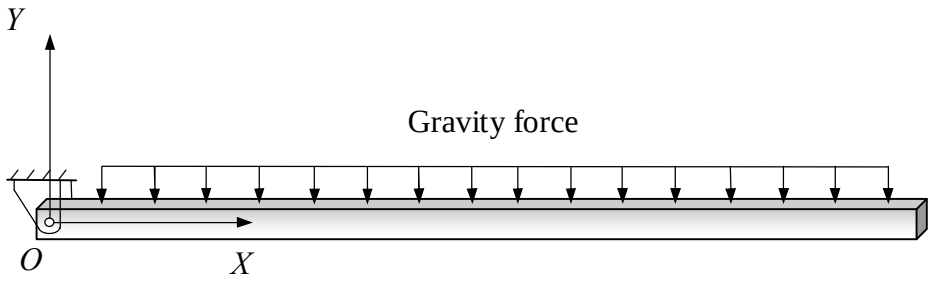

Figure 46 The free falling flexible pendulum

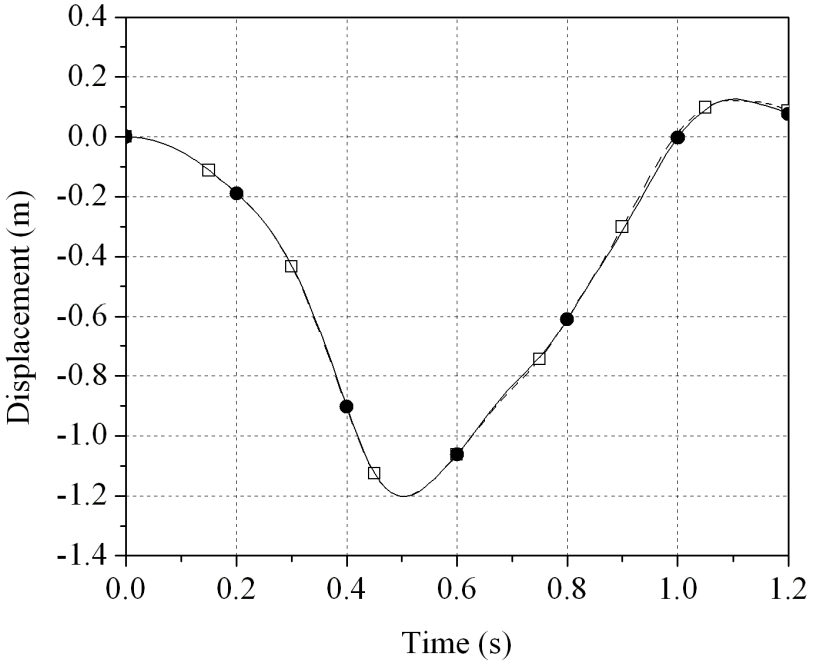

Figure 47 Tip vertical displacement for the 0.04×0.04 m^2 cross section model (--□-- TDBE12; —●— TDBE16)

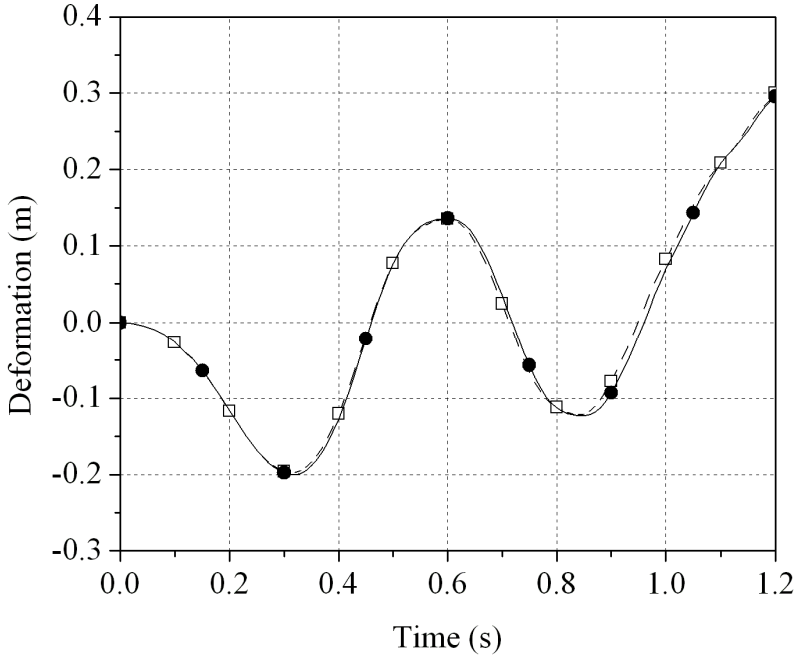

Figure 48 Midpoint transverse deformation for the 0.04×0.04 m^2 cross section model (--□-- TDBE12; —●— TDBE16)

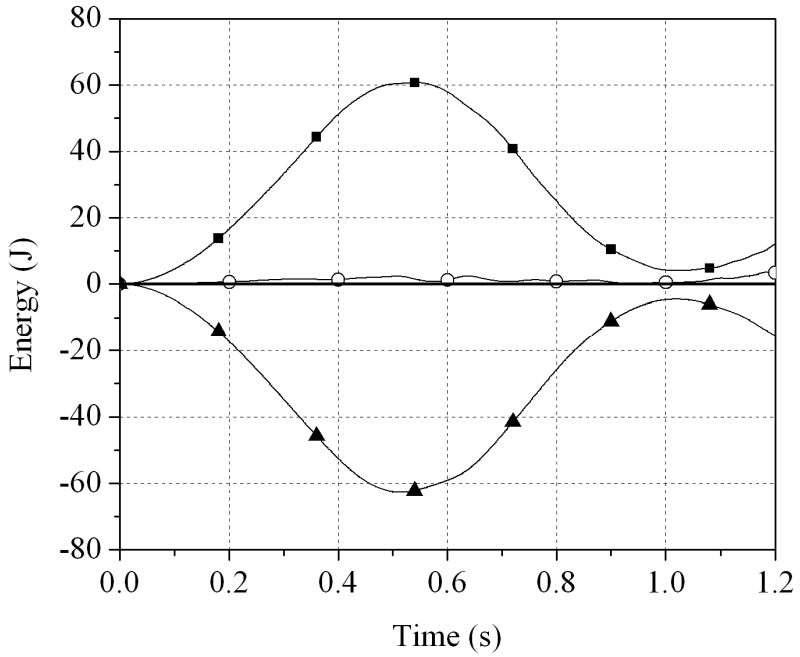

Figure 49 Energy balance for the 0.04×0.04 m^2 cross section TDBE16 model
(—■— kinetic energy; —○— elastic energy; —▲— potential energy; —— total energy)

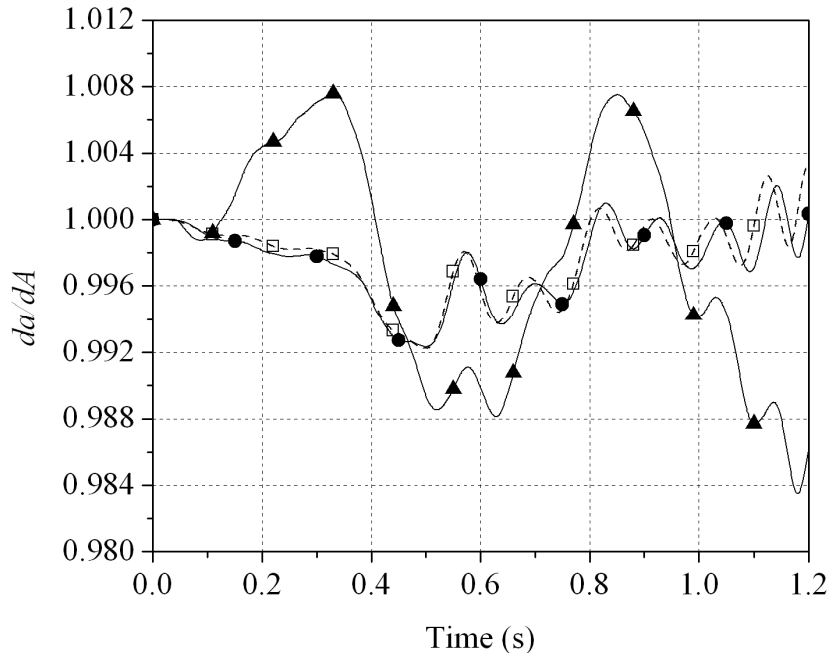

Figure 50 Area ratio at x = 0.6m for the 0.04×0.04 m^2 cross section model
(—□— TDBE12; —▲— y = 0.016m (TDBE16); —●— y = 0.0m (TDBE16))

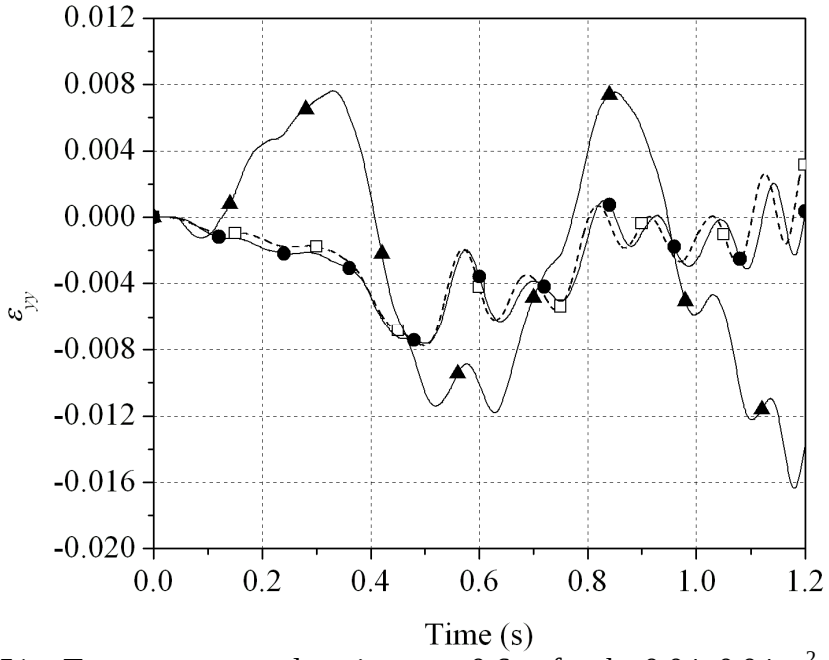

Figure 51 Transverse normal strain at x = 0.6 m for the 0.04×0.04 m^2 cross section (—□— TDBE12; —▲— y = 0.016 m (TDBE16); —●— y = 0.0 m (TDBE16))

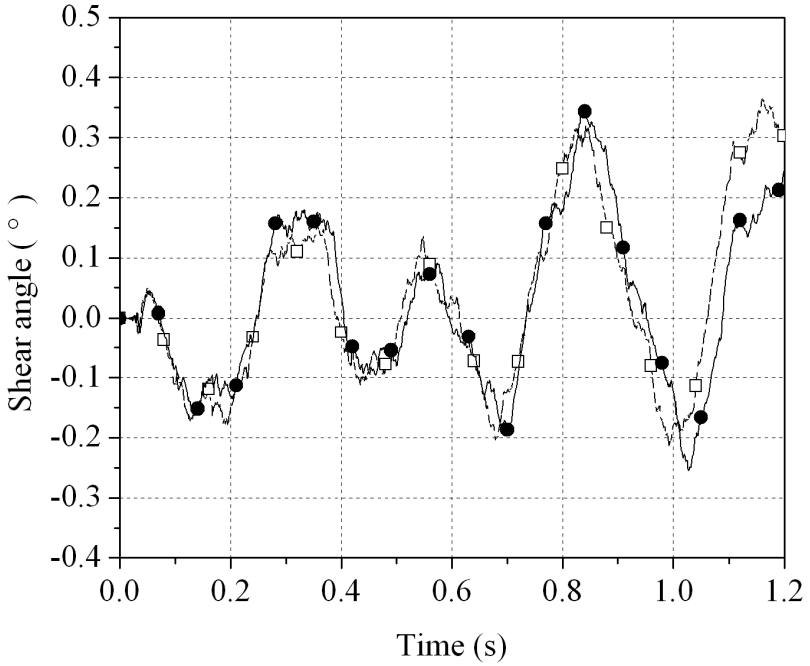

Figure 52 Midpoint shear angle of the 0.04×0.04 m^2 cross section model (--□-- TDBE12; —●— TDBE16)

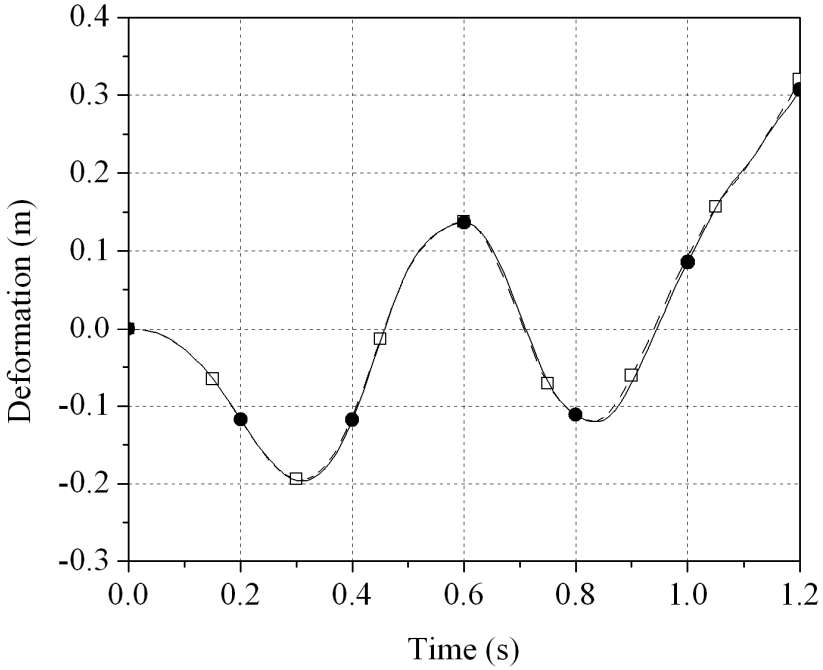

Figure 53 Midpoint transverse deformation for 0.04×0.04 m^2 cross section TDBE12 model (--□-- 6 elements; —●— 8 elements)

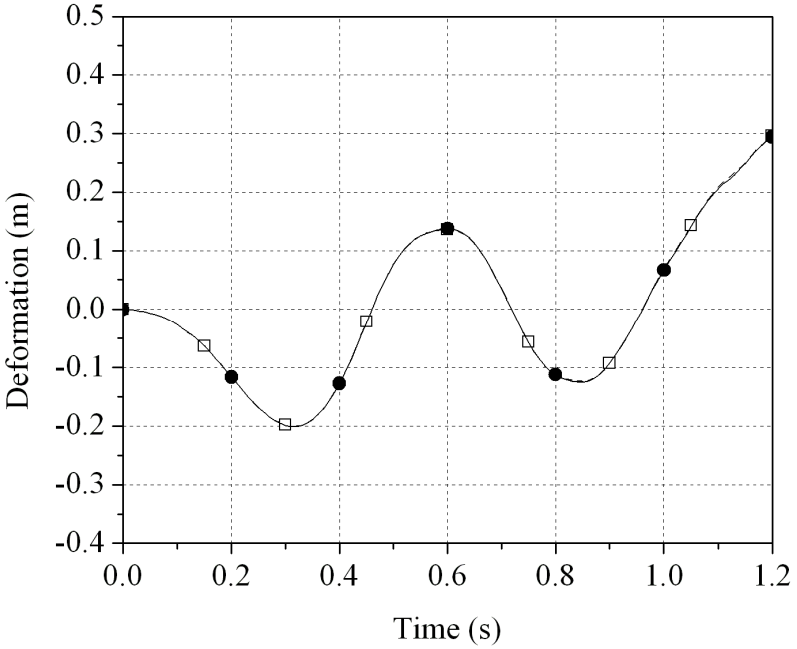

Figure 54 Midpoint transverse deformation for 0.04×0.04 m^2 cross section TDBE16 model (--□-- 6 elements; —●—8 elements)

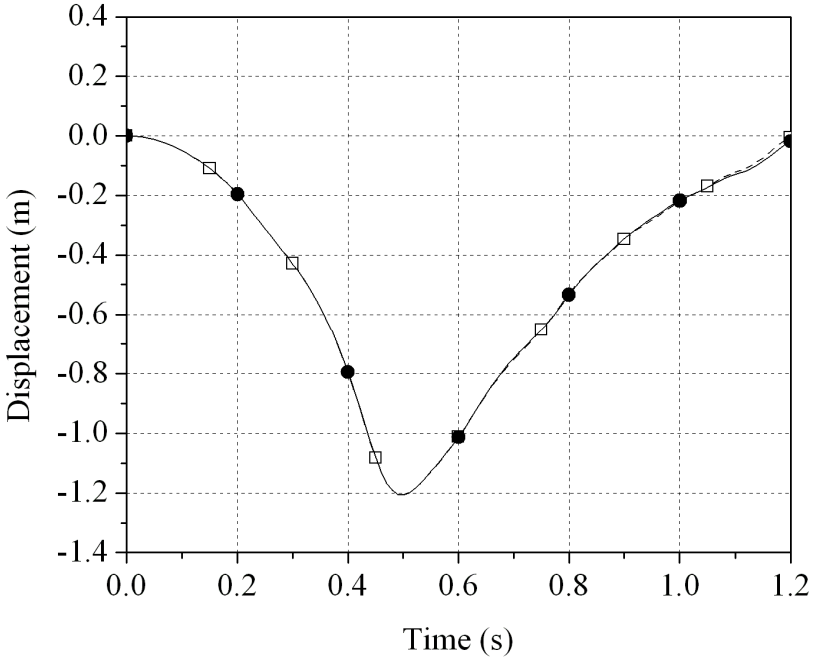

Figure 55 Tip vertical displacement for the 0.02×0.02 m^2 cross section model
(--□-- TDBE12; —●— TDBE16)

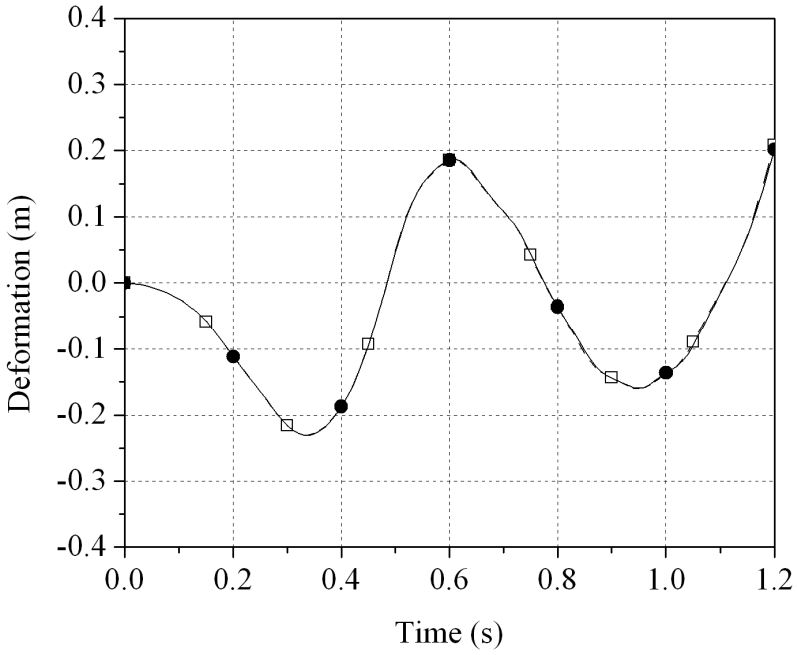

Figure 56 Midpoint transverse deformation for the 0.02×0.02 m^2 cross section model
(--□-- TDBE12; —●— TDBE16)

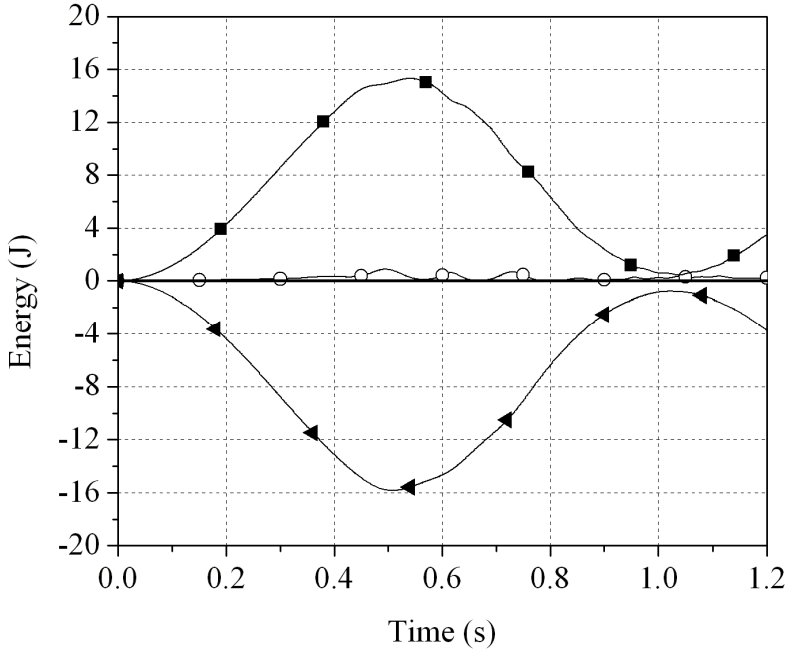

Figure 57 Energy balance for the 0.02×0.02 m^2 cross section TDBE16 model
(—■— kinetic energy; —○— elastic energy; —▲— potential energy; —— total energy)

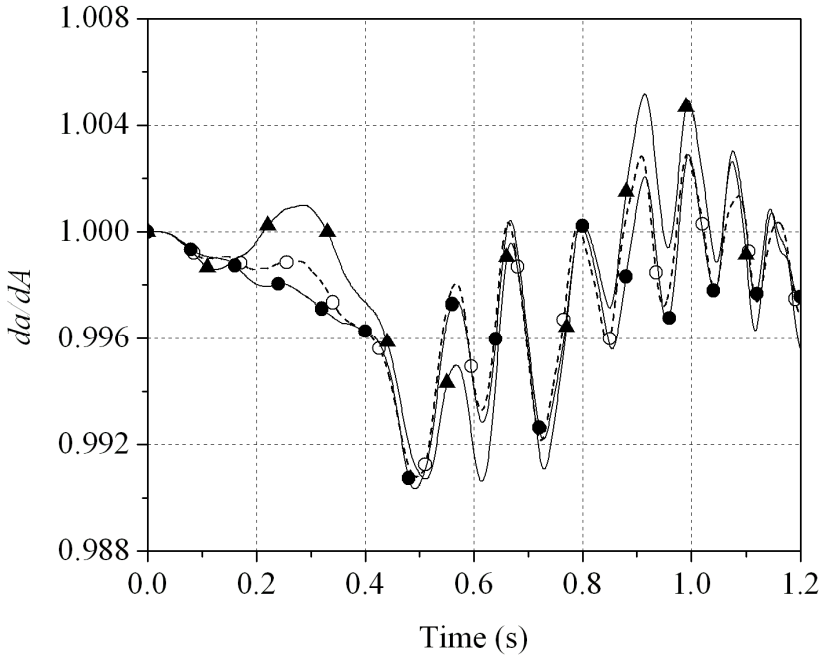

Figure 58 Area ratio at x = 0.6 m for the 0.02×0.02 m^2 cross section model
(—○— TDBE12; —▲— y = 0.008m (TDBE16); —●— y = 0.0m (TDBE16))

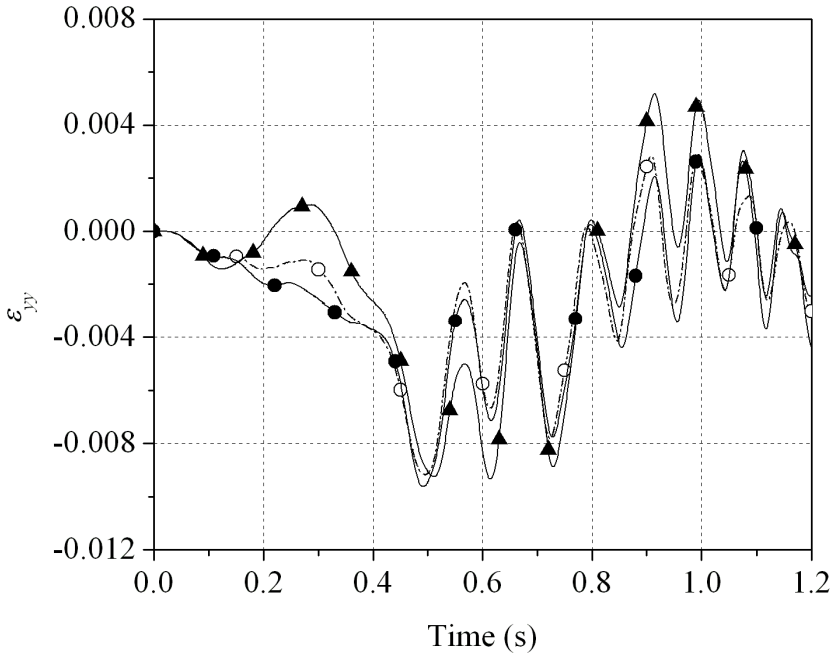

Figure 59 Transverse normal strain at x = 0.6 m for the 0.02×0.02 m^2 cross section model (—○— TDBE12; —▲— y = 0.008m (TDBE16); —●— y = 0.0m (TDBE16))

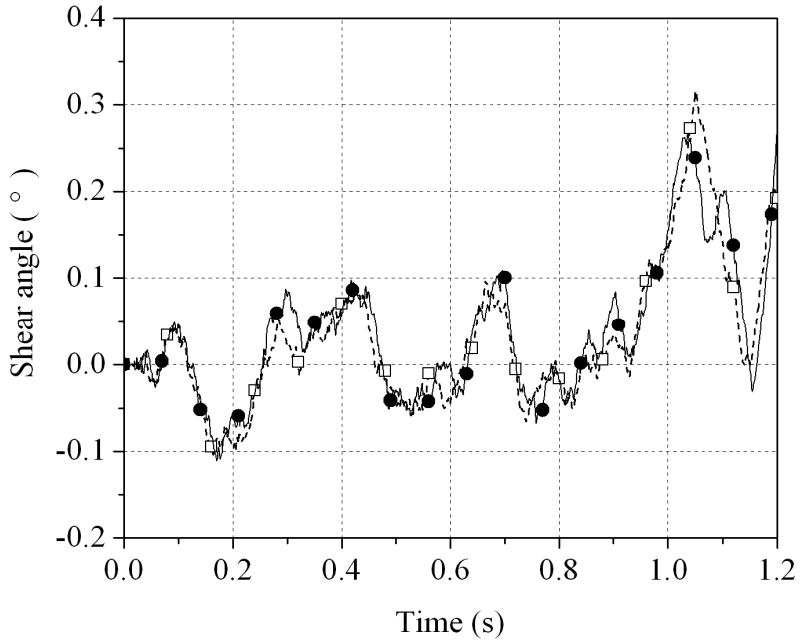

Figure 60 Midpoint shear angle of the 0.02×0.02 m^2 cross section model (--□-- TDBE12; —●— TDBE16)

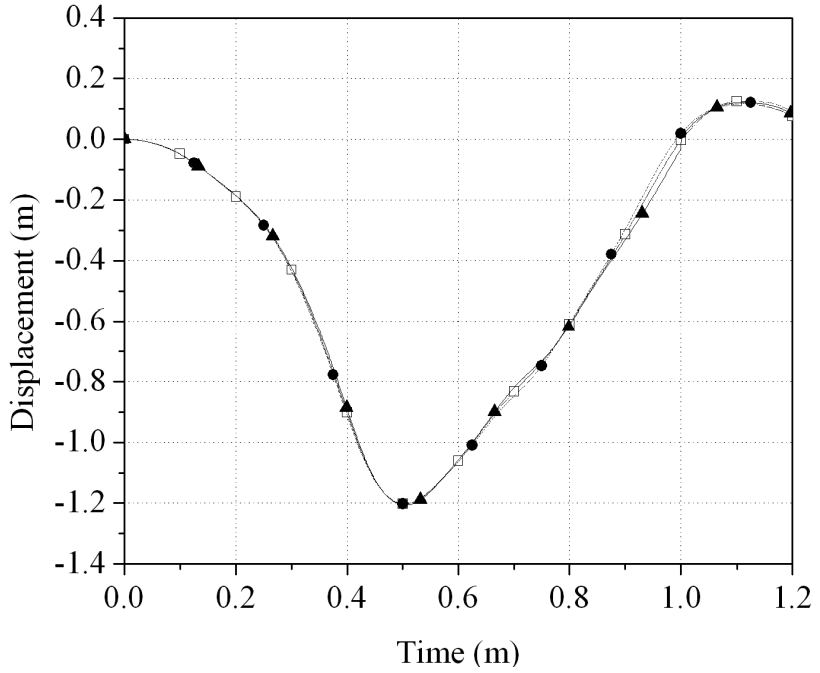

Figure 61 Tip vertical displacement for the 0.04×0.04m^2 cross section model
(--□-- TDBE12; —●— TDBE16; —▲—BEAM188)

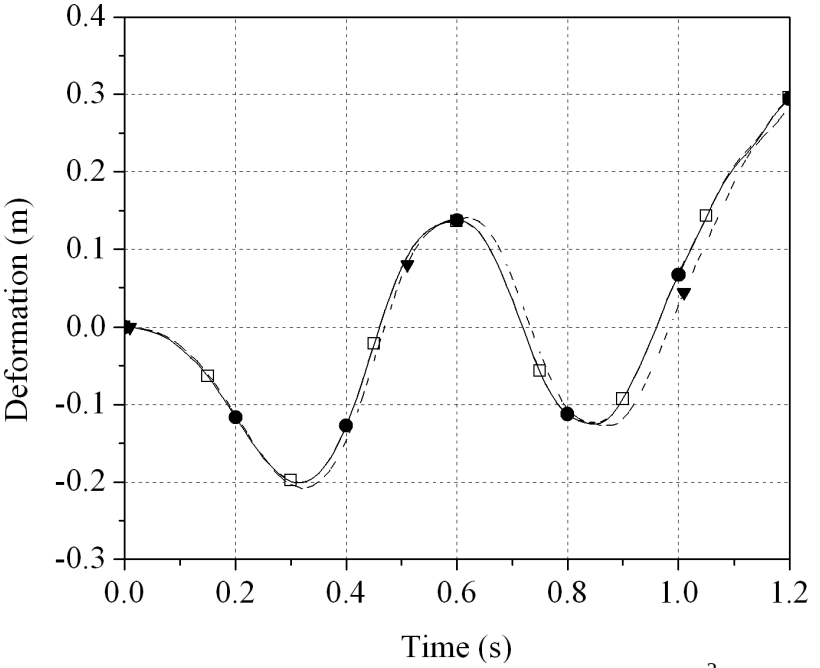

Figure 62 Midpoint transverse deformation for the 0.04×0.04 m^2 cross section model
(--□-- TDBE12; —●— TDBE16 ; --▲-- BEAM188)

5.6. Concluding Remarks

Most existing finite element beam formulations assume that the cross section of the beam remains rigid regardless of the amplitude of the displacement. Fully parameterized ANCF finite elements, however, relaxes this assumption and allow for the deformation of the cross section. In this chapter, the effect of the order of interpolation on the modes of deformation of the beam cross section using ANCF finite elements is examined. To this end, a new two-dimensional shear deformable ANCF beam element is introduced. The new finite element employs a higher order of interpolation, and allows for new cross section deformation modes that cannot be captured using previously developed shear deformable ANCF beam elements. The element developed in this study relaxes the assumption of planar cross section; thereby allowing for including the effect of warping as well as for different stretch values at different points on the element cross section. The displacement field of the new element is assumed to be cubic in the axial direction and quadratic in the transverse direction. Using this displacement field, expressions for the element extension, shear and the cross section stretch were used to study the effect of the order of interpolation. The change in the area of the cross section is measured using Nansonôs formula. The differences between the cross section deformation modes obtained using the new higher order element and those obtained using the previously developed lower order elements were highlighted. Numerical examples were presented in order to compare the results obtained using the new finite element and the results obtained using previously developed ANCF finite elements. The results obtained in this study showed a good agreement between the TDBE12 and TDBE16 models for deformation and strain measures at the element centerline. Nonetheless, the

results show that the TDBE16 model captures variations along the cross section lines that cannot be captured using the TDBE12 model.

CHAPTER 6

CONCLUSIONS AND FUTURE WORK

6.1 Conclusions

The main contribution of this thesis is to introduce a new unified approach for modeling the contact geometry and ligament deformation in bio-mechanics applications using ANCF finite elements. In this unified computational environment, one method was used for the development of accurate geometry as well as for performing the analysis. The main features that characterize and distinguish the model proposed here are: a) ANCF geometry and analysis are integrated to study the femur/tibia contact and large ligament displacements, b) the methods used are general and can be applied to other biomechanics systems, c) the model is dynamic and is more appropriate for studying human activities as compared to the quasi-static models, d) this model relates the knee mechanical properties and the contact forces produced, e) the model is simple and easy to implement in other types of biomechanical systems. The model considered in this thesis demonstrated the importance of the integration of geometry, FE, and MBS algorithms.

In the model presented in Chapter 2, new finite element/multibody system models are developed for the ligament/bone insertion site constraints. Two ANCF finite elements are employed; the first is the fully parameterized beam element, while the second is the gradient deficient cable element. The fully parameterized ANCF beam element allows for using different ligament/bone insertion site constraint models. The partially and fully clamped ligament/bone joints are considered. The partially clamped joint allows for the cross section deformation at the ligament/bone insertion site. This cross section deformation can be measured using Nansonôs formula.

The analysis reported in Chapter 2 has shown that the fully parameterized ANCF beam element allows for more modes of deformation at the knee ligament/bone insertion site as compared to the gradient deficient cable element which cannot capture the expected change in the ligament cross section. The numerical results demonstrate that the new computational finite element/multibody framework using the simplified two ligament model with either the beam or cable element can yield useful data in regard to the change in length and strains of either the LCL or MCL regardless of the insertion site constraints (fully clamped or partially clamped). In addition, the analysis demonstrates that the ligament-to-bone direct connection which is a progression of elastic type fibrocartilage, collagen and bone that can deform (as a result of stress concentrations) under a prescribed cyclic motion precludes the application of the fully clamped beam which does not allow such deformation (Benjamin M, et al. 2006).

The data shows higher strains for both ligaments than the quasi-static finite element models reported in the literature (Weiss et al., 2001; Peña et al., 2006). The higher strains are the result of the integration of the fully parameterized ANCF beam finite element model into a dynamic multibody computational framework that captures the large displacement and change in the ligament cross section resulting from the prescribed cyclic motion. High strains are also justified in the simple model considered in Chapter 2, because two ligaments only were considered and the femur was subjected to a relatively high speed of rotation. The two ligaments considered carry the entire load which in reality is shared by other ligaments and tissues of the knee joint.

Two general formulations based on ANCF finite elements for modeling the contact geometry in bio-mechanics applications are presented in Chapter 3. In one method, ANCF

volume geometry is converted to surface geometry using a parametric relationship that reduces the number of independent coordinate lines. In the second method, ANCF surfaces can be directly used without the need for using the parametric relationship. Each contact surface is described in a parametric form using two surface parameters that enter into the ANCF finite element geometric description.

Two formulations, the elastic and constraint, are used in this thesis to predict the femur/tibia contact forces. A set of nonlinear algebraic equations that depend on the surface parameters is developed and used to determine the location of the contact points. In both methods, the assumptions of non-conformal contact are used. In the constraint method, if no degrees of freedom are specified, the femur has five degrees of freedom with respect to the tibia, and the normal contact forces are obtained as reaction forces using the technique of Lagrange multipliers. In the elastic contact formulation, penetration between the bodies is allowed; this penetration and its derivative enter into the calculation of the contact forces. In the elastic contact formulation, if no degrees of freedom are specified, the femur has six degrees of freedom with respect to the tibia. The numerical results obtained in Chapter 3 show a good agreement between the results obtained using the constraint and elastic contact formulations.

In Chapter 4, the formulation of the boundary conditions of the partially clamped joint is investigated using two different models that employ the cross section and the tangent frames. The fully parameterized ANCF beam element, which allows for the deformation of the cross section, is employed in the investigation. The numerical results demonstrate that the new computational finite element/multibody system framework using the simplified knee model with either the cross section frame or tangent frame can yield useful data in regard to the change in

length and strains of either the LCL or MCL. The data shows higher strains for both ligaments than the quasi-static finite element models reported in the literature (Weiss et al., 2001; Peña et al., 2006). The higher strains are the result of the integration of the fully parameterized ANCF beam finite element model and contact constraint formulation into a dynamic multibody computational framework that captures the large displacement and change in the ligament cross section resulting from the prescribed cyclic motion. Also, the use of the constraint contact formulation, the pretension in the cruciate ligaments and the fact that the knee joint model is not symmetric, have an important effect on the results obtained in this thesis.

In general, the tangent frame and the cross-section frame are not the same and they differ due to the rotation of the cross section as the result of the shear and torsion effects. In most applications, the difference is small, permitting without producing significant errors the use of either frame. Nonetheless, the results of the example used in this thesis show that the cross section frame has a better convergence characteristics as compared to the tangent frame.

Most existing finite element beam formulations assume that the cross section of the beam remains rigid regardless of the amplitude of the displacement. Fully parameterized ANCF finite elements, however, relaxes this assumption and allow for the deformation of the cross section. In Chapter 5, the effect of the order of interpolation on the modes of deformation of the beam cross section using ANCF finite elements is examined. To this end, a new two-dimensional shear deformable ANCF beam element is introduced. The new finite element employs a higher order of interpolation, and allows for new cross section deformation modes that cannot be captured using previously developed shear deformable ANCF beam elements. The element developed in this thesis relaxes the assumption of planar cross section; thereby allowing for including the

effect of warping as well as for different stretch values at different points on the element cross section. The displacement field of the new element is assumed to be cubic in the axial direction and quadratic in the transverse direction. Using this displacement field, expressions for the element extension, shear and the cross section stretch were used to study the effect of the order of interpolation. The differences between the cross section deformation modes obtained using the new higher order element and those obtained using the previously developed lower order elements were highlighted. Numerical examples were presented in order to compare the results obtained using the new finite element and the results obtained using previously developed ANCF finite elements. The results obtained in this thesis show a good agreement between the TDBE12 and TDBE16 models for deformation and strain measures at the element centerline. Nonetheless, the results show that the TDBE16 model captures variations along the cross section lines that cannot be captured using the TDBE12 model.

6.2. Limitations and Future Work

As in many modeling projects, the knee model presented in this investigation has limitations. It is important to point out that the current model does not have representations of the patella, patellar tendon, joint capsule, skin and muscles. Attachment of the medial meniscus periphery to the tibial cartilage is not modeled. The description of the cruciate ligaments and menisci is very simple. Geometry of the knee structures was obtained using a physical knee model. Furthermore, the femur and tibia surfaces are assumed to be symmetric in order to simplify and check the results of the contact geometry and forces. The material properties of the ligaments are based on the model proposed by Pena et al. (2006); these material properties are not specimen-specific. These limitations may have significant influence on the model's predictive capacity depending

on the purpose of its utilization. Some of these issues can be addressed by the Dynamic Simulation Laboratory team. As future work ANCF can be used to model ligaments, menisci, muscles and the geometry of the femur and tibia condyles without any limitations.

It is difficult to validate the present model because of the limited amount of experimental data that describe the dynamics behavior of the human knee joint. Most of the data that describe the joint response are obtained using static or quasi-static models. Because the model presented in this thesis allows for the simulation of very dynamic scenarios, at this point, the validation can only be based on qualitative evaluation of joint response by comparison with data published in the literature.

The procedures developed in this research can be used in modeling ligament, muscles, and soft tissues (LMST). The integration of geometry, finite element, and multibody system algorithms, as defined in this thesis, is necessary for developing bio-mechanics models that capture significant details that cannot be captured using existing multibody system algorithms.

APPENDIX A

The shape function $\mathbf{S}$ used in Chapter 2 for the fully parameterized three-dimensional ANCF beam element is defined as

$$\mathbf{S} = [s_1\mathbf{I} \quad s_2\mathbf{I} \quad s_3\mathbf{I} \quad s_4\mathbf{I} \quad s_5\mathbf{I} \quad s_6\mathbf{I} \quad s_7\mathbf{I} \quad s_8\mathbf{I}] \tag{A.1}$$

where $\mathbf{I}$ is a 3 × 3 identity matrix, and s_l, $l = 1, 2, \ldots, 8$, are the shape functions defined as

$$\left.\begin{aligned} s_1 &= 1 - 3\xi^2 + 2\xi^3, & s_2 &= l\left(\xi - 2\xi^2 + \xi^3\right) \\ s_3 &= l\left(\eta - \xi\eta\right), & s_4 &= l\left(\varsigma - \xi\varsigma\right) \\ s_5 &= 3\xi^2 - 2\xi^3, & s_6 &= l\left(-\xi^2 + \xi^3\right) \\ s_7 &= l\xi\eta, & s_8 &= l\xi\varsigma \end{aligned}\right\} \tag{A.2}$$

where $\xi = x/l$, $\eta = y/l$, $\varsigma = z/l$, and l is the length of the finite element in the reference configuration. In the case of cable elements, the shape function matrix $\mathbf{S} = [S_1\mathbf{I} \quad S_2\mathbf{I} \quad S_3\mathbf{I} \quad S_4\mathbf{I}]$ can be defined as:

(A.3)

where I is a 3 × 3 identity matrix. In this equation, the shape functions are written as follows:

$$S_1 = 1 - 3\xi^2 + 2\xi^3, \qquad S_2 = l(\xi - 2\xi^2 + \xi^3), \quad S_3 = 3\xi^2 - 2\xi^3, \quad S_4 = l(-\xi^2 + \xi^3) \tag{A.4}$$

where $\xi = x/l$ and l is the length of the element.

APPENDIX B

In this appendix, it is shown that, for a given x, the area ratio as defined by Nansonôs formula is independent of the coordinate y in the case of the TDBE12 model. To this end, a unit vector **n** is defined normal to cross section surface in the current configuration as

$$\mathbf{n} = \frac{\begin{bmatrix} r_{,y2} & -r_{,y1} \end{bmatrix}^T}{\left|\mathbf{r}_{,y}\right|} \tag{B.1}$$

where $\mathbf{r}_{,y} = \begin{bmatrix} r_{,y1} & r_{,y2} \end{bmatrix}^T$. It follows that

$$\mathbf{J}^T\mathbf{n} = \begin{bmatrix} \dfrac{J}{\left|\mathbf{r}_{,y}\right|} & 0 \end{bmatrix}^T \tag{B.2}$$

Substituting into Equation 7 for the expression of J and using $\mathbf{n}^T\mathbf{J}\mathbf{J}^T\mathbf{n} = \left(J/\left|\mathbf{r}_{,y}\right|\right)^2$, one can show that $da/dA = \left|\mathbf{r}_{,y}\right|$. Since the gradient vector $\mathbf{r}_{,y}$ is independent of y in the case of the TDBE12 model, the area ratio in this case will be also independent of y. This is not the case, however, for the TDBE16 model.

CITED LITERATURE

Abbas, L.K., Rui, X., and Hammoudi, Z.S.: Plate/Shell Element of Variable Thickness Based on the Absolute Nodal Coordinate Formulation. IMechE Journal of Multibody Dynamics 224: 127-141, 2010.

Abdel_Rahman, E.M., Hefzy, M.S.: Biomechanics of the Human Knee Joint in Compression: Reconstruction, Mesh Generation and Finite Element Analysis Three-Dimensional Dynamic Behavior of the Human Knee Joint under Impact Loading. Medical Engineering and Physics 20: 276 ï 290.

Amis, A.A., Bull, A.M.J., Gupte, C.M., Hijazi, I., Robinson, J.R.: Biomechanics of the PCL and Related Structures: Postero-lateral, Postero-medial and Menisco-femoral Ligaments. Knee Surgery, Sports Traumatology, Arthroscopy 11: 71-281, 2003.

Ashraf T., Beard, D.J., Newman J.H.: Symmetrical vs. Asymmetrical total Knee Replacement a Medium Term Comparative Analysis. The Knee 10: 61-66, 2003.

Bartel, D.L., Davy, D.T., and Keaveny, T.M.: Orthopaedic Biomechanics: Mechanics and Design in Musculoskeletal Systems. Pearson/Prentice Hall, New Jersey, USA, 2006.

Bei, Y., Fregly, B.: Multibody Dynamic Simulation of the Knee Contact Mechanics. Journal of Medical Engineering and Physics 26: 777-789, 2004.

Bendjaballah, M.Z., Shirazi-adl, A., and Zukor, D.J.: Biomechanics of the Human Knee Joint in Compression: Reconstruction, Mesh Generation and Finite Element Analysis. The Knee 2: 69ï 79, 1995.

Benjamin M., Toumi H., Ralphs J.R., Bydder G., Best T.M. and Milz S.: Where Tendons and Ligaments Meet Bone: Attachment Sites ('entheses') in Relation to Exercise and/or Mechanical Load. Journal of Anatomy 208: 471-490, 2006.

Bertozzi, L., Stagni, R., Fantozzi, S.,Cappello, A.: Biomechanical Modeling from In-Vivo Data. Lecture Notes in Computer Science 4650: 133-160, 2008.

Blankevoort, L., and Huiskes, R.: Validation of a Three-Dimensional Model of the Knee. Journal of Biomechanics 29: 955-961, 1996.

Blankevoort, L., Kuiper, J.H., Huiskes, R., Grootenboer H.J.: Articular Contact in a Three-Dimensional Model of the Knee. Journal of Biomechanics 24: 1019-1031, 1991.

Cheng, R.C.K., Brown, T.D., Andrews, J.G.: Non-Uniqueness of the Bicompartmental Contact Force Solution in a Lumped-Parameter Mathematical Model of the Knee. Journal of Biomechanics 23: 353-355, 1990.

Cheng, C.K.: A mathematical model for predicting bony contact forces and muscles forces at the knee during the human gait. PhD Dissertation, Iowa City: The University of Iowa, USA, 1988.

Crisfield, M. A., and Moita, G. F.: A Co-Rotational Formulation for 2-D Continua Including Incompatible Modes. International Journal for Numerical Methods in Engineering 39: 2619-2633, 1991.

Donahue, T.L.H., Hull, M.L., Rashid, M.M., and Jacobs, C.R.: A Finite Element Model of the Human Knee Joint for the Study of Tibio-Femoral Contact. J Biomechanical Engineering, 124: 273-280, 2002.

Drake, R.L., Bogl, W., and Mitchell, A.W.M.: Gray's Anatomy for Students, Elsevier, Ontario, Canada, 2005.

Dufva, K., Sopanen, J.T., and Mikkola, A.: A Two-Dimensional Shear Deformable Beam Element Based on the Absolute Nodal Coordinate Formulation, Journal of Sound and Vibration 280: 719-738, 2005.

Elias, J.J.,Wilson D.R., Adamson, R., Cosgarea A.J.: Evaluation of a Computational Model used to predict the Patella Femoral Contact Pressure Distribution. Journal of Biomechanics 37: 295-302, 2004.

Engel, K., Herpers, R., and Hartmann, U.: Biomechanical Computer Models, Theoretical Biomechanics. Vaclav Klika, 2011.

Fung, Y.C.: Biomechanics.: Mechanical Properties of Living Tissues. 2nd ed. Springer-Verlag, New York, 1993.

Gantoi, F.M., Brown, M.A., and Shabana, A.A.: ANCF Finite Element/Multibody System Formulation of the Ligament/Bone Insertion Site Constraints. J Computational and Nonlinear Dynamics 5: 031006-1 - 031006-9, 2010.

Gantoi, F.M., Brown, M.A., and Shabana, A.A.: ANCF Modeling of the Contact Geometry and Deformation in Biomechanics Applications. Technical Report # MBS2012-2-UIC, Department of Mechanical Engineering, University of Illinois at Chicago, Chicago, 2012.

Garcia-Vallejo, D., Mayo J., Escalona J.L., and Dominguez J.: Efficient Evaluation of the Elastic Forces and the Jacobian in the Absolute Nodal Coordinate Formulation. Nonlinear Dynamics 35: 313-329, 2004.

Garcia-Vallejo, D., Escalona, J.L., and Mikkola, A.: A New Locking-Free Shear Deformable Finite Element Based on Absolute Nodal Coordinates. Nonlinear Dynamics 50: 249-264, 2007.

Garcia-Vallejo, D., Mayo, J., and Escalona, J.L.: Three-Dimensional Formulation of Rigid-Flexible Multibody Systems with Flexible Beam Elements. Multibody System Dynamics 20: 1-28, 2008.

Garcia-Vallejo, D., Mayo, J., Escalona, J.L., and Dominguez, J.: Modelling Three-Dimensional Rigid-Flexible Multibody Systems by Using Absolute Coordinates. 12th IFToMM World Congress, Besancon, June 18-21, 2007.

Gerstmayr, J., and Shabana, A.A.: Analysis of Thin Beams and Cables Using the Absolute Nodal Coordinate Formulation. Nonlinear Dynamics 45: 109-130, 2006.

Gerstmayr, J., Matikainen, M.K., and Mikkola, A.: A Geometrically Exact Beam Element Based on the Absolute Nodal Coordinate Formulation. Multibody System Dynamics 20: 359-384, 2008.

Gerstmayr, J. and Irschik, H.: On the Correct Representation of Bending and Axial Deformation in the Absolute Nodal Coordinate Formulation with an Elastic Line Approach. Journal of Sound and Vibration 318: 461-487, 2008.

Gerstmayr, J., and Matikainen, M.K.: Analysis of Stress and Strain in the Absolute Nodal Coordinate Formulation. Mechanics Based Design of Structures and Machines 34: 409-430, 2006.

Guess, T. M., Thiagarajan, G., Kia, M. and Mishra, M.: A subject Specific Multibody Model of the Knee with Menisci. Medical Engineering & Physics 32: 505-515, 2010.

Hussein, B. A., Sugiyama, H., and Shabana, A. A.: Coupled Deformation Model in the Large Deformation Finite-Element Analysis: Problem Definition. Journal of Computational and Nonlinear Dynamics 2: 146-154, 2007.

Hussein, B. A., Weed, D., and Shabana, A. A.: Clamped End Conditions and Cross Section Deformation in the Finite Element Absolute Nodal Coordinate Formulation. Multibody System dynamics 21: 375-393, 2009.

İşcan, M.Y.: Forensic Anthropology of Sex and Body Size, Forensic Science International. Forensic Scince International 147: 107-112, 2005.

Kapandji, I.A.: The Physiology of the Joints. Edinburgh: Churchill Livingstone, 1970.

Kennedy, J.C., Weinberg, H.W., Wilson, A.S.: The Anatomy and Function of the Anterior Cruciate Ligament. The Journal of Bone and Joint Surgery 56-A: 223-235, 1974.

Kerkkanen K. S., Sopanen, J.T., and Mikkola, A.: A Linear Beam Finite Element Based on the Absolute Nodal Coordinate Formulation. ASME Journal of Mechanical Design 127: 620-624, 2005.

Koyama H., Sugiyama, H., and Yamashita H.: Gradient Deficient Curved Beam Element Using the Absolute Nodal Coordinate Formulation. Journal of Computational and Nonlinear Dynamics 5(2): 021001.1- 8, 2010.

LaPrade R. F., Engebretsen A. H, Thuan V. L., Johansen S., Wentorf F. A., and Engebretsen L.: The anatomy of the medial part of the knee. The Journal of Bone and Joint Surgery (American) 89: 2000-2010, 2007.

Leondes, C. T.: Biomechanical Systems Technology, Vol. 1: Computational Methods. World Scientific Publishing Co. Pte. Ltd., USA, 2007.

Machado, M., Flores P., Pimenta Claro, J.C., Ambrosio, J., Silva, M., and Completo, A.: Development of a Planar Multibody Model of the Human Knee Joint. Nonlinear Dynamics 60(3): 459-478, 2010.

McLean, S.G., Su, A., and Van den Bogert, A.J.: Development and Validation of a 3-D Model to Predict Knee Joint Loading during Dynamic Movement. Journal of Biomechanical Engineering 125: 864ï 874, 2003.

Meister B.R., Michael S.P., Moyer R.A., Kelly J.D., and Schneck C. D.: Anatomy and Kinematics of the Lateral Collateral Ligament of the Knee. The American Journal of Sports Medicine 28: 869-878, 2000.

Mikkola, A. and Shabana, A.A.: Comparison between ANCF and B-Spline Surfaces. Proceedings of the Second Joint International Conference on Multibody System Dynamics, Stuttgart, Germany, May 29 ï June 1, 2012.

Milner, C.E.: Functional Anatomy for Sport and Exercise. New York: Routledge, 2008.

Moffat, K.L., Sun, W.S, Pena, P.E., Chahine, N.O., Doty, S.B., Ateshian, G. A., Hung, C.T., and Lu, H.H.: Characterization of the Structure-Function Relationship at the Ligament-to-Bone Interface. Proceedings of the National Academy of Sciences 105: 7947 ï 7952, 2008.

Mohamed A.A., Brown M., Shabana A.A.: Study of the ligament tension and cross-section deformation using nonlinear finite element/multibody system algorithms. Multibody System Dynamics 23: 227-248, 2010.

Mommersteeg T.J.A., Blankevoort L., Huiskes R., Kooloos J.G.M., Hendriks J.C.M.: The Effect of Variable Relative Insertion Orientation of Human Knee Bone Ligament Bone Complexes on the Tensile Stiffness. Journal of Biomechanics 28(6): 745-752, 1994.

Mow, V.C., and Hayes, W.C.: Basic Orthopedic Biomechanics. Philadelphia: Lippincott-Raven Publishers, 1997.

Nachbagauer, K., Gerstmayr, J., Sinwel, A.S., and Irschik, H.: A Linear and Quadratic Planar Finite Element Based on Absolute Nodal Coordinate Formulation. Proceedings of the 1st Joint International Conference on Multibody System Dynamics, Lappeenranta, Finland, May 25-27, 2010.

Nordin, M., Frankel, V.H.: Basic biomechanics of the musculoskeletal system. 3rd ed. Lippincott Williams & Willkins, 2001.

Ogden, R.W.: Non-Linear Elastic Deformations. Dover Publications, 1984.

Omar, M.A., and Shabana, A.A.: A Two-Dimensional Shear Deformable Beam for Large Rotation and Deformation Problems. Journal of Sound and Vibration 243(3): 565-576, 2001.

Pedowitz, R.A., O'Connor, J.J., and Akeson, W.H.: Daniel's Knee Injuries: Ligament and Cartilage, Structure, Function, Injury, and Repair. Second Edition, Lippincott Williams & Willkins, 2003.

Peña, E., Calvo, B., Martínez, M.A., and Doblaré, M.: A Three-Dimensional Finite Element Analysis of the Combined Behavior of Ligaments and Menisci in the Healthy Human Knee Joint. Journal of Biomechanics 39(9): 1686-1701, 2006.

Piazza, S.J., Delp, S.L.: Three-Dimensional Simulation of Total Knee Replacement Motion During a Step-up Task. Journal of Biomechanical Engineering 123: 599 ï 606, 2001.

Sanborn, G.G., Shabana, A.A.: On the Integration of the Computer Aided Design and Analysis using the Finite Element Absolute Nodal Coordinate Formulation. Journal Multibody System Dynamics 22: 81-197, 2009.

Sasaki, K., Neptune, R.R.: Individual Muscle Contributions to the Axial Knee Joint Contact Force during Normal Walking. Journal of Biomechanics 43: 2780ï 2784, 2010.

Schwab, A.L., and Meijaard, J.P.: Comparison of Three-Dimensional Flexible Beam Elements for Dynamic Analysis: Classical Finite Element Formulation and Absolute Nodal Coordinate Formulation. Journal of Computational and Nonlinear Dynamics 5 (1):011010-1 ï 011010-10, 2010.

Shabana, A.A., Yakoub, R.Y.: Three Dimensional Absolute Nodal Coordinate Formulation for Beam Elements: Theory. ASME Journal of Mechanical Design 123 (4): 606-613, 2001.

Shabana, A.A.: Dynamics of Multibody Systems. 3rd ed. Cambridge: Cambridge University Press, 2005.

Shabana, A.A.: Computational Continuum Mechanics. Second Edition, Cambridge University Press, Cambridge, UK, 2012.

Shabana, A.A., Zaazaa, K. E. and Sugiyama, H.: Railroad Vehicle Dynamics: a Computational Approach. Taylor & Francis/CRC, Boca Raton, FL, USA, 2008**.**

Silva, J.F., and Flores, P.: Dynamic Modeling and Analysis of the Knee Joint. Proceedings of the National Conference on the Dynamics of Multibody Systems, Guimaraes, Portugal, December 6-7, 2007.

Song, Y., Debski, R.E., Musahl V., Thomas M., Woo S.L.: A Three-Dimensional Finite Element Model of the Human Anterior Cruciate Ligament: a Computational Analysis with Experimental Validation. Journal of Biomechanics 37: 38-390, 2004.

Sopanen, J.T., and Mikkola, A.: Description of Elastic Forces in Absolute Nodal Coordinate Formulation. Nonlinear Dynamics 34 (1): 53-74, 2003.

Sugiyama, H., Escalona, J.L., and Shabana, A.A.: Formulation of Three-dimensional Joint Constraint Using the Absolute Nodal Coordinates. Nonlinear Dynamics 31: 167-195, 2003.

Sugiyama H., Gerstmayr J., and Shabana A.: Deformation Modes in the Finite Element Absolute Nodal Coordinate Formulation. Journal of Sound and Vibration 298(4-5)1129-1149, 2006.

Sugiyama, H., and Suda, Y.: Non-linear Elastic Ring Tire Model Using the Absolute Nodal Coordinate Formulation. Proceedings of the Institution of Mechanical Engineers, Part K: Journal of Multi-body Dynamics, 211-219, 2009.

Tian, Q., Zhang, Y., Chen, L., and Yang, J.: Simulation of Planar Flexible Multibody Systems with Clearance and Lubricated Revolute Joints. Nonlinear Dynamics 60: 489-511, 2010.

Timoshenko, S.P., and Goodier, J.N.: Theory of Elasticity. New York: McGraw-Hill, 1970

Vollebregt, E.A.H.: Survey of Programs on Contact Mechanics Developed by J.J. Kalker. Vehicle System Dynamics 46(1): 85-92, 2008.

Wang, C.J.: Injuries to the Posterior Cruciate Ligament and Posterolateral Instabilities of the Knee. Chang Gung Med Journal 25: 288-297, 2002.

Weed D., Maqueda L., Brown M., and Shabana A.: A Multibody/Finite Element Nonlinear Formulation of a Two-Ligament Knee Joint. Proceedings of the 2008 ASME International Mechanical Engineering Congress and Exhibition, Boston, U.S.A, 407-416, 2008.

Weiss, J., Maker, B., and Govindjee, S.: Finite Element Implementation of Incompressible, Transversely Isotropic Hyperelasticity. Computer Methods and Applications in Mechanical Engineering 135: 107-128, 1996.

Weiss, J.A. and Gardiner J.C.: Computational Modeling of Ligament Mechanics. Critical Reviews in Biomedical Engineering 29(4): 1-70, 2001.

Yamaguchi, G.: Dynamic Modeling of Musculoskeletal Motion. Kluwer Academic Publishers, Dordrecht, Netherlands, 2001.

Yakoub, R.Y., and Shabana, A.A.: Three Dimensional Absolute Nodal Coordinate Formulation for Beam Elements: Implementation and Applications. ASME Journal of Mechanical Design 123: 614-621, 2001.

VITA

Name Florentina Marina Gantoi

Education

University of Illinois at Chicago, Chicago IL.

Ph.D. / Department of Mechanical & Industrial Engineering (2008-present).

Pitesti University , Romania

B.Sc. / Department of Mechanical Engineering (2001-2006).

Teaching Experience

University of Illinois at Chicago, Chicago IL, USA (2008-2013)**.**
Teaching assistant for the following courses:

- Thermodynamics
- Theory of Vibration
- Computational Multibody Dynamics
- Continuum Mechanics
- Design and Machinery

Professional Membership

– Society of Automotive Engineers (SAE): member since 2013.
– American Society of Mechanical Engineers (ASME): member since 2008.

Reviewing

– ASME Journal of Computational and Nonlinear Dynamics
– ASME IDETC/CIE 10th International Conference on Multibody Systems, Nonlinear Dynamics and Control, 2012.

Publications

Journal Publications

*Pengfei Li, **Gantoi, F.M,** and Shabana, A. A.: Higher Order Representation of the Beam Cross Section Deformation in Large Displacement Finite Element Analysis. Journal of Sound and Vibration 330(26): 6495-6508, 2011.

***Gantoi, F.M.,** Brown, M., and Shabana, A. A.: ANCF Finite Element/Multibody System Formulation of the Ligament/Bone Insertion Site Constraints. Journal of Computational and Nonlinear Dynamics 5(3):031006-031015.

Gantoi, F.M., Brown, M., and Shabana, A. A.: Finite Element Modeling of the Contact Geometry and Deformation in Biomechanics Applications. Journal of Computational and Nonlinear Dynamics 5(3):031006-031015.

* Used in making the current thesis.

Conference papers

Gantoi, F.M., Brown, M., and Shabana, A. A.: ANCF Modeling of the Contact Geometry and Deformation in Biomechanics Applications. Proceedings of the 2012 ASME International Design Engineering Technical Conferences& Computers and Information in Engineering Conference, Chicago, IL, August 12-15, 2012.

Shabana, A., **Gantoi, F.M**. and Brown, M.: Integration of Finite Element and Multibody System Algorithms for the Analysis of Human Body Motion. Proceedings of the IUTAM Symposium on Human Body Dynamics: from Multibody Systems to Biomechanics, University of Waterloo, Waterloo, Canada, 2011.